MICRO AIRCRAFT DESIGN

Final Report:
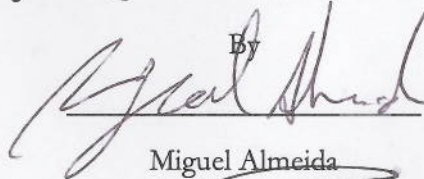
Submitted to the Faculty of the

WORCESTER POLYTECHNIC INSTITUTE

In fulfillment of the requirements for

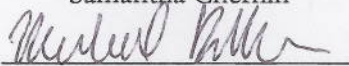## MAJOR QUALIFYING PROJECT
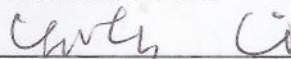
By

Miguel Almeida

George Asare

Alex Brown

Samantha Chernin

Michael DiMilia

Jamie Donahue

Thomas Hlavenka
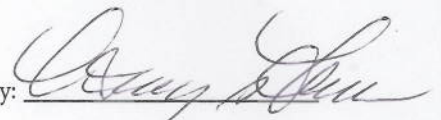
Alexander Korza

Yutong Li

April 27th 2017

Approved by:

Professor Anthony B. Linn, Advisor

Table of Contents

Table of Figures

Table of Tables

ACROYNMS AND NOMENCLATURE

DBF – Design, Build, & Fly

RAC – Rated Aircraft Cost

NiMH – Nickel Metal Hydride

NiCad – Nickel Cadmium

AMA – Academy of Model Aeronautics

UAV – Unmanned Aerial Vehicle

L/D – Lift to Drag Ratio

TMS – Total Mission Score

Cl_{max} – Maximum Coefficient of Lift

Cl_{cruise} – Cruise Coefficient of Lift

CL – General Coefficient of Lift

CD – General Coefficient of Drag

Cm – General Coefficient of Moment

Alpha – Angle of Attack

V_{stall} – Stall Speed

MAV – Micro Aerial Vehicle

ECS – Electronic Speed Controllers

MDF – Medium Density Fiberboard

CL-alpha – Lift Curve Slope

CLo – Zero Angle Lift

RPM – Revolutions per minute

m/s – meter per second

Kg- Kilograms

N – Newton's

ρ – Density

c_{bar} – Mean Aerodynamic Chord

Re – Reynolds Number

TE – Trailing Edge

LE – Leading Edge

V_{cruise} – Cruise Speed

ABSTRACT

The goal of this MQP was to design, build, and fly a UAV that can successfully complete the four missions of the AIAA DBF 2017 competition while optimizing the team's score and meeting the general competition requirements. The UAV was an electric-driven, radio controlled aircraft that must be powered by nickel batteries, and fit inside a fixed-dimension, watertight launch tube in a folded storage configuration. The UAV must be capable of unfolding from the storage configuration to the flight configuration without the use of any tools, all moveable components be self-locking and self-aligning. The UAV must complete three flight missions that evaluate aircraft speed and the ability to carry a payload and one ground mission, a drop test that evaluates the aircrafts durability when placed in its storage container.

ACKNOWLEDGEMENTS

INTRODUCTION

We set out on this project with two distinct but interdependent goals: (1) to fulfill our MQP requirements in full realization of the learning objectives set out by WPI and (2) to compete and place in the AIAA's highly competitive DBF competition, making a name for both WPI aerospace and ourselves. DBF provides a unique educational opportunity to students, where a team of undergraduates—with years of combined learning experience in aerospace theory—coalesce these lessons in the production of a micro aerial vehicle (MAV). In this way, the DBF competition serves as a unifier between the theory of WPI's undergraduate studies and the real-world practice of aircraft production, a true testament to WPI's motto, "Lehr und Kunst."

LITERATURE REVIEW

This year's DBF competition focused on the production of a portable fixed-wing MAV capable of folding into a tube and being easily deployed from its folded state. The most obvious real-world applications of such a MAV would be for the military, which is most likely where the project draws its inspiration from; the Switchblade MAV (see Figure 1) is a tube-launched, portable fixed-wing MAV that is being developed by the company, AeroVironment, under a US Army contract. One of the biggest design challenges with a portable UAV is to include enough wing area to fly, but still be able to fit into a tube. To overcome these challenges, AeroVironment's design (1) uses folding, flat plate wings mounted on the forward and aft sections of the fuselage and (2) is configured for a tube launch, which helps overcome the lower stall speed presented by designs with less lifting surface. Accommodating these unique features, the Switchblade weighs 2.5 kg, launches from a 60 cm long tube, and flies at speeds of up to 80 km/h for up to 40 minutes [1]. For comparison, our final MAV, Gompei Volanti, also weighs 2.5 kg, can be launched from an 89 cm long tube, and can fly at speeds in excess of 80 km/h for an unknown duration (due to pilot fatigue).
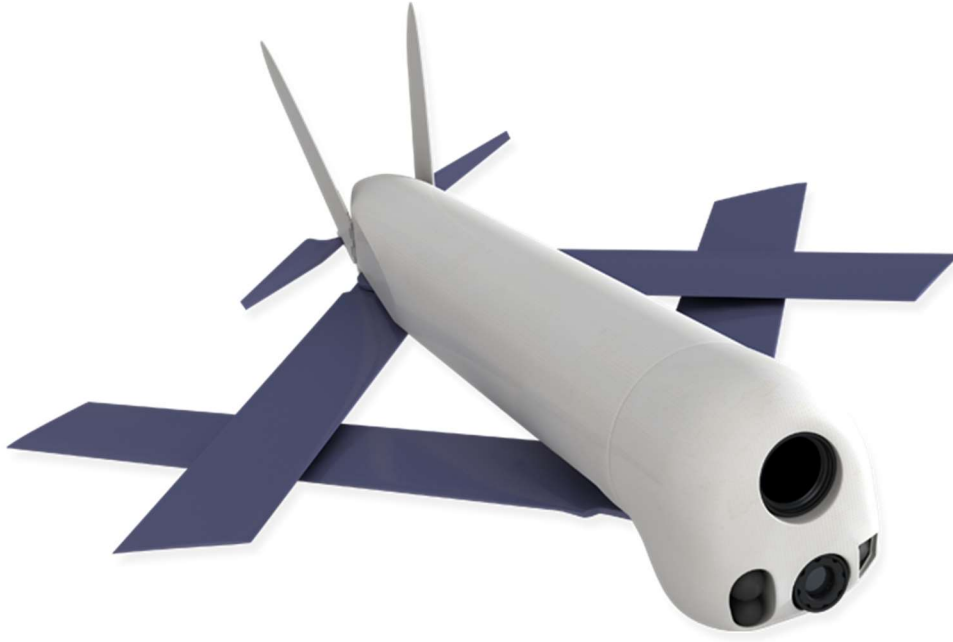
FIGURE 1: SWITCHBLADE MAV 2

The application of drones is defined by their payload, and in the Switchblade's case, its payload of plastic explosives and optical sensors for first person view (FPV) flight make it a uniquely destructive indirect fire and quick reconnaissance weapon. The Switchblade's design features were implemented to solve the Army's very real problem of lack of information during the chaos of ambushes [3]. Soldiers, who only have the cover of the vehicles in their convoy, need a way to quickly identify and eliminate threats without exposing themselves to unnecessary danger. Calling in air support takes too long for this application, and the soldiers under fire may struggle to identify where they are being shot from without an aerial perspective. Having a portable fixed-wing MAV solves both of these problems, as it can be deployed quickly, accurately identify enemies, and eliminate them without putting the soldiers in danger.

However, the applications of portable fixed-wing MAVs are not limited to military applications. There is a growing need for MAVs in commercial applications, and many of those, such as precision agriculture, prefer fixed-wing MAVs due to their combination of speed, range, and endurance that multi-rotors will never match [4]. Having fixed-wing MAVs be portable would reduce the hassle and expenses of getting these MAVs and their pilots to the people that need them. This would save time and money, thus making the commercial MAV industry more viable.

In these ways, our project has been validated as a solution to real world problems in both the military and commercial realms. These applications were further considered at various points in our design, as we prioritized cost and durability, which allowed us to build a MAV that stayed within the relatively low budget of our MQP and have hard landings without significantly affecting the structural integrity of our MAV.

EXECUTIVE SUMMARY

This report analyzes the process of engineering Gompei Volanti, Worcester Polytechnic Institute (WPI)'s entry to the AIAA's 2017 Design/Build/Fly Competition. Gompei Volanti is a tri-folding, carbon fiber-epoxy matrix composite, single engine tractor aircraft capable of carrying an 18-oz. (3 hockey pucks) payload and folding into an 8-inch diameter tube. The scope of the analysis includes trade-off studies, design, manufacturing, and testing.

Design Process

Design decisions were made after conducting a trade-off analysis that analyzed both practical concerns, like ease of manufacturing, and scoring concerns to create the highest scoring plane possible. Carbon Fiber was selected for its high strength-to-weight ratio. This is important because the tube diameter limits the chord length of the wing, and in order to achieve a desired wing area, the wingspan and aspect ratio must be increased, which increases bending stresses on the wing. The tri-folding aspect of the design, maximizes wing area that can fit into the tube, while adhering to a conventional design for simplicity's sake. A single engine tractor was selected because the tube restricts the aircraft to a center mounted engine, and the mass distribution of the tri-folding design makes a forward-mounted propulsion system advantageous.

Key Mission Requirements and Design Features

To win DBF, not only do you have to design an aircraft that meets the mission and performance characteristics, but you also need to optimize your total score. The use of trade-offs was extremely

important in this aspect. The key mission requirements and features that increase the aircraft

performance and score are the empty weight, hand-launched takeoff, and tube size and weight.

Empty Weight: The aircrafts empty weight impacts the score drastically as it is one of the leading

components in the Rated Aircraft Cost (RAC) which is what our report and total mission score gets

divided by to get our final score.

Tube Weight and size: The aircraft needs to fit in a tube of a length-to-width ratio of at least 4, but

also the tube weight and size heavily influences our total score, being a part of the RAC.

Hand Launched: The takeoff requirement for this year's completion is hand-launched. This

condition requires a high lift for takeoff due to the relatively low speed at which the aircraft is being

thrown.

System Performance Capabilities

The design features that were decided to be most critical in maximizing our aircraft's system

performance are specified below:

- Max Takeoff Weight: 2.3455 kg

- Empty Weight: 1.7 kg

- Reliable hand launched takeoff + secure payload storage for M2 and M3

- Top speed: 21+ m/s

- Stall speed: 9.5 m/s

- RAC: 3.04 kg-m

The final design of Gompei Volanti is a conventional, high wing monoplane configuration with a single tractor motor and no landing gear. To substitute landing gear, the fuselage belly has 4 layers of carbon fiber, instead of 2. The aircraft is equipped with a folding carbon fiber 2 blade propeller, 10-cell NiMH Battery, and an E-flite motor, all of which minimizes weight and improves performance. The team's goal was to maximize our total score while optimizing performance and mission requirements.
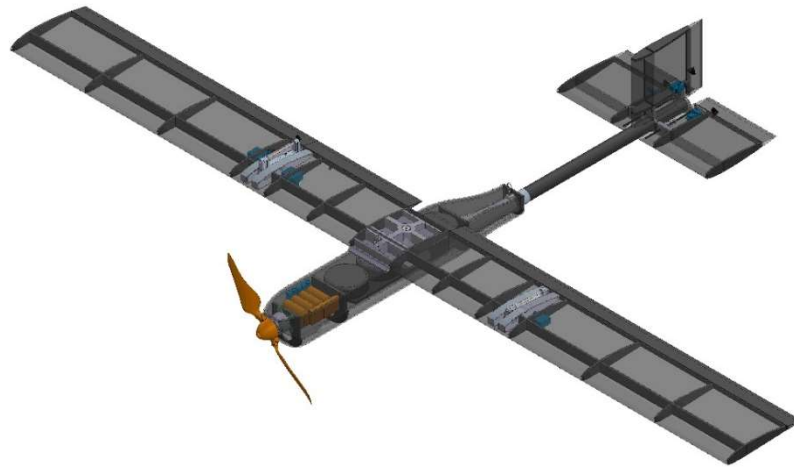
FIGURE 2: CAD MODEL

MANAGEMENT SUMMARY

The WPI team consists of eighteen students: 9 seniors, 6 juniors, 2 sophomores, and 1 freshman. We consider our team a green DBF team as we only have two members that were originally familiar with DBF before joining as part of their senior design project. The goal for this year's DBF team is to create a fully functionally and optimized aircraft and at the same time build a foundation for the next generation.

Team Organization

As a team we divided into four design subgroups: structures, aerodynamics, propulsion, and stability and control, each of which is led by two seniors and has approximately two or three underclassmen. The subgroups are not meant to be rigidly organized, as groups will move and change as the design process finishes and the manufacturing process begins. These subgroups are coordinated by the Design and Testing Coordinators, who are in charge of ensuring cooperation and communication

within and between teams. The Team Leader is charged with keeping the subgroups accountable for their work, as well as enforcing the timeline. The team also appointed a Resource Manager who is in charge of the budget, procurement, and public relations. Finally, our pilot is a freshman AMA member who has been flying model UAV's with his father since a young age, and the backup pilot is a senior AMA member who has been taking flying lessons since the beginning of the summer.

Responsibilities of each subgroup:

- **Structures**: Materials research, CAD designers, structural analysis, building plan, head builders of the UAV

- **Aerodynamics**: Airfoil Selection, Lift/Drag calculation, critical performance parameters, aerodynamic analysis (both in computer programs and wind tunnel)

- **Propulsion**: Determine the type of motor, battery, and propeller to meet thrust and power requirements

- **Stability and Control**: Determine control scheme by identifying servos, linkages, receiver/transmitter and control battery, design of control surfaces, monitor center of gravity aerodynamic center for stability
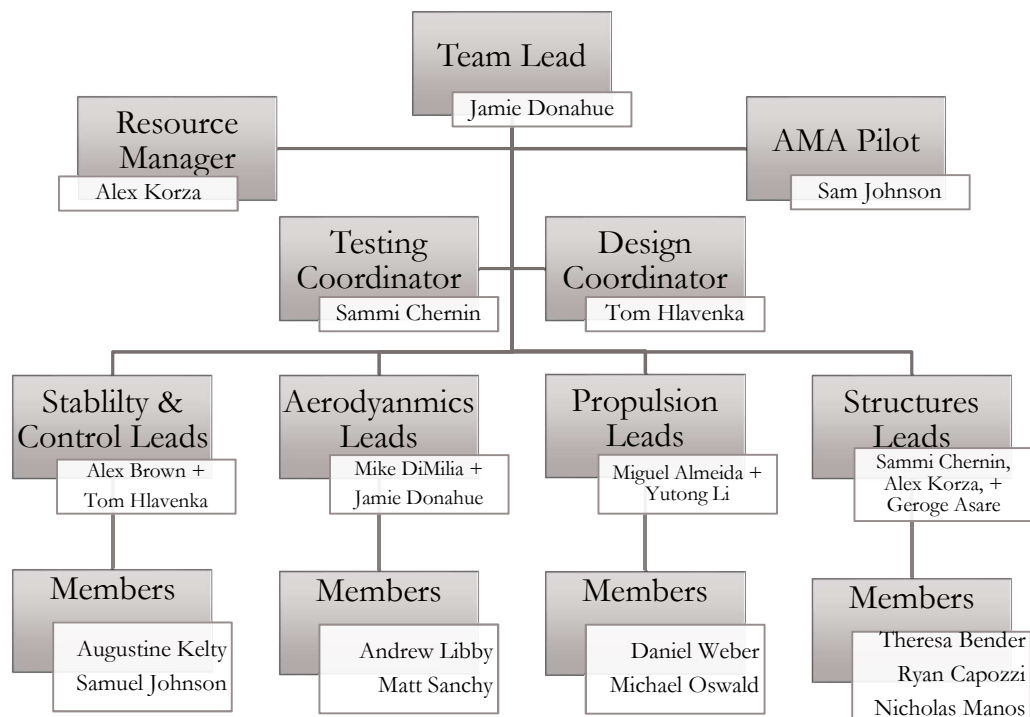
FIGURE 3: TEAM ORGANIZATION CHART

14

Project Milestones

At the beginning of our project we established a timeline to keep track of manufacturing schedules, material orders, travel plans, and the team's major milestones. The schedule was managed by the team leader to insure that our objectives were met within the allotted time and that we will have a tested and flight ready aircraft before April 20th. The project spanned across the entire year (August 2016 – April 2017). The DBF Timeline is displayed below in Figure 3 with the intent of visualizing our team's goals in a timely and organized fashion.
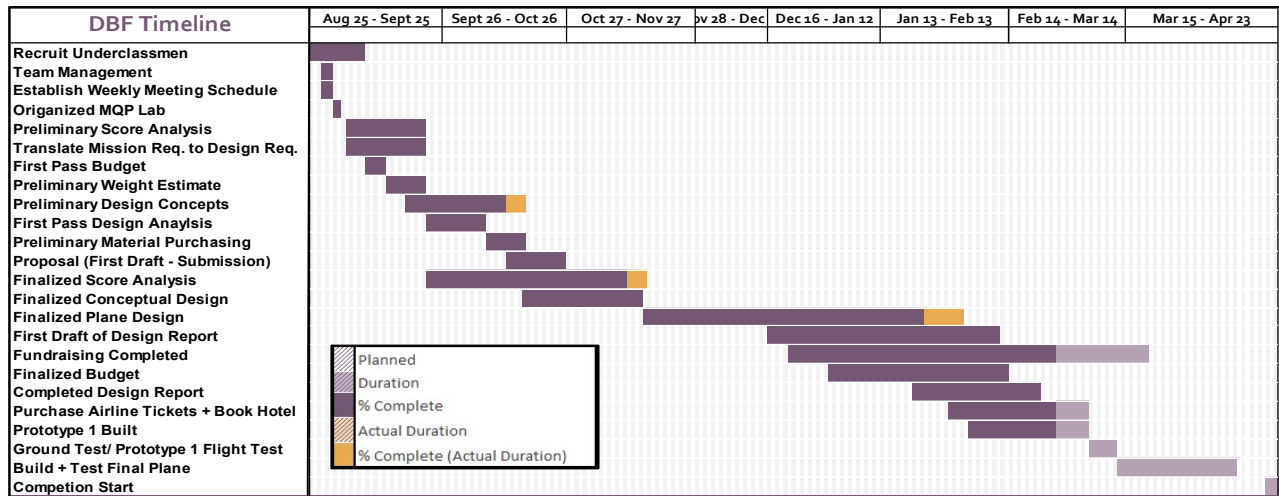
FIGURE 4: PROJECT TIMELINE

Project Budget

The project budget is split into our 4 subgroups in addition to our Travel expenses. Travel includes all expenses related to going to the competition in Tucson, Arizona including flights, housing, food, and rental cars. The Structures budget will cover material acquisition, manufacturing tools, and testing apparatus for structural tests. Stability and Controls includes the parts required for control surfaces, like servos and a secondary battery, as well as RC Hardware like a controller and receiver. Propulsion includes the primary battery, motor, and propeller. Aerodynamics includes 3D printed airfoils

and testing apparatus for aerodynamic tests in WPI's wind tunnel. Our total predicted budget amounts to $9,615. Figure X below show the breakdown of the predicted budget and the funding sources.
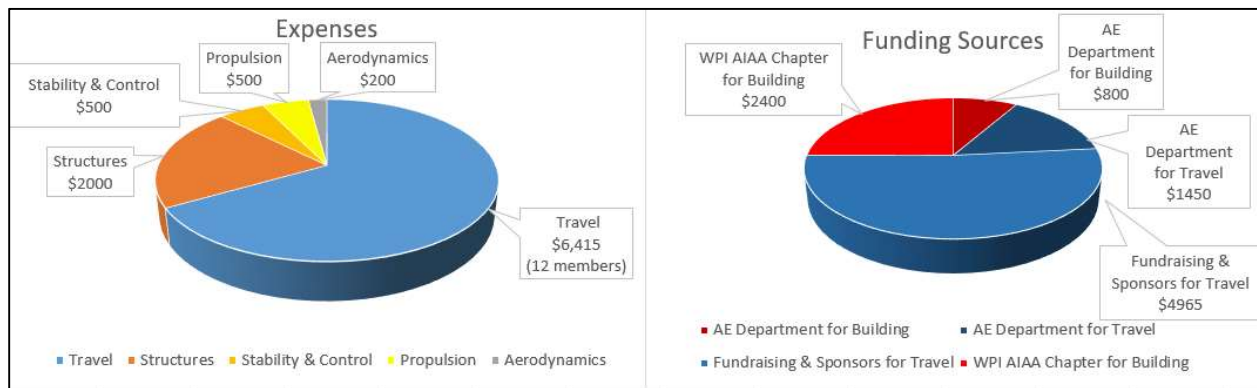
FIGURE 5: PROJECT BUDGET

We are getting these funds from three main sources: WPI's Aerospace Engineering (AE) Department, WPI's AIAA Student Chapter, and Fundraising/Sponsors. The AE Department provides $250 for every student working on the project as their Major Qualifying Project, which for us amounts to $2250 in funding. We used this to acquire initial materials for building. We subsequently sought funding from WPI's student government via our AIAA student chapter. This covered the remaining $2400 in the building cost, but could not cover travel costs. The remaining travel costs, after AE Department funding, will be split between fundraising and sponsorships. Sponsorships will be sought out via connections made during the senior team members' past internships. Fundraising will be conducted around the WPI campus and will complete the funds for our budget.

CONCEPTUAL DESIGN

Our team is required to design, build, and fly a UAV that can successfully complete the four missions of the competition. All of the conceptual designs and structure fabrication will be done by the team itself. The UAV is an electric-driven, radio controlled UAV powered by NiCad or NiMH battery, that will fit inside a fixed-dimension, watertight launch tube in a folded storage position. The UAV must be capable of unfolding from the storage position to the flight configuration without the use of any tools or removing parts.

The UAV must complete three flight missions and one ground mission:

- **Mission 1** – Complete three (3) laps with no payload

- **Mission 2** – Complete three (3) laps with three (3) regulation hockey pucks in UAV

- **Mission 3** – Complete (N) number of laps with (N) number of pucks, where N is the maximum number of laps and pucks decided by the teams

- **Ground Mission** – Complete three (3) drops from a height of 12 inches without sustaining major damage. The drops are a flat drop with the long axis of the tube parallel to the ground surface, and a drop on each end of the long axis perpendicular to the ground surface.

The flight course for each mission is a 1000 foot straightway on each side with a 360 degree loop. The two turns on each end are determined by the turning radius of the UAV. The payload for the missions is a regulation hockey puck, with a diameter of 3 in (0.0762 m), thickness of 1 in (0.0254 m) and a weight of 6 ounces (0.17 kg). The flight window for every mission is five minutes, starting at the moment the UAV leaves the launcher's hand. On a side note, the ground mission and mission one must be completed in order to attempt missions two and three. Additionally, to receive points for a mission, the UAV must have a successful landing without major damage.
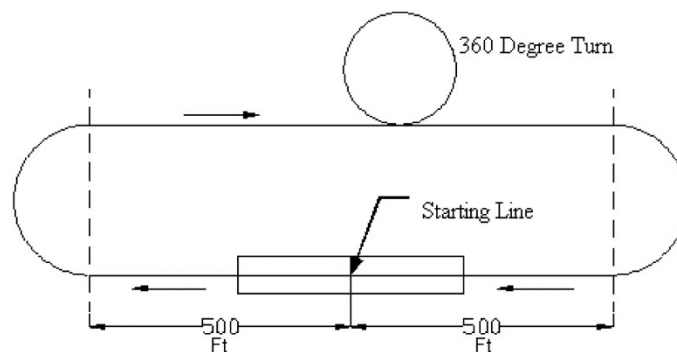
FIGURE 6: MISSION COURSE

Mission and Design Requirements

With the given competition requirements, a list of design constraints was then written up in order to ensure that any design would meet the requirements. The table below outlines the mission requirements and how they were translated into design requirements.

TABLE 1: MISSION TO DESIGN REQUIREMENTS

Mission Requirements		Design Requirements
Fit inside a sealed right cylindrical launch tube with a L/D ratio of at least 4		UAV would need some form of folding wing
Manually transition to the launch configuration in a self-locking manner		The joints of the folding wing could not use screws or some other form of manual lock
Carry at least 3 hockey pucks internally		The plane needs to have a high L/W ratio to maximize pucks carried to weight of the plane
Have the range and velocity necessary to complete at least 3 laps within 5 minutes		The battery and motor must be designed with a limiting velocity and duration in mind
Be capable of being hand launched		The stall velocity had to be under the velocity at which a team member could throw the plane

We decided a folding wing would be an optimal choice because its span lends well to reducing the length and weight of the tube, which would maximize our score. The scoring algorithm was defined as follows. Where the total mission score (TMS) is the success rate for all three missions and rated aircraft cost (RAC).

$$SCORE \ = \ Written \ Report \ Score \ * \ Total \ Mission \ Score \ / \ RAC$$

$$TMS \ = \ 1 + 2 * (Min\_time/N\_time \ + (4 * [N\_(laps * pucks)/Max\_(la \quad * pucks)] + 2)$$

$$RAC \ = \ (EmptyWeigh \qquad + \ TubeWeight \ * \ (Length \ + \ Circumference$$

Configurations Considered

We first started looking into possible configurations for our aircraft by identifying the most important design parameters and weighting them based on mission requirements. Using four configurations—Conventional, Flying Wing, Bi-Plane, and Canard—and a scoring matrix we were able to evaluate tradeoffs and decide on the best configuration for this design challenge.

TABLE 2: CONFIGURATION SCORING MATRIX

Design Parameters	Weight	Conventional	Flying Wing	Bi-Plane	Canard
Weight	80%	2	1	3	2
Stability	40%	1	3	2	2
Efficiency	30%	2	1	3	2
Folding Complexity	50%	2	1	2	1
Structure Strength	40%	1	3	1	2
Landing Gear Integration	10%	1	3	1	2
Plane Length/Dia Ratio	30%	1	1	3	1
Hand Launch-ability	20%	1	2	3	1
Total Score	-----	4.3	4.7	6.2	4.7

Scoring Legend	Value
1	BEST
2	OK
3	WORST

Based on Table 2, the Conventional configuration was chosen. From there we started drawing up possible plane designs. From those, two main configurations were considered, a tri folding wing and a side folding wing. The tri-fold wing featured two joints along the wing where the outer wing panels would fold up. The wing would then rotate to be parallel to the fuselage. The side folding wing had wings that folded down and then back to be parallel to the fuselage. Table X below shows the comparison:

TABLE 3: CONFIGURATION SCORES

	Score	Weight (kg)	Number of Joints	Tube Length (m)	Tube Diameter (m)	Chord Length (m)	Wing Span (m)
Bi-fold	287.5	1.64	4	0.945	0.2	0.2	1.63
Tri-fold	406.1	1.54	6	0.72	0.18	0.163	2.02
Side-fold	334.8	1.5	7	1.03	0.1676	0.16	2.06

Bi-Fold

Tri-Fold

Side-Fold
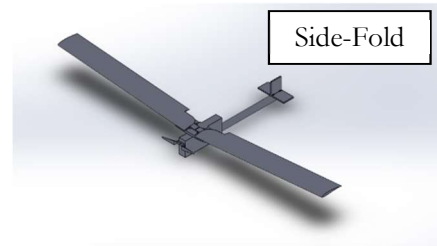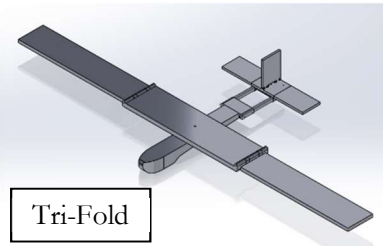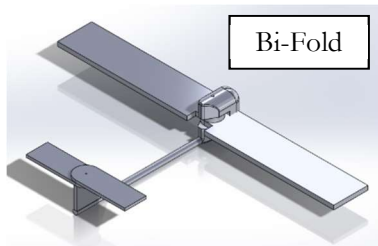
Component Weighting and Selection Process

When it came to weighting the importance of components and selecting the right ones for our configurations, we analyzed the official scoring algorithm and did research on the advantages and disadvantages of the various components. One particular situation that we handled was deciding to use a ducted fan or a propeller; although a ducted fan does produce more thrust, the speed required to get the benefits is out of the range of our aircraft. As a result, we went with the propeller.

Final Conceptual Design Configuration

In order to decide between these two main concepts, rough designs were created and scored based on their major design parameters. For example, the tri-fold had a minimum launch tube length of ⅓ the wing span, while the side-fold had a minimum launch tube length of ½ the wing span. It was determined because of this main difference, the tri-fold would lead to a better score based on the conditions given. Therefore the tri-fold was chosen as our final configuration.

PRELIMINARY DESIGN

Design Methodology

Using the constraints given and the finalized conceptual configuration, the team moved onto making a plane that will optimize score and complete all three missions and the ground test. Once the team's goals were aligned we started doing analyzing and testing propulsion systems, aerodynamic components, and structural designs. Once the research was done we moved straight into the deign analysis which required multiple computer programs to compute. The design process involved several iterations as general and performance characteristics were interchanged and updated, such as the weight of the aircraft after switching materials or resizing the wing to meet lift requirements. The iterative process is absolute necessary when optimizing the aircraft performance. Each subgroup understood their individual limitations and capabilities which led to improved designs.

Design Trades

A detailed analysis of the scoring algorithm with regards to design constraints was created. It was clear from the algorithm that trade-offs would need to be made in the design of the UAV. An aircraft that could carry more pucks or fly more laps would need to be heavier than a plane that barely met the requirements of 3 pucks and 3 laps.

In order to estimate the plane that would have the highest score, a MATLAB program was written that would optimize the tradeoffs between payload capacity, velocity, and weight. This program was designed to iterate over and create design parameters for planes with various empty weights, payload capacities and velocities. It would then plot the empty weight versus plane score, as well as print the design parameters of the highest scoring aircraft found.

The program worked first by iterating over weights and velocities in a user defined range. Since we had defined our estimated lift coefficients, the code was able to calculate the necessary wing area using the lift equation for the given weight and velocity. Then by calculating drag using various equations for various forms of drag, the necessary thrust could be calculated, from which the code could estimate a motor and battery size for a five-minute mission. Once all these elements were calculated, the code could

produce an actual weight for the plane based on the weight of the individual parts and the carbon fiber composite we would be using. If this actual weight was greater than the initial given weight, that plane configuration would not have enough to fly and was thrown out. Otherwise, if the actual weight was less than the original weight, the score for that configuration was stored to be plotted after the iteration was fitted.

Figure X below gave us a lot of valuable information. We first noticed that each distinct line of points corresponds to a specific number of laps. For each lap count, plane score drops off quickly with weight, so minimizing the weight of our plane was significant. Additionally, we could see that it only made sense to carry three pucks - the additional structural weight necessary to carry additional pucks was not offset in the score by the additional points from the pucks.
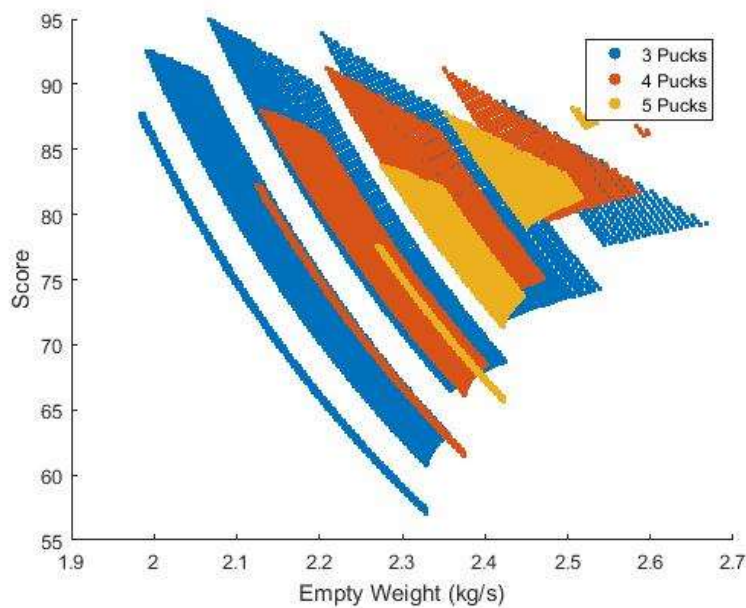
FIGURE 7: SCORE OPTIMIZATION

Having decided on carrying only three pucks, we then hid the other puck counts to examine the plot more closely.
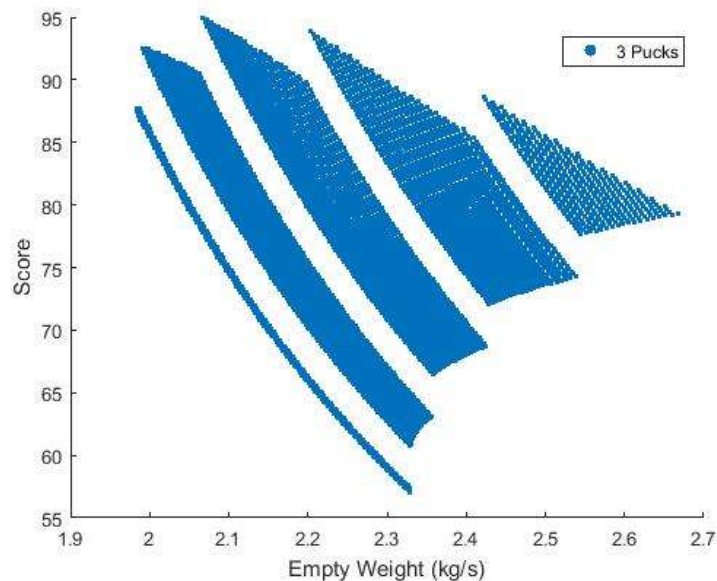
FIGURE 8: THREE PUCK SCORE ANALYSIS

From this plot we can see there is an optimal lap count/airspeed. Up to a certain point, it makes sense to carry a slightly heavier motor/battery in order to fly more laps, but past that points the weight begins to lose you more points than are gained from the additional laps. According to this initial MATLAB estimation, our optimal weight and airspeed would be approximately 1.6 kg at 20 m/s.

Our design work then moved to a more in depth excel sheet where we were able to look more in depth at a specific plane and less at general score trends. The final numbers from this excel sheet were an empty weight of 1.7kg and an airspeed of 21 m/s.

Mission Model

In order to model the mission accurately, the mission was split into five phases - cruise, takeoff, climb, turn, and landing.

Takeoff: Takeoff was a focal point in our design - our stall speed was limited by the hand launch constraint, and so producing as much lift as possible at that speed was crucial.

Climb: In order to reach a safe altitude as determined by the judges at the event, the aircraft will climb for approximately 16 seconds at 10 degrees, reaching an estimated 35 meters above sea level.

Cruise: The cruise speed was determined in order to allow the plane to utilize full throttle, matching the static thrust of the climb phase of the mission, while also completing as many laps as was optimal during the mission.

Turn: Completing the turn phase as quickly as possible would allow us to finish our laps quickly, so fast turns are optimal. We accomplished this by designing to a 60 degree bank angle and 24 meter turn radius. The turn phase also uses maximum thrust.

Aerodynamic Characteristics

Stall Speed Analysis

We made a model of our aircraft using a 1 meter long 2x4 piece of wood to simulate the fuselage with a wooden dowel to represent the wing. We weighted the aircraft to accurately simulate our actual aircraft. We then videoed team members throwing the simulated aircraft several times. We analyzed the videos using the Open Source Physics Tracker educational tool. Using a set reference length and coordinate system, the software tracked the aircraft and calculated things such as length traveled, velocity and acceleration. On average we found the throws were between 10 and 12 meters per second. See figure 6 for a screenshot of the tracker coordinate system overlaid on a video and a velocity vs time graph from the program.

FIGURE 9: STALL SPEED ANALYSIS
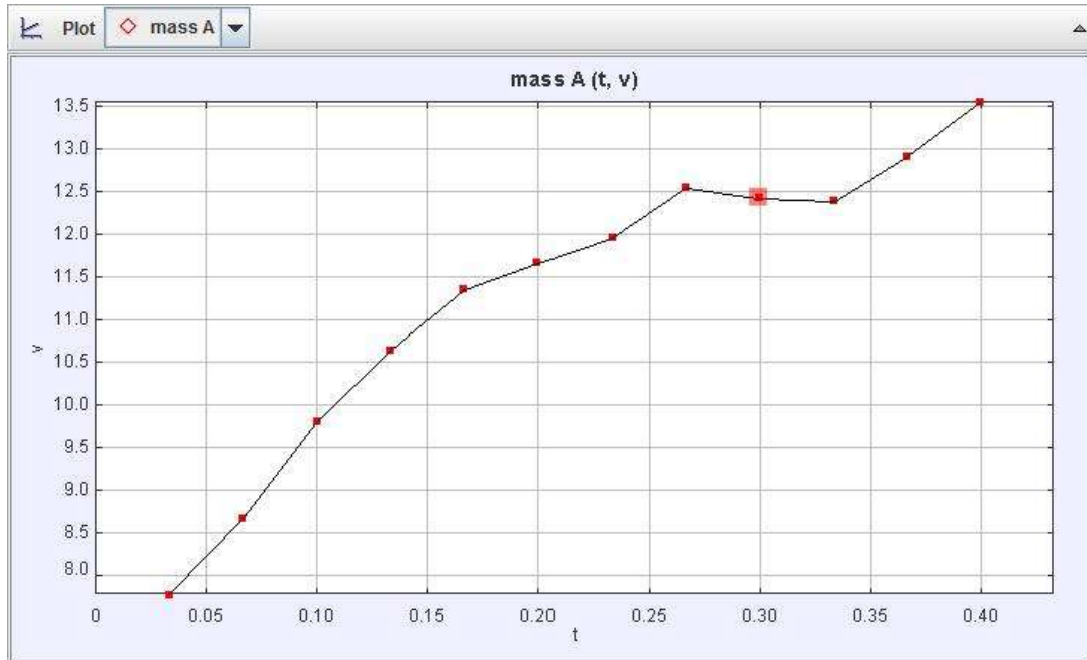
FIGURE 10: ACCELERATION ANALYSIS

Wing Airfoil Selection

The selection of the wing airfoil for this mission posed an interesting problem. It was, therefore, necessary to find an airfoil that had as high a Cl_{max} as possible, but the Cl_{cruise} needed to match up exactly such that the angle of attack was close to zero in cruise. By setting the lift at cruise and the lift at takeoff equal to each other, the following equation relating Cl_{cruise} and Cl_{max} was created.

$$Cl_{cruise}/Cl_{max} = V_{stall}^2/V_{cruise}^2$$

With the stall and cruise speed defined as 9.5 m/s and 21 m/s respectively, the ratio of lift coefficients had to be approximately 0.2.

Additionally, an airfoil with a high lift to drag ratio at cruise and stall was optimal. The higher the lift to drag ratio, the smaller the wing and the lighter the plane would be overall as well as decreasing the size of the motor and battery for the same airspeed.

24

The aerodynamics team was able to analyze multiple airfoils using the UIUC Airfoil Coordinates Database and the XFLR5 program. We were able to narrow down our top three airfoils (Selig-9037, Selig-9000, and Eppler-387) and then proceed with the extensive analysis. Let it be noted that the all airfoils are were increased from their original 9% t/c (thickness to chord ratio) to 12% t/c. We chose t/c to be 12% due to it having more favorable stall characteristics for this mission. For thin airfoils, a serve stall typically occurs at the leading edge (LE) which makes recovery very difficult and almost impossible unless you have a professionally trained pilot. Whereas thicker airfoils typically have a smoother stall at the trailing edge (TE) and can be recovered by an amateur pilot.
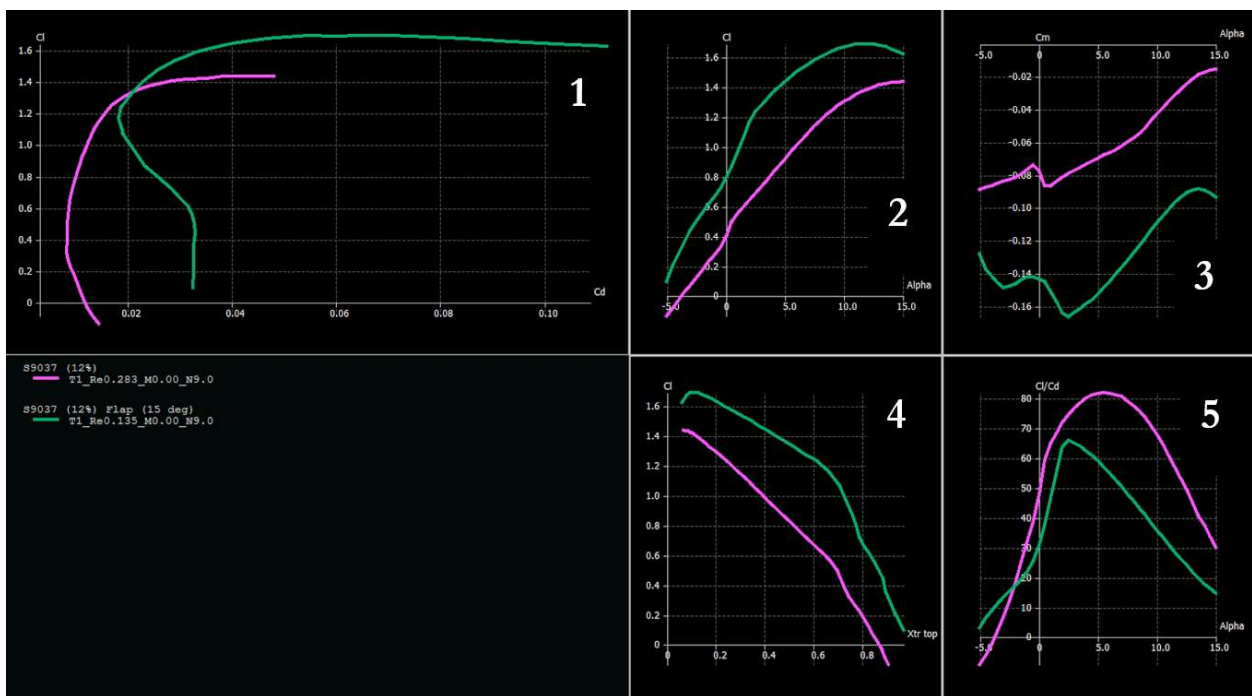
FIGURE 11: SELIG 9037 AERODYNAMIC DATA

Figure X above shows the aerodynamic profile for the Selig-9037 (S9037) airfoil. The plots above Plots above show (1) CL vs CD curve, (2) CL vs alpha, (3) Cm vs alpha, (4) CL vs Xtr top, and (5) L/D vs alpha. This profile included both takeoff (green) and cruise (magenta) conditions. To correctly simulate the cruise and takeoff conditions we needed to find the Reynolds number.

The follow calculation was used to find the Reynolds number at both conditions:

$$Re = (\rho * V * c_{bar})/\mu$$

Where ρ is the density in kg/m^3, c_{bar} is the mean aerodynamic chord of the wing in m, and μ is the air viscosity in N*s/m^2. The density and air viscosity were determined based on the historical weather data from Tucson, AZ during mid-April.

For takeoff condition the Reynolds number was calculated using the stall speed the velocity, and at the cruise condition the Reynolds number was calculated using the cruise speed. The values for ρ, μ, and c_{bar} where the approximately the same for each conditions since we assumed that the difference between takeoff altitude and cruise altitude is negligible. Respectfully, the takeoff Reynolds number and cruise Reynolds number are 134613.36 and 282688.

This process was repeated for the other two airfoils. The Selig-9000 (S9000) profile is shown below in Figure X and following is the Eppler-387 (E387) profile in Figure X.

A comparison of the three airfoils is described in the table below. Reminder that the (%) represents the t/c value. Also, the CL ratio below is based on the Cl_{cruise} of each airfoil at an angle of attack of 0.51 degrees and the max CL at 15 degree flaps for all airfoils. For takeoff we approximated an initial angle of attack of ~10 degrees.

TABLE 4: AIRFOIL COMPARISONS

Wing Airfoil	Cl Ratio	L/D cruise	L/D stall
S9037 (12%)	0.222	45.1	35
S9000 (12%)	0.184	35.7	32
E387 (12%)	0.235	39.8	27

From the table a first look would tell you that the E387 is the best choice, but if examined closely the S9037 airfoil is the optimal pick. The E387 does indeed have a better CL ratio, but the problem with this airfoil is that the stall occurs at a very low angle of attack (6.5 degrees) so it cannot make it to 10 degrees for takeoff whereas the S9037 stalls at 12 degrees, almost double that of the E387. Also the L/D ratio at cruise and stall is substantially better if using the 9037 airfoil. The S9037 had a Cl_{max} of approximately 1.7 at 10 degrees with flaps deployed (15 degrees), and a Cl_{cruise} of 0.378 (No flaps), giving a lift coefficient ratio of 0.222, which meets our initial goal of 0.2.

The plots above for the S9000 show (1) CL vs CD curve, (2) CL vs alpha, (3) Cm vs alpha, (4) CL vs Xtr top, and (5) L/D vs alpha. This profile included both takeoff (green) and cruise (red) conditions.
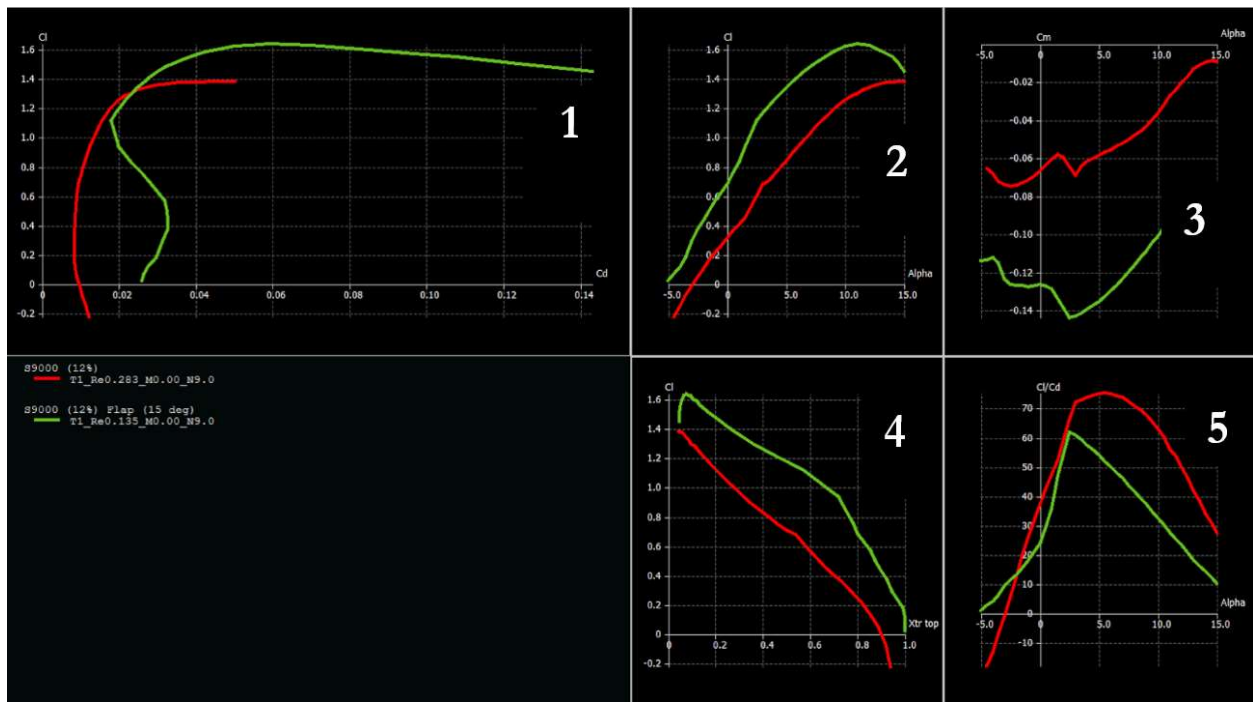
FIGURE 12: SELIG 9000 AERODYNAMIC DATA
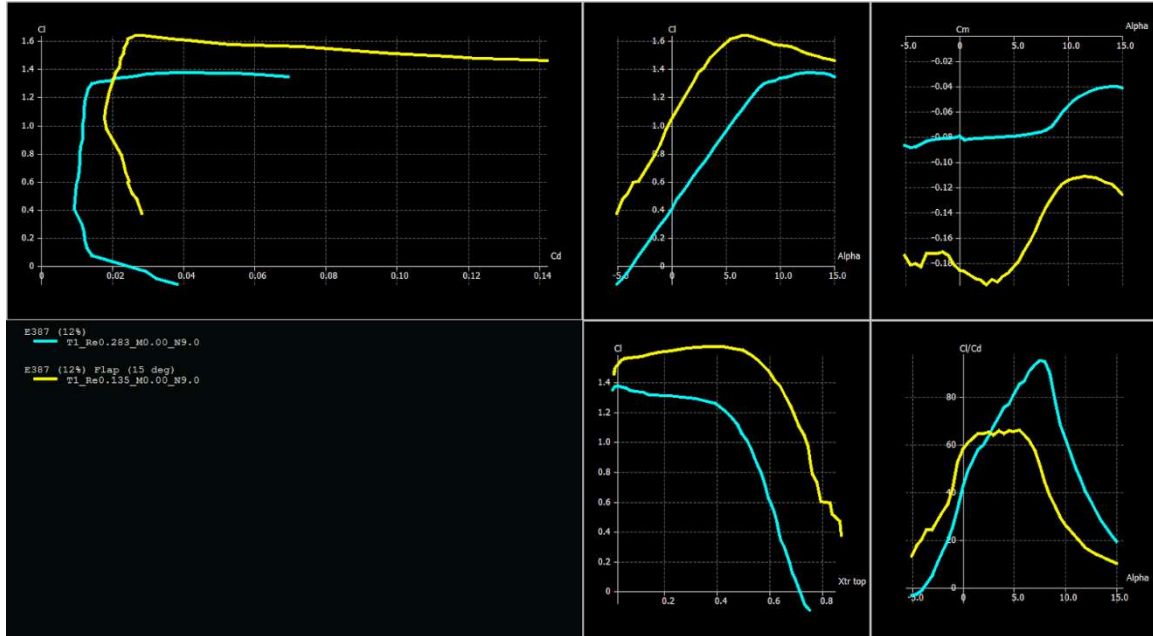
FIGURE 13: EPPLER 387 AERODYNAMIC DATA

The plots above for the E387 show (1) CL vs CD curve, (2) CL vs alpha, (3) Cm vs alpha, (4) CL vs Xtr top, and (5) L/D vs alpha. This profile included both takeoff (yellow) and cruise (aqua) conditions.

With the S9037 airfoil and a wing area of 0.3033m^2, the aircraft generates a minimum of 21.56 N of lift both during cruise and takeoff. This is equal to the weight of the plane. At takeoff we have a much lower speed, but a much higher angle of attack which cancel each other out, leading to equivalent lift. At the higher angle of attack, the thrust is vectored upward adding additional force in the upward direction. Flying at full throttle during both parts of the mission, the dynamic thrust at takeoff is much close to the static thrust of the motor. This additional thrust will be used to allow the aircraft to climb.

The lift being equal in both stages of the mission assumes worst case scenario for the hand launch. From our initial hand launch tests of a plane shaped object weighing approximately 2kg, hand launches varied between 9 and 11 m/s. A lift of 21.56N assumes a stall speed of 9.5 m/s. This is slightly higher than the lower end of our tests, as the plane has a small amount of time to gain speed after leaving the hand. Additionally, multiple hand launches are allowed before the mission is considered a failure, allowing multiple attempts to throw the plane above stall speed.

Tail Airfoil Selection

We chose a symmetric airfoil for the tail for several reasons. (1) It is easy to manufacture, (2) the wing moment can be countered by changing the incident angle on tail instead of using a cambered airfoil without an incident angle, (3) can use the same airfoil for the vertical tail, and (4) the analysis is simplified and less mistakes are made.
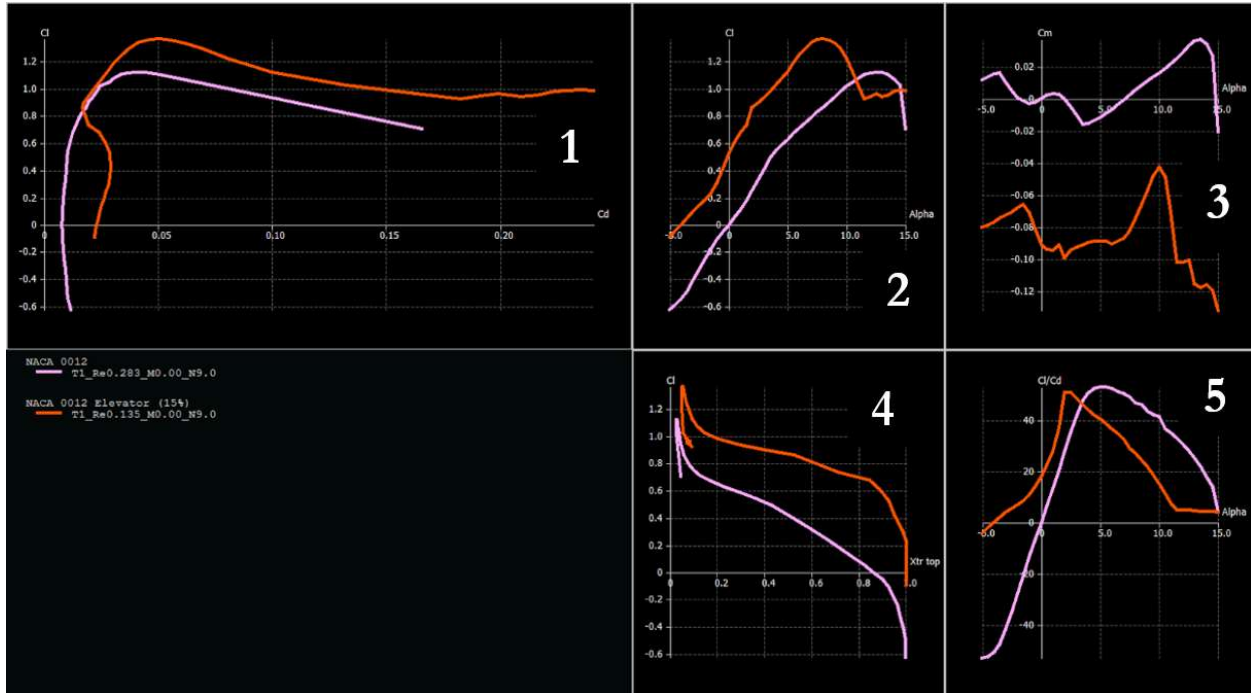
FIGURE 14: NACA 0012 AERODYNAMIC DATA

The tail airfoil we choose was the NACA0012, keeping t/c at 12%. The following plot shows the aerodynamic characteristics of the NACA0012 airfoil. Included in these plots is a Cm versus alpha curve however, the longitudinal stability of the aircraft is outlined in a later section using this NACA0012 airfoil.

The plots above for the NACA0012 show (1) CL vs CD curve, (2) CL vs alpha, (3) Cm vs alpha, (4) CL vs Xtr top, and (5) L/D vs alpha. This profile included both takeoff (orange) and cruise (pink) conditions.

Drag Analysis

In order to estimate drag, four different types of drag were calculated based on estimates of wing and fuselage shape and size.

Skin Friction Drag is drag caused by the friction between a surface and the air passing over it. The skin friction drag was calculated by multiplying the total surface area by the skin friction coefficient and the dynamic pressure. Skin friction drag was estimated to be 0.5738N.

Pressure Drag is caused by turbulent wakes behind objects. The main cause of this kind of drag is the fuselage as it is the least streamlined of all bodies on the aircraft. The fuselage CD was estimated

based on similarly shaped objects, and calculated by multiplying that Cd by the dynamic pressure and the surface area. The pressure drag was estimated to cause 0.0714N of drag.

Induced Drag is a form of drag that is caused by the redirection of airflow around an airfoil. This form of drag is based on the lift coefficient and was calculated to cause 0.2526N of drag.

The parasitic drag of the wing was measured experimentally on a smaller scale and verified using XFLR5. Scaling our fit to the larger plane, we estimated the wing parasitic drag to cause 0.6677N of drag during cruise. These drags totaled together gave us our total maximum drag number of 1.5655N of drag at cruise, and a final lift to drag ratio of 13.8. Because both drag and lift increase with airspeed, a plot of necessary thrust vs airspeed was created.
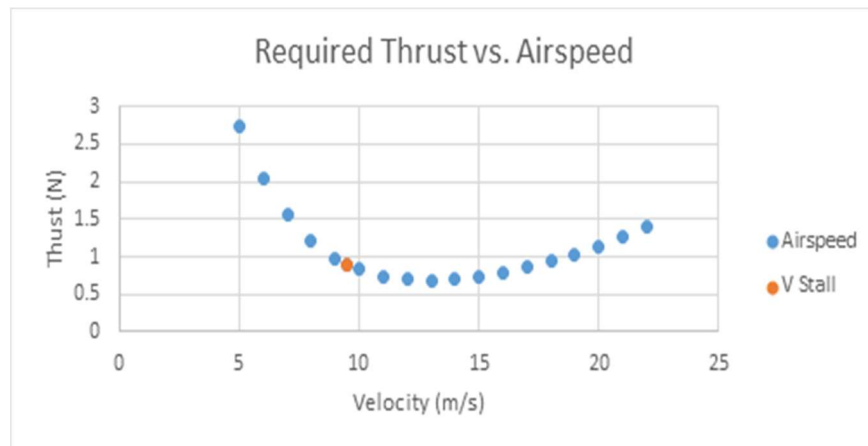
FIGURE 15: REQUIRED THRUST VS. AIRSPEED

Stability and Control

The longitudinal and lateral stability of an aircraft are critical elements of aircraft design. There are two types of stability: static stability and dynamic stability. Static stability is the natural tendency of an aircraft to gain its equilibrium after it is disturbed, and dynamic stability is the tendency of an aircraft to damp out oscillations and return to steady state. Various parameters contribute to the stability of an aircraft, including vertical and horizontal tail ratios, tail distance, and center of gravity location.

The tail distance was confined by the size of the tube we were aiming for, so it was necessary to design for longitudinal stability around that constraint by modifying the center of gravity location, horizontal tail size, and tail incidence angle.

30

Longitudinal stability was achieved around our cruise angle of attack of approximately zero degrees. The moment coefficient vs angle of attack plot is given below.
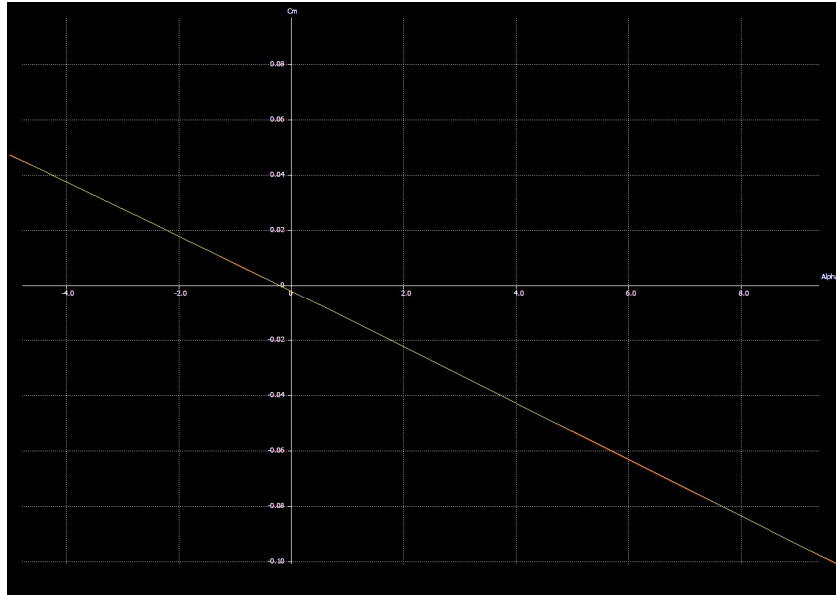
FIGURE 16: LONGITUDINAL STABILITY

In order to calculate dynamic stability of the entire aircraft, stability derivatives were calculated to be as follows:

TABLE 5: LONGITUDINAL STABILITY DERIVATIVES

X_u	-0.015794	C_{xu}	-0.0037559
X_w	0.66281	C_{xa}	0.15762
Z_u	-1.9253	C_{zu}	-0.0001
Z_w	-21.857	C_{La}	5.1978
Z_q	-2.6739	C_{Lq}	7.1447
M_u	2.7e-08	C_{mu}	3.60e-08
M_w	-0.42675	C_{ma}	-0.57014
M_q	-1.0619	C_{mq}	-15.938

TABLE 6: LATERAL STABILITY DERIVATIVES

Y_v	-1.1091	C_{Yb}	-0.26376

Yp	0.053869	CYp	0.014896
Yr	0.89238	CYr	0.24676
Lv	-0.042602	Clb	-0.0058901
Lp	-3.5807	Clp	-0.57566
Lr	0.43914	Clr	0.0706
Nv	0.81172	Cnb	0.11223
Np	-0.25532	Cnp	-0.041047
Nr	-0.65689	Cnr	-0.10561

Using these values, settling times for various modes were estimated. With no control input, the settling time for the Phugoid mode was approximately 135 seconds, while the settling time for the roll convergence mode was 0.86 seconds. We calculated neutral point and static margin (see Table X) to determine the static stability of our aircraft. With a static margin of about 0.2 our aircraft will be somewhat sensitive to control input. Because our CG is adjustable, we will be able to adjust the static margin to reduce sensitivity, and improve flight characteristics during flight testing based on our pilot's preferences.

Neutral Point and Static Margin Calculation to determine Static Stability	
Property	Definition
Static Margin	Neutral Point wrt chord - CG wrt chord
Neutral Point	h_ac+((a_t/a_bar)*V_barH*(1-de/da)
h_ac	aerodynamic center of main wing
a_t	lift curve slope of tail
a_bar	lift curve slope
	a_wb*[1+(a_t/a_wb)*(S_t/S)*(1-de/da)
a_wb	lift curve slope of wing-body
S_t	tail lifting surface
S	main wing lifting surface
de/da	ratio of change in incidence angle and angle of attack
	(4.44*(1-M^2)^(1/2))*(((1/AR)-(1/(1+AR^1.7)))*((10-3*lamda)/7)*((1-(l_battv/b))/((2*lbart/b)^0.33))*(cos(Lamda)))^1.19
M	mach number
	u/342
u	cruise speed
AR	aspect ratio
	b/c_bar
b	wingspan
c_bar	aerodynamic chord
lamda	taper ratio
l_battv	vertical distance between chords
l_bart	distance between 1/4 chords of main wing and tail
Lamda	wing sweep angle
V_barH	horizontal tail volume ratio
	(S_t/S)*(l_bart/c_bar)
Neutral Point	0.355727559
Static Margin	0.2

FIGURE 17: STATIC MARGIN CALCULATIONS

Mission Performance

Using this chart, we were able to plot the thrust as well as the load on the battery over the course of the mission, keeping in mind the mission profile. The first stage of the flight corresponds to take-off (first 12 seconds of flight), followed by a series of cruising periods, and turning periods (up to 258 seconds of flight) where the peak of amperage requirements occurs at the turns. The final stage of the flight is landing (from 258 seconds to 266 seconds of flight).
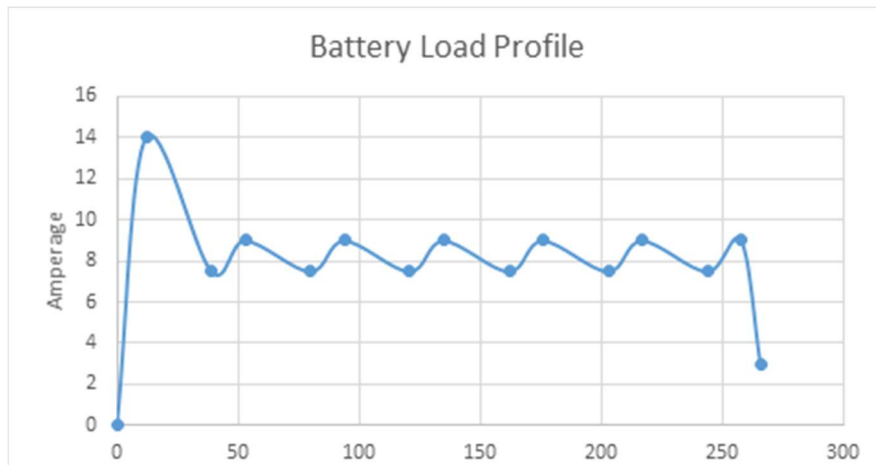
FIGURE 19: BATTERY LOAD PROFILE
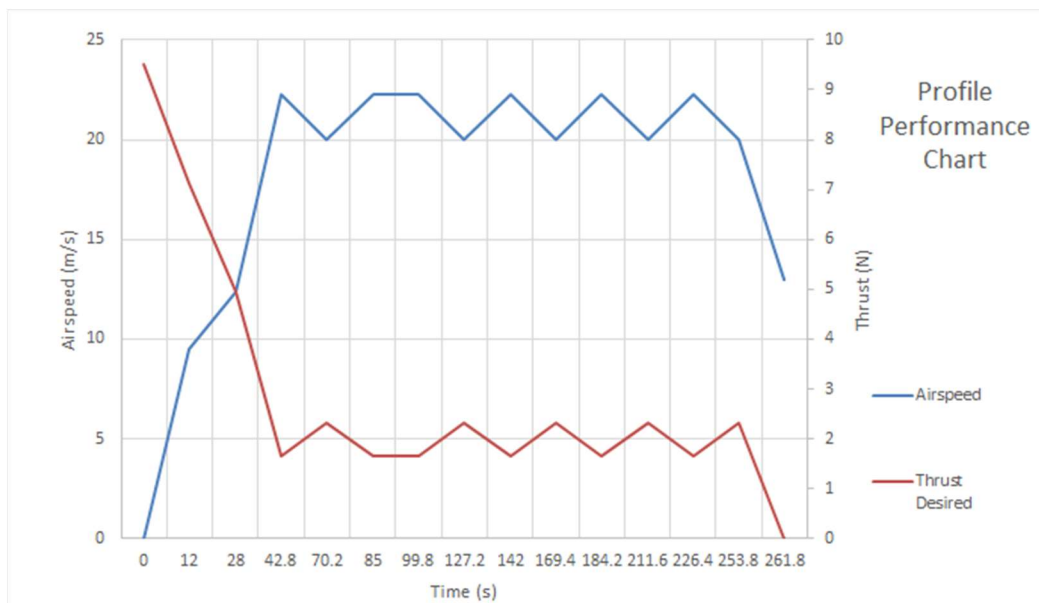
FIGURE 18: BATTERY PERFORMANCE PROFILE

By charting out the entire mission model, including velocity, thrust, and energy required, we were able to predict that our final UAV would be able to fly for the full five minute mission duration and complete six full laps in that allotted time.

TABLE 7: PROPULSION MISSION PERFORMANCE

Input	Cruise	Takeoff	Climb	Turn
Velocity (m/s)	22.2500	9.5000	12.3500	20.0000
Climb Angle (Degree)	X	X	10	2
Bank Angle (degree)	0.0000	0.0000	0.0000	60.0000
Turning Radius (m)	X	X	X	23.5653
Thrust (N)	1.6696	1.4652	4.9473	2.3212
Static Thrust(N)	9.4604	3.9922	8.4647	9.0272
Static Thrust (g)	965.3468	407.3653	863.7431	921.1414
Static Wattage (W)	193.5774	63.1377	163.4542	180.1229
Power (W)	146.0085	60.4753	154.8648	143.9209
Altitude (m)	X	X	35	X
Time (s)	27.3978	12	16.32040218	14.8065
Repeat	6.0000	1	1	6.0000
Energy (J)	24001.8329	725.7035	2527.4563	12785.8066
Current (A)	13.5	5.6	14.3	13.3
Total Time (s)	289.5			
Total Energy (J)	40579			

PRELIMINRY DESIGN

Final Design

Gompei Volanti measures 1.13 meters in length, with a wingspan of 1.7014 meters in the unfolded position. In the folded position, after the tail boom has been retracted and the wings folded, the overall width is reduced to 0.1780 meters, and the length is reduced to 0.8232m.

Structural Characteristics/Capabilities

Most parts of the aircraft were built out of a carbon fiber composite material, with some parts being reinforced with foam for additional rigidity. This material was chosen for its high strength, ease of manufacturing and lightweight. It was discovered early in manufacturing that the carbon fiber composite was too flexible for certain structurally important parts of the aircraft, and therefore had to be reinforced with ⅛" foam.

The wings made of this carbon fiber composite, and strengthened with a spar at the quarter chord and ribs placed throughout the wing, proved strong enough to sustain the design wing loading of 7.74 kg/m^2.

Most joints used in the folding wing and tail were machined out of aluminum in order to prevent a catastrophic failure during flight. These parts are also not easily replaceable, as they were glued to the wing. The large surface area at the attachment point ensured a secure gluing site, but make it impossible to replace a wing joint without replacing at least one of the wing panels it is attached to. Additionally, if the joint buckled under the wing loading during flight, the failure would not be recoverable and the plane would inevitably crash.
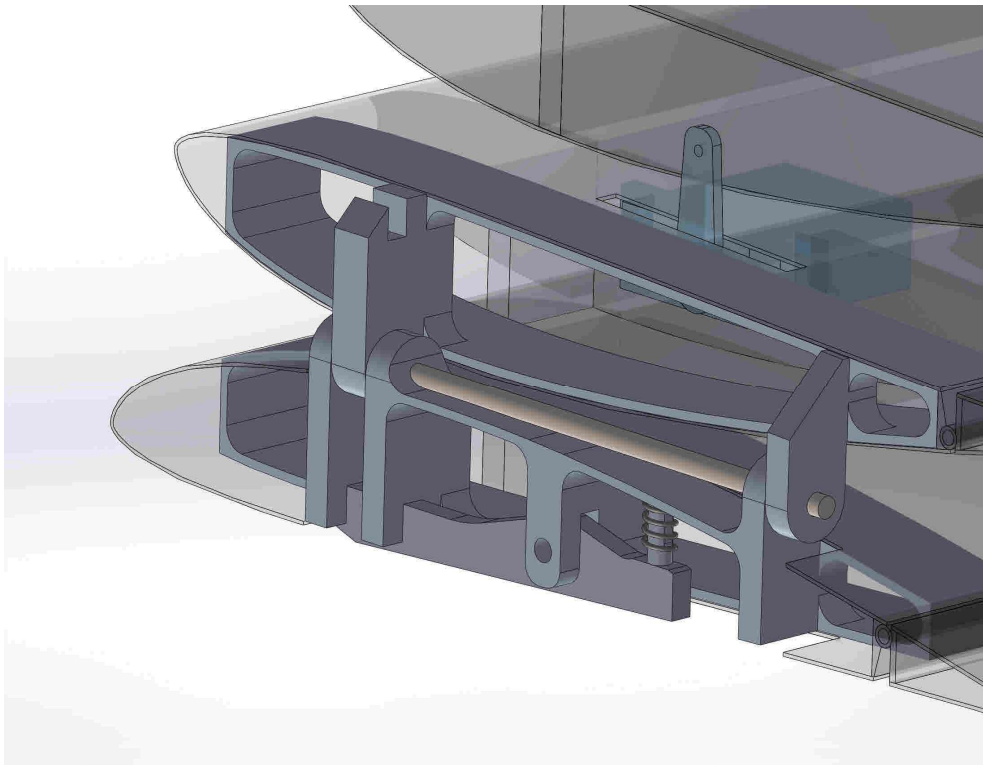
FIGURE 20: WING FOLDING MECHANISM

System and Subsystem Design/Selection/Integration

The main systems considered when designing the plane were the propulsion and control systems. For the propulsion system, it was critical that we selected the system including the motor, battery, and propeller. The system was designed to match the mission profile that was determined to give the optimal score.

Motor Selection

There are basic types of electric motors in the market: brushless and brushed. The brushed motors generate a relatively big amount of heat due to the large internal resistance and require the user to change the brush after a certain time of usage, also the output power of brushed motor is smaller than the brushless one for the waste of electric energy in generating heat. The brushless motor can provide higher output power with little heat generation. Based on the comparison above, our selection is the brushless motor.

There are two divisions of brushless motors: out-runner and in-runner. In-runner motor can provide higher RPM value but with low torque. On the other hand, the out-runner motor provides lower RPM value with a higher torque. Since the aircraft is designed to carry hockey pucks as payload and need to start the flight with a high acceleration, we chose to use the out-runner brushless electric motor.

According to the discussion above, the two motors we first chose are AXI 2820 and E-flite Park 480. The detailed specifications of these two motors are listed in the table below.

TABLE 8: MOTOR

Park 480		AXI 2820/12	
KV	1020	KV	990
Current	22A	Current	22A
Max Current	28A For 15s	Max Current	45A For 15s
Max Power	400W	Max Power	650W
Battery	6 to 10 cell (NiMH)	Battery	8 to 14 cell (NiMH)
Propeller	10x7–12x6	Propeller	10x7–12x6

Weight	87g	Weight	151g

The Park 480 has a lighter weight and a lower maximum power, while the AXI 2820 has a heavier weight and a higher maximum power. We did a series of performance tests (Detailed Design) to determine which motor to use.

Since the Park 480 has a higher KV value, which suggests that it can increase more RPM with per volt added, it will be more sensitive to the voltage raised of the battery pack. After doing a series of wind tunnel tests, we found out that the performances of these two motor are compatible to each other, so we chose the Park 480 as the motor to use due to the lighter weight. We decided to choose E-flite 30-Amp Pro as the corresponding ESC.

Propeller Selection

The decision of propeller selection depends on the corresponding motor and battery. We first set a range of propeller based on the specifications of the two motors listed in Table 2: from 10*7 to 12*6. The aircraft we designed can be folded into a tube, so that we decided to use folding propeller for the folding convenience. The final selection is Aeronaut CAM Folding Propellers. This series of propellers are made of carbon fiber, which have higher strength and a light weight.

Battery Pack Selection

According to the competition rules, we are only allowed to use either Nickel–metal hydride battery (NiMH) battery or Nickel–cadmium (NiCad) battery. We decided to use the NiMH battery since the NiCad is generally heavier and has the memory effect, which will cause the lower battery charged capacity. Since the aircraft has a high current draw during each mission, we looked for the NiMH battery that has a higher C rating, which is the parameter that indicates the amount of continuous current draw the battery cell can support. Based on the current estimation in Table 1, our desired battery cell should handle the current up to 25 amp with a safety factor of 1.8.

We did a massive research on NiMH battery cell and created a database of different cells with specifications. We concluded from the database that the energy and the weight of the battery cell follow a linear relationship, which is shown in the figure below.
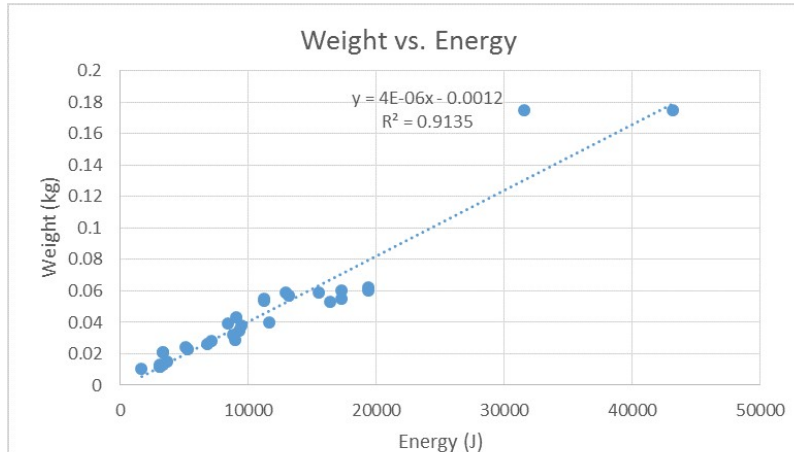
FIGURE 21: BATTERY COMPARISON

TABLE 9: BATTERY WEIGHT ESTIMATION

Battery Weight Estimation			
Input		**Output**	
Safety Factor (#)	2	**Energy (J)**	81157.35403
Number of cells in Series (#)	9	**Weight(kg)**	0.3389
Constant (kg/J)	4.18E-06	**Voltage (V)**	10.8
		Capacity in mAH	2087.380505

We chose the safety factor to be 2 since there will be many unpredicted factors affect this theoretical estimation. Based on this estimation, we chose several cells to do deeper research.

Cell	Capacity (mAH)	Number of Cell	Voltage (V)	Weight (g)
XCell X2/3A 1600	1600	1	1.2	22
ELITE 2100	2100	1	1.2	32.8
ELITE 1700	1700	1	1.2	28.3

| Sanyo HR-45AU | 2150 | 1 | 1.2 | 35 |
| Sanyo HR-AAU | 1650 | 1 | 1.2 | 28 |

TABLE 10: MOTOR SPECIFICATIONS COMPARISON

We prefer the aircraft to have excessive energy by the end of the mission instead of running out of power, so that we choose the Elite 2100 as the battery cell due to its large capacity and high discharge rate.

Elite 2100 Pack	
Size	4/5A
Cell Weight (g)	32.8
Number of Cells	9
Pack Weight	300 g
Capacity (mAH)	2100
Discharge Rate (A)	30

FIGURE 22: MOTOR AND BATTERY SELECTION

Electronic Speed Control (ESC) Selection

We chose ESC for propulsion based on the current data we got from the wind tunnel test (Performance Results). The highest current value recorded during the test is 16.4 amps. Accounting for safety factor, we narrowed the range of ESC to those from 25 amp to 30 amp. Our selection is E-flite 30A Pro Switch Mode for the light weight as well as it is the same brand as the motor, which can provide us a higher compatibility during actual performance.

TABLE 11: PROPULSION SYSTEM selection

Propulsion System	
Battery Cell	Elite 2100mAH 4/5A
Number of Cells	9
ESC	E-flite 30A Pro Switch Mode ESC
Propeller	11*7 Aeronaut Folding Propeller
Motor	E-flite Park 480

Control System

Control systems were also of critical importance as the flaps being in the up position is critical to a successful launch. Post launch, the plane was designed so that a failure in the control systems would allow the plane to slowly lose speed and glide to the ground. Seven servos were used to actuate various control surfaces over the body of the aircraft, including flaps, ailerons, elevators and a rudder. The servos were connected to the receiver by wire through the inside of the plane, either down the wing span or up through the tail boom, and connected to their respective control surfaces with a servo arm. The motor and all servos were programmed to match the fail-safe mode during loss of transmit signal. The fail-safe position is as follows: throttle closed, full up elevator, full right rudder, full right aileron, and full flaps down.

Weight and Balance

The final aircraft weighed 2.3455 kilograms, slightly over our initial estimate. The center of mass is located 14 centimeters behind the nose of the wing, or approximately 7 centimeters behind the leading edge of the wing. This point is slightly ahead of the neutral point of 8 centimeters behind the leading edge.

Sub-assemby	Function	Component	No. Components	CG distance from x = 0 (mm)	Weight (N)	Moment (N*mm)
Fuselage				208.76	12.0047913	2506.120232
	Structures	Fuselage Shell	1			
	Tail Harness	Pull Ring	1			
		Bushing	2			
	Payload	Pucks	3			
	Main Wing Joint	Internally Threaded Shoulder	1			
		Lock Groove	1			
		Washer	1			
		Screw	1			
	Propulsion	Prop Battery Pack	1			
		Motor	1			
		Spinner	1			
		Prop Blade	2			
	Controls	Reciever Battery	1			
		ESC	1			
		Controls Battery Pack	1			
Main Wings				340.74	9.080136	3093.965541
	Structures	Ribs	14			
	2nd Wing Joint	Machined Component Inner	2			
		Machined Component Outer	2			
		Rod	2			
		Compression Spring	2			
		Catch	2			
	Main Wing Joint	Pull Ring Retracting Plunger	1			
	Controls	Ailerons	3			
		Aileron Joint - Tube	13			
		Servos	3			
		Servo Horn	3			
Tail				848.42	2.3178087	1966.475257
	Structures	Tail Boom	1			
		Tail Rib	6			
	Tail Harness	Tail Bushing	1			
	Tail Joint	C-channel	2			
		Hinge Plate	4			
		Elevator Joint - Tube	2			
		Conical Compression Spring	2			
	Rudder	Symmetric Airfoil	1			
	Elevator	Symmetric Airfoil	2			
	Controls	Servos	3			
		Servo Horns	3			
				Total:	23.402736	7566.56103

CG = 323.3195054
CG wrt chord = 0.355727559

TABLE 12: WEIGHT AND BALANCE

Rated Aircraft Cost (RAC)

The Rated Aircraft Cost (RAC) was then calculated, using the equation given in the rules statement. Again, $RAC = (EmptyWeightmax + TubeWeight) * (Le \quad + Circumference$. Therefore, the RAC of our aircraft was 3.04 kilogram-meters.

Mission and Flight Performance

We performed battery-motor-propeller test and decided optimal selection accordingly. The figure shown below is the performance results in the wind tunnel.
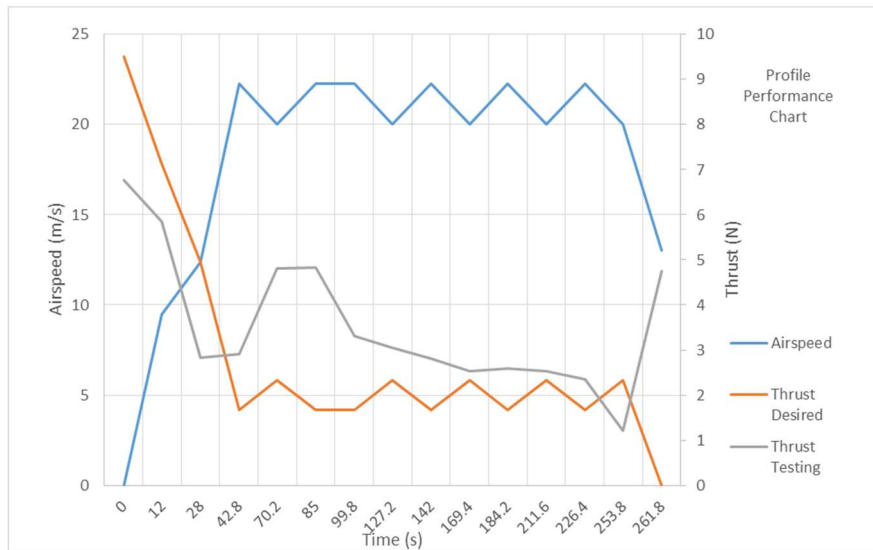
FIGURE 23: MISSION AND FLIGHT PERFORMANCE

After analyzing the data, we determined that the recommended combination of motor, propeller, and battery should be the E-flite Park 480 motor, with an 11*7 propeller, and a battery pack of nine 1.2V, 2100mAh cells rated for 30A continuous current draw.

With the propulsion confirmed we were able to finalize our flight parameters. Outlined in the table below is the determined flight characteristics.

Clmax	1.59
Clcruise	0.3014
Airspeed	21.15 m/s

Cruise Angle of Attack	0.51 degrees
Lift	21.68 N
Drag	1.5655 N
Vstall	9.5 m/s

TABLE 13: KEY PERFORMANCE PARAMETERS

Based on these parameters, the aircraft will be able to carry three hockey pucks and fly for five minutes, completing a maximum of six laps for Mission 3.

Drawing Package
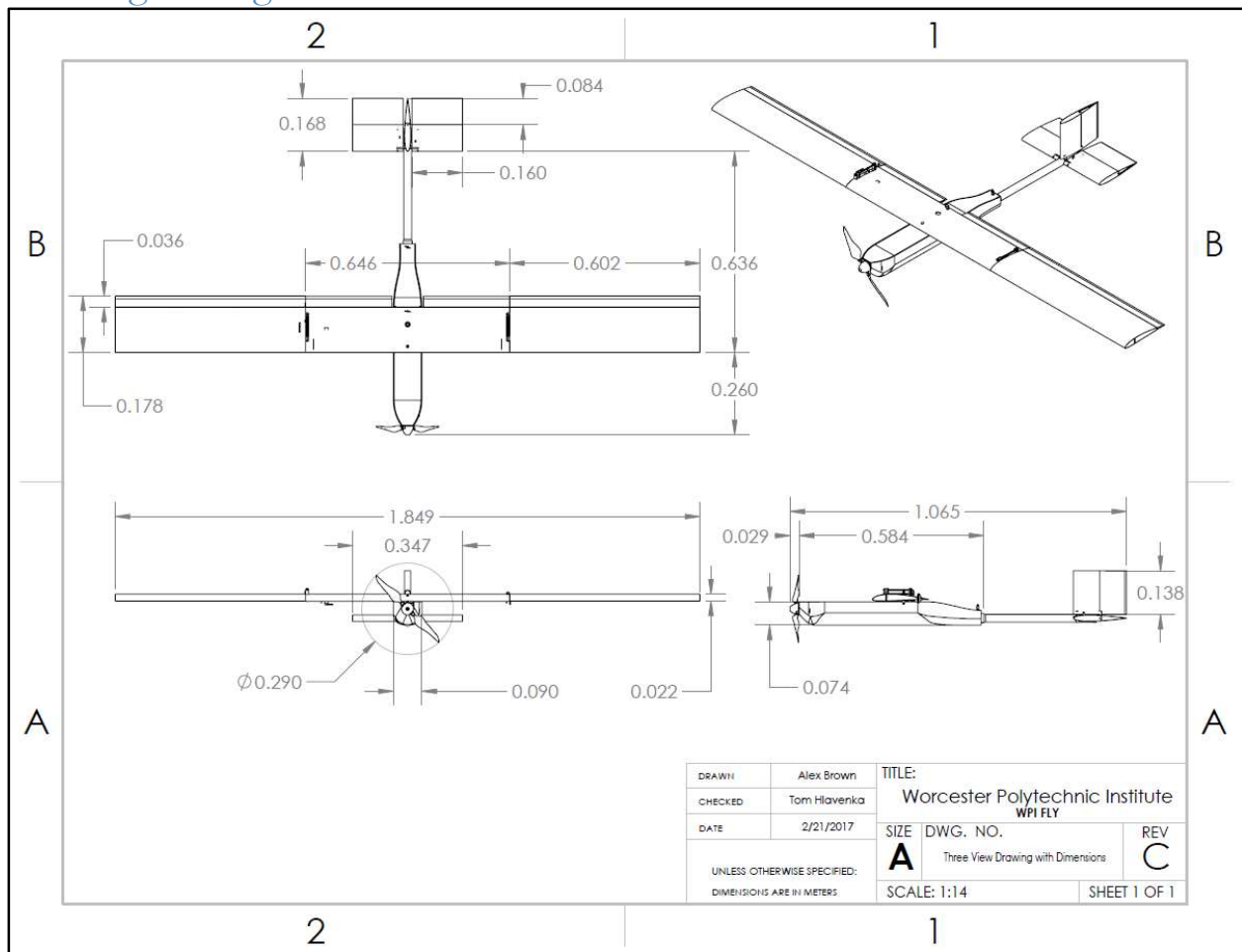
FIGURE 24: THREE VIEW CAD MODEL
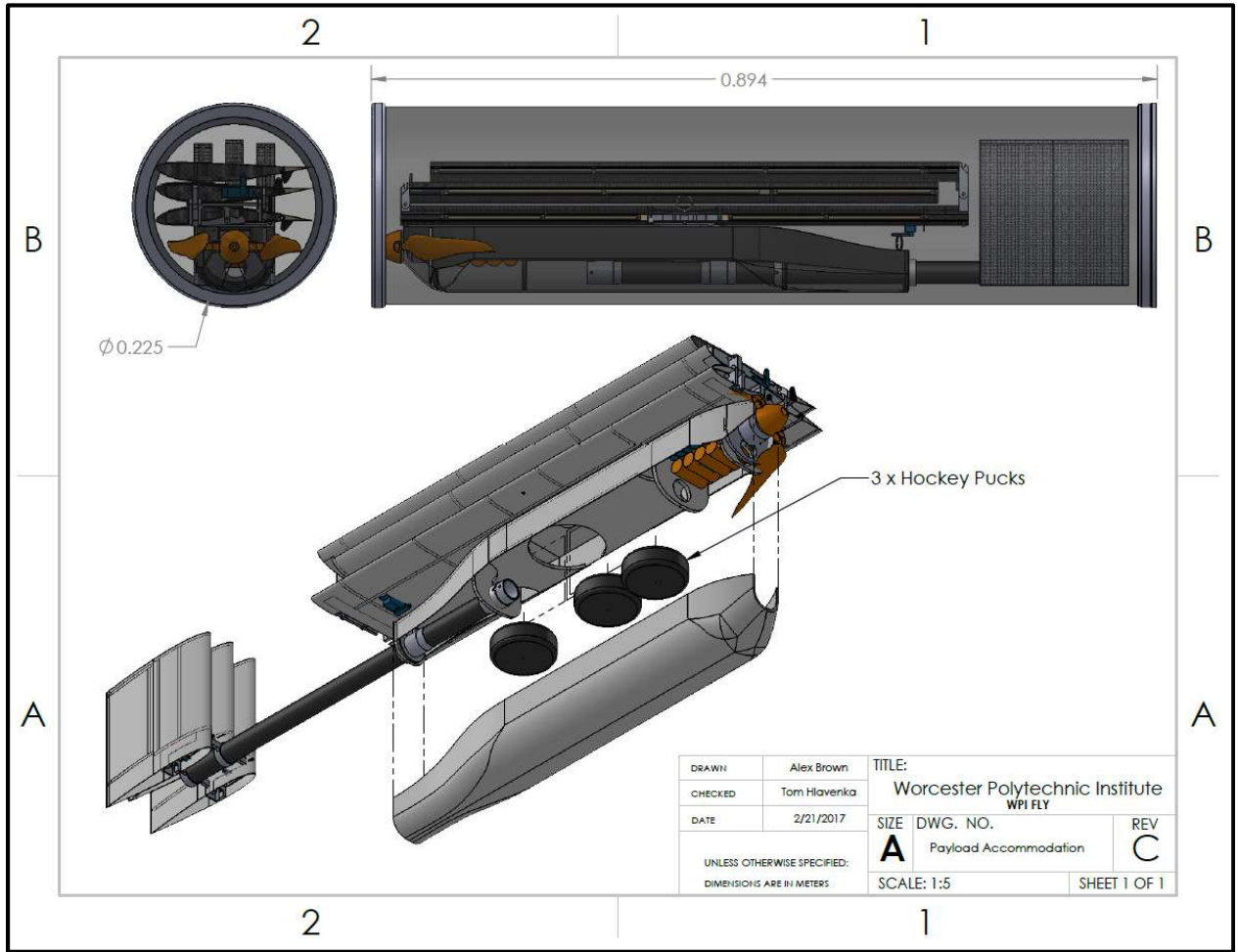
FIGURE 25: STRUCTURAL ARRANGEMENT CAD MODEL

Components

Item	Quantity	Name	Description
1	2	Propeller Blade	Aeronaut 12 x 6
2	1	Spinner	Aeronaut Turbo 40 mm
3	1	Motor	T-Motor AS2820 800 KV
4	1	Main Battery	10 Cell NiMH 2100 mAh
5	1	Receiver Battery	5 Cell NiMH 400 mAh
6	1	Speed Control	Spider 40A ESC
7	1	Receiver	Spectrum AR 6260
8	3	Flap / Aileron Servo	HS-5070MH
9	3	Elevator/ Rudder Servo	HS-5070MH

Joints

Item	Description
A	Right Wing Joint
B	Left Wing Joint
C	Rotating Wing Joint
D	Telescoping Tail Boom
E	Tail Joint

DRAWN	Alex Brown	TITLE:
CHECKED	Tom Hlavenka	Worcester Polytechnic Institute
DATE	2/21/2017	WPI FLY

SIZE A DWG. NO. Systems Layout Drawing REV C

UNLESS OTHERWISE SPECIFIED: DIMENSIONS ARE IN METERS

SCALE: 1:8 SHEET 1 OF 1

FIGURE 26: SYSTEMS LAYOUT CAD MODEL
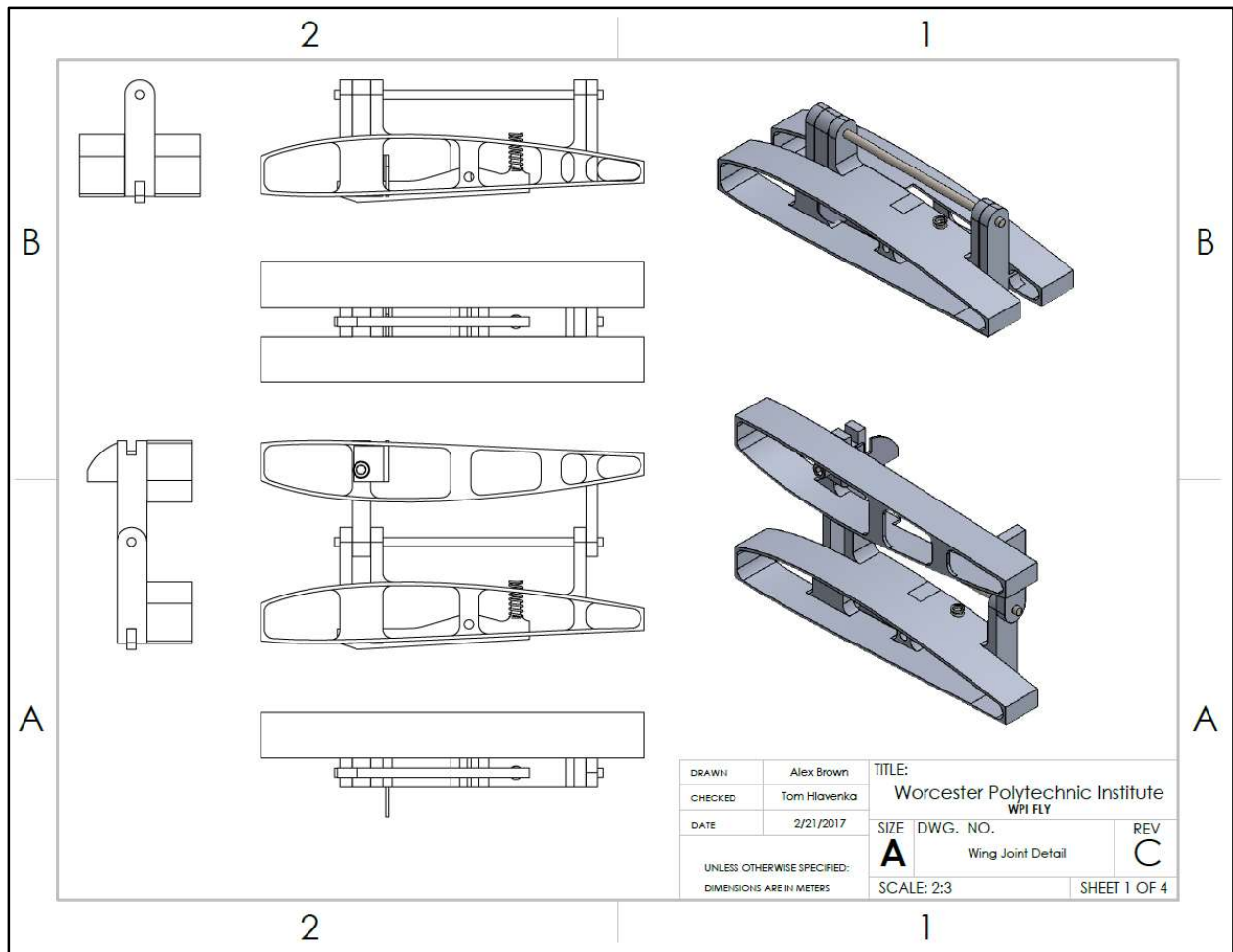
FIGURE 27: WING JOINTS CAD MODEL

MANUFACTURING PLAN AND PROCESSES

Investigated Manufacturing Processes

The goal in manufacturing was to design the lightest weight UAV with a high lift-to-drag ratio that maintains structural integrity and stability while meeting the mission goals. To do this, our goals were to (1) identify the material with the highest strength-to-weight ratio that is within our manufacturing capability, (2) create a design that minimizes weight and induced drag while being sufficiently stable and strong to withstand the forces and moment on the UAV, and (3) optimize the volume usage of the tube with connections, such as pivots and hinges. We also created a list of secondary goals for risk mitigation measures, which included land-ability, simplicity, and component repair-ability.

Our first tests were conducted on small samples. These tests found that two layers of 3K 2x2 weave carbon fiber held sufficient strength and was light enough for the skin of our aircraft. We then conducted secondary tests on wing samples to determine how well our evaluation of the strength-to-weight ratio of the material translates to that of the component. The torsional rigidity test proved that our initial results would be sufficient for the UAV. Finally, we built and conducted tertiary tests on the UAV as a whole. These tests included ground testing, drop testing both in the tube and fully assembled outside of the tube, and flight tests.

Selected Manufacturing Process
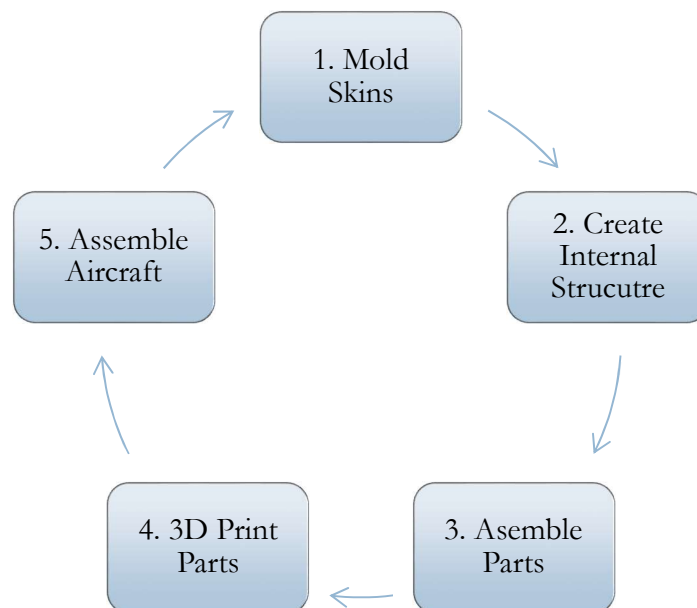
FIGURE 28: MANUFACTURING CYCLE

After much research and analysis of material weight vs. strength, we selected a range of Carbon Fiber based composites as the material of choice for both the skin and structural components of the aircraft. Vacuum-bagging was selected as the ideal technique to mold the composite as the necessary resources were readily available to us and several members of the team had experience with the technique. Extensive testing was done to analyze the benefits of various weaves of carbon fiber. Using the chart below, different weaves of carbon fiber were selected for different parts of the aircraft, based on required strength. Generally, the lightest carbon fiber that was rigid and strong enough to maintain structural integrity was chosen for each part of the UAV.

We used three-quarter inch thick layers of MDF built up to the necessary thickness to create each of the mold blocks for our parts. From there, we machined three separate mold sections based off our CAD model of the UAV: a wing section, the fuselage, and a tail section. Once each mold was machined, we sanded them down and finished them with Epoxy Sealing and Finishing Resin to ensure a perfectly smooth finish for the mold.

Each mold section was created by cutting out the appropriately sized piece of carbon fiber or fiberglass cloth, impregnating it with the epoxy resin and layering it into the mold. An average of two layers of Carbon fiber or fiberglass cloth were used per mold to maximize the strength to weight ratio of the part. From there, the vacuum bag was placed over it and the part was put into an enclave set at 115°F to cure for fourteen hours.

For the folding hinges in the tail and wing, the team chose to use 3D printed parts from a Markforged Mark Two Rapid Prototyping Machine. The Mark Two has a double filament head and primarily prints a nylon plastic in various user chosen densities. The MarkTwo has a second print head that allows the user to add a second filament of either fiberglass, Kevlar, or carbon fiber to reinforce the part. After evaluating several sample parts, the team decided to print the folding wing joints, the folding tail joint assembly, and the rotating wing pivot using a 50% nylon density, reinforced with carbon fiber in critical areas to ensure structural strength. The 3D printed parts were compared to aluminum parts and the aluminum parts were ultimately chosen because of their ideal relative strength to weight ratio and ease of construction. A second set of backup aluminum joints were created in the case of failures.

Each of the six separate wing skins were glued to the various hinges and reinforced with spars created from a Carbon fiber- 1/8" foam core composite "club sandwich" to create the three folding wing sections. The wing sections were set on the main fuselage body using a pivot on a spring to keep the wing flush with the fuselage. An aluminum plate was attached to the top of the fuselage to ensure that the locking mechanism functioned properly, and to provide extra support for the lock post. The six separate tail skins were set into three separate tail sections using the same club sandwich and attached to the folding assembly, which was then glued into the end of the retractable boom. Finally, the collapsing boom was secured into its track in the main fuselage body. Finally the wiring, electrical, and mechanical components were inserted.

Once the structural adhesive was entirely dry, the ground test was performed to ensure that all components were correctly assembled and functional for flight tests.

Manufacturing Milestones
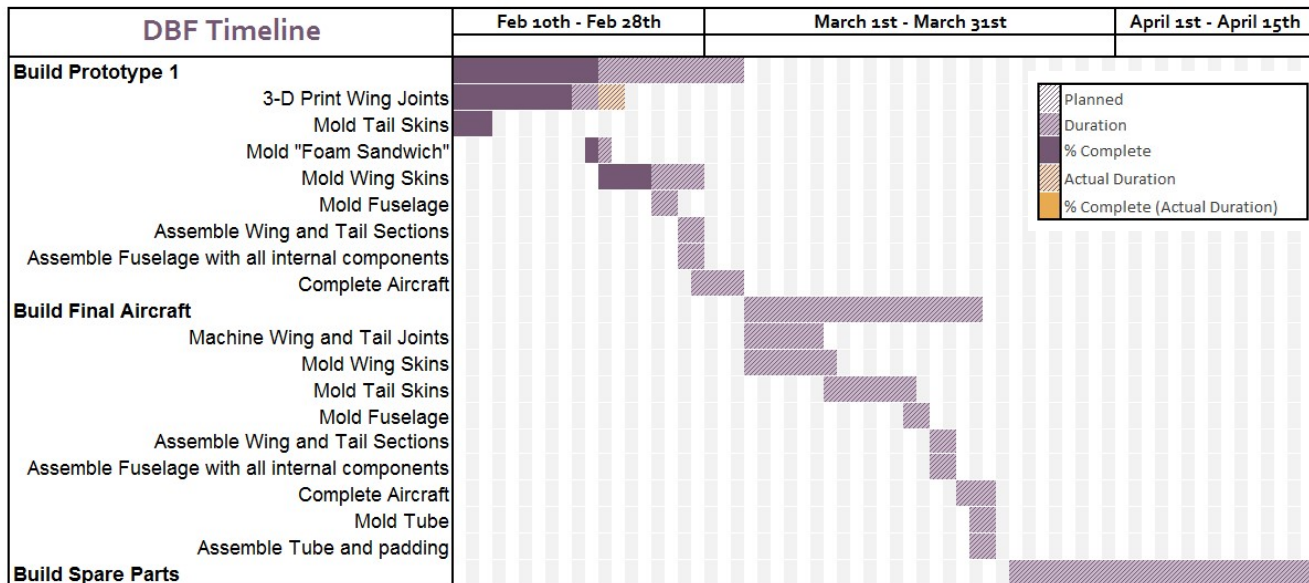
FIGURE 29: MANUFACTURING TIMELINE

The manufacturing team carefully outlined the timeline up through the complete assemble of the plane. Considering the extended time needed for creating composites the schedule is very aggressive.

Manufacturing Composites

1. **Critical Materials**

   a. Glue

   b. MDF

   c. Milling Bits

   d. CNC Mill

   e. Mold Finishing Epoxy

   f. Sandpaper

   g. Mold release wax

   h. Composite fiber

   i. Epoxy resin and Hardener

   j. Epoxy measuring tools

   k. Epoxy container

   l. Spreader

   m. Peel Ply

   n. Release Film

   o. Breather

   p. Vacuum Bag

   q. Sealing Tape

   r. Sealing Plate

   s. Oven

   t. Vacuum Pump

   u. Vacuum fittings

2. **Critical Skills**

   a. SolidWorks

   b. Esprit (or other CAM Software)

   c. HAAS Machine Tool Operation

    d.   Epoxy-Mold Finishing, Sanding

    e.   Vacuum bagging, Composite Layup

3. **Process Order**

    a.   Select General Plane Configuration

    b.   Overall part Geometry and shape and Size requirements

    c.   Create a model of the finished part in Solid works

    d.   Create a model of a mold for the finished part

    e.   Acquire the milling bits required to machine mold geometry within reasonable tolerance.

    f.   Glue together a MDF block from which the mold can be machined.

    g.   Create CAM for the Mold,

    h.   Schedule machine time, Machine the mold

    i.   Epoxy finish, and sand the machined Mold

    j.   Apply wax, Laminate Layup and Vacuum Bag

    k.   Oven Cure

    l.   Remove part from mold, remove films and cut to size

    m. Clean Mold and Sealing Plate

Manufacturing Aluminum Joints

1. **Critical Materials**

    a.   Aluminum Stock

    b.   3-d Printer

    c.   Manual Milling Machine

    d.   Manual Lathe

    e.   CNC-Mill

    f.   Tooling

2. **Critical Skills**

    a.   SolidWorks

    b. Stress Analysis

    c. Machining

    d. HAAS Machine Tool Operation

    e. Esprit (Or other CAM Software)

3. **Process Order**

    a. Select General Plan Configuration

    b. Select Specific Joint Type and Location

    c. Define Attachment Geometry & Method

       i. Wing Skin Thickness and Profile (Glue)

       ii. Tail Skin Thickness and Profile (Glue)

       iii. Tail Boom Cross Section and Diameter (Glue)

       iv. Fuselage Component Placement and Attachment Points (Screws)

       v. Servo Location and Servo Geometry (Screws)

    d. Calculate Stresses and refine Joint Geometry for Different Materials

       i. Flight and Test Loads

          1. Glue Surface Area

          2. Pin Diameter and Material

          3. Critical Joint Cross Sections

    e. Select Locking Mechanism

       i. Un-lock when subject to extreme loading

       ii. Likely Failure Modes

       iii. Compliance or Looseness

       iv. Self-Locking Mechanism

       v. Stress-Geometry Considerations

    f. Design Joint Concept and Refinement for Manufacturability

       i. 3-d Printed

          1. Part Orientation

          2. Reinforcement Type and Location

3. Wall Thickness

4. Print-Support Removability

    ii. Aluminum Parts

        1. Milling Fixtures

        2. Origin Location

        3. Stock Size & Geometry

        4. Part Orientation

        5. Depth of Cut Limits

        6. Minimum Wall Thickness

        7. Milling Bit Radius

        8. Tool Clearance

        9. Tool Entry

        10. Post-CNC Machining Operations

g. Manufacturing

    i. 3-d Printed Parts

        1. Set up a meeting with WPI Academic and Research Computing (ARC) to communicate part orientation, reinforcement, density, color, and select the appropriate printer.

    ii. Aluminum Parts

        1. Acquire Stock

        2. Square Stock ends for repeatable Zeroing

        3. Develop CAM

        4. Acquire necessary bits and tooling

        5. Schedule machine time and machine parts

In order to design the joints that allow our aircraft to fold to fit into a small tube, the location of these joints, the way which they folded and the size of related components had to be determined. Although it was tempting to delay concept work on joints until this geometry had been solidified, it would have set the project behind so current best estimates were used to start the design of the joints. Stress

calculations were integrated into the "Design Spreadsheet" so design updates would automatically update stress calculations, and redefine joint geometry. Bending moment and Shear loads were calculated at the Folding Wing Joint for both the wing and the tail. This moment was then used to estimate the forces which the latch, and hinge pin on the wing joint would be subjected. It was found that an approximate force of 303N in shear would be present at the glue interface in the joint during a wing-tip test. The stresses on the hinge pin, and pin bearing surfaces were substantial in that the yield strength of the pin was exceeded for some materials if the pin were 3mm in diameter. Carbon Fiber, and ABS pins of such small diameter were determined to be definitely unsafe. Steel or Aluminum pins would be necessary for the wing joint to maintain a reasonable safety factor. These stresses revealed the magnitude of force to expect on the latching mechanism. In order for a robust latch to be created in a 3-d printed material with inferior strength properties it was believed that a pin-in a hole type latch would be necessary to provide the necessary stiffness without making the joint bigger or heavier. An aluminum latching mechanism would be strong enough, and small enough, and produced to fine enough tolerances that more convenient spring-latch in single- shear could be utilized without raising strength, stiffness, weight, or size concerns.

Aircraft Dimensions Calculater			
Vertical Tail Height	0.1682	Distance From Wingtip to Joint	0.5602
Vertical Tail chord	0.1639	Shear force at Joint (N)	11.5138
Vertical Tail AR	1.0267	Moment at Joint (N-M)	6.4497
Wing Space	0.5602	Distance Between Pins	0.0162
Tail Space	0.2327	Pin Diamater (m)	0.003
Space between Wing Rudder	0.0689	Pin Length in Contact (m)	0.004
Distance To Pivot from Back of Fusalage	0.5128	Pin Area	0.0000
Wing Panel Length	0.5602	Number of Pin Areas in Shear	1
Center Chord	0.1769	Pin Y Shear Stress	1.629E+06
Outer Chord	0.1769	Pin Y Shear Force	1.151E+01
Wing Percent Thickness	0.12	Pin X Shear Force	3.975E+02
Center Thickness	0.0212	Pin X Shear Stress	5.623E+07
Outer Thickness	0.0212	Pin Shear Stress	5.625E+07
Length to center of hinge right	0.0212	Pin Shear Force (N)	3.976E+02
Length to center of hinge left	0.0318	Area of Pin Seat	1.200E-05
Hinge top Thickness	0.005	Stress on Pin Seat	3.313E+07
Hinge Height Low	0.0262	Area of Pin Holder	2.800E-05
Hinge Height High	0.0368	Stress on Pin Holder	1.420E+07
Tail Percent Thickness	0.0900	Shear Strength of Epoxy (Wipe, Sand,Wipe)	3450000
Elevater Chord	0.1639	Force on Glue Area	303.84
Elevater Span	0.2530	Glue Area Needed	1.761E-04
Elevater Thickness	0.0147	Saftey Factor for Glue	2.00
Rudder Thickness	0.0147	Area in mm^2	176.14
Material	Density	Shear Strength	Yield Strength
Aluminum 6061	2700	207000000	310000000
Steel A36	8050	266250000	355000000
Carbon Fiber (Unidirectional, Protruded)	1550	41300000	1650000000
ABS-Plastic	1600	31500000	42000000
Material	Pin Saftey Margin (Stress/Stress)	Seat Saftey Margin	n Holder Saftey Marg
Aluminum 6061	3.7	9.4	21.8
Steel A36	4.7	10.7	25.0
Carbon Fiber (Unidirectional, Protruded)	0.7	49.8	2.9
ABS-Plastic	0.6	1.3	2.2

FIGURE 30: SECTION OF THE MAV DESIGN SPREADSHEET DEVOTED TO STRESS AND DIMENSION CALCULATION

The geometry of the wing joint necessitated an airfoil-shaped glue bonding area where the joint could be glued to the load-carrying wing skin. The joints also had to make accommodations for aileron- and flap servos, while positioning the wing-hinge location properly so the wing could fold.

Both a 3-d printed and aluminum part were designed. Both parts were manufactured, and attempts were made to get both 3-d printed and aluminum joints into a functional state.

3-d printed parts were designed and manufactured first, because they had fewer manufacturability design restrictions and it was perceived that there would not be difficulty having the parts printed. The first design had too thin a wall, and the printer filament did not bond properly to adjacent filaments. Fiber reinforcement was also only available in walls printed in plane with a vertical thickness exceeding 2 mm and a width of more than 4 mm. A second version of the 3-d printed parts was designed taking into account these new design restrictions, while also incorporating a mounting location for the servo. When finished, the 3-d printed part without servos weighed (X) grams and even after a couple days tinkering, the joint could not be made to self-latch. Surface finish was poor, and hole alignment issues made it difficult for a small spring to push the latching pin through the latching-hole even when the holes were drilled to a larger size.
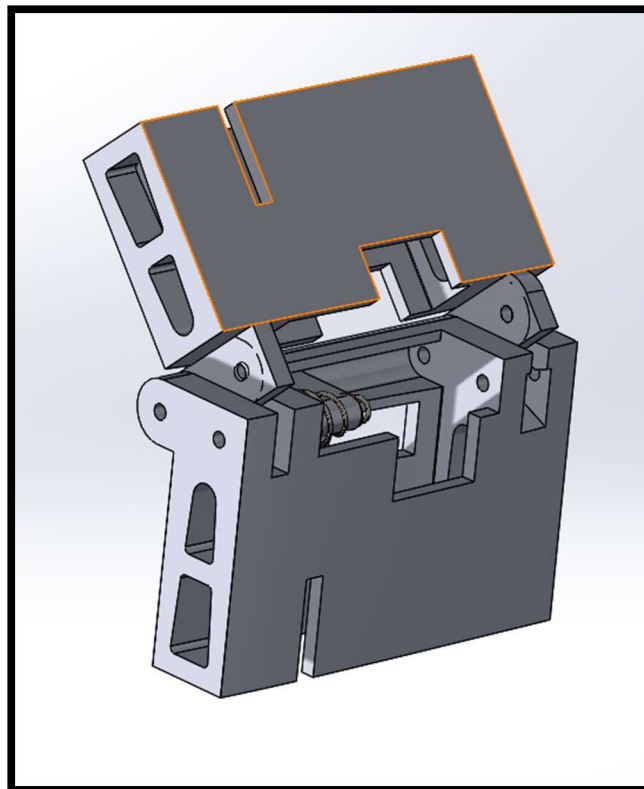
FIGURE 31: SOLIDWORKS FOR A 3-D PRINTED WING JOINT

Ultimately 3-d printed parts proved to take a long time to produce, they were expensive as our parts required carbon reinforcement to meet stiffness and strength requirements, and the precision and finish of the resulting parts was ultimately poor.

Aluminum joints were designed and manufactured when it was beginning to become apparent that 3-d printed joints were not capable of delivering the performance we demanded. Ultimately both joints had similar geometry, however wall thickness and glue surface area could be reduced due to the greater strength, and better glue adhesion of aluminum. The joints were designed around a minimum wall thickness of 1.27 mm however machining mistakes and experience would later show that thinner walled parts (down to about 0.5 mm) were definitely viable if carefully machined and designed.

After the Haas machine tools on campus were used to carve the joints general structure, holes were drilled for pivot pins, and slots were cut for the latching arm using a manual mill in the Higgins machine shop. Performing these operations in a CNC mill was possible however no CNC mills could be easily configured to mill the holes and slots we needed as a result it was easier to perform these operations by hand.
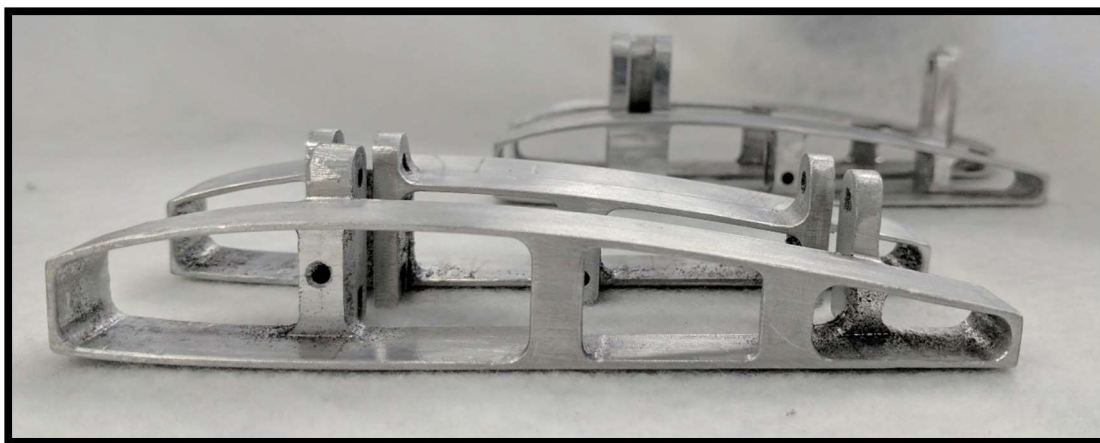
FIGURE 32: ALUMINUM WING JOINT PIECES UNASSEMBLED BUT OTHERWISE FINISHED

To fixture the joints while they were being machined it was decided that machining the thin walled parts out of a larger aluminum block and leaving behind tangs that supported the part would be easiest.

Creating specialized fixtures to hold the parts as they were machined was simply a complexity which we wanted to avoid, and the additional wasted material was not a concern due to our low production volume. Not having extensive machining experience, or experience making CNC toolpaths meant that we were already facing a significant manufacturing learning curve, so we pushed ahead with manufacturing methods we thought were easiest.
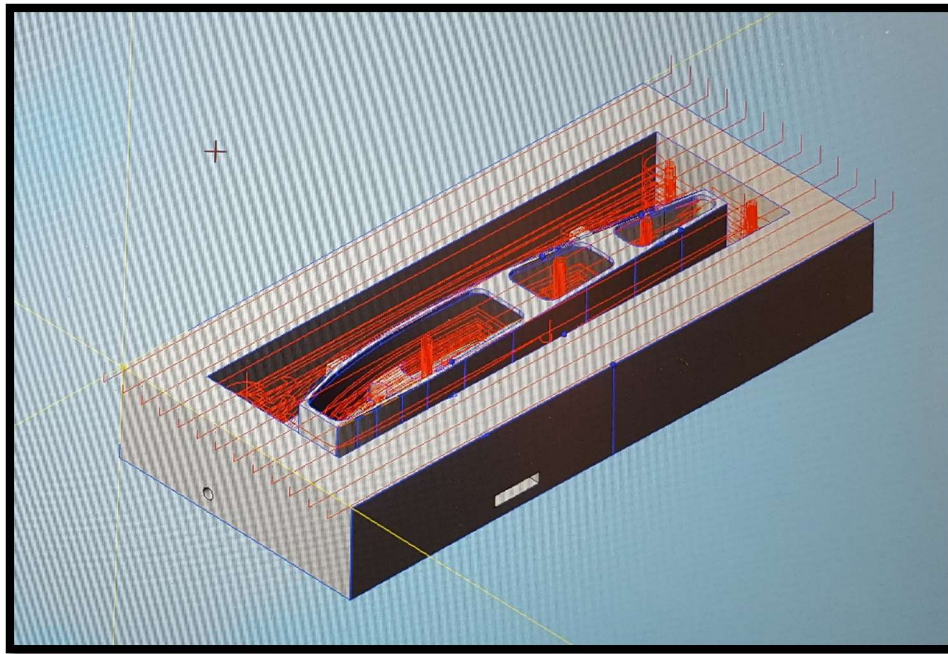
FIGURE 33: TOOLPATHS CREATED IN ESPRIT FOR ONE SIDE OF A WING JOINT

Initially servo mounts were not integrated into the design for fear that servo mounting geometry would impossible to machine. The second version of the wing joints which was ultimately manufactured but not integrated into an aircraft integrally mounted the two wing ailerons. Aluminum servo mounting plates were ultimately glued to the first set of joints, imitating a fully machined servo mount to provide a sturdy, accessible, and aerodynamic mounting location for servos.

 Tail loads were found to be exceptionally low, (only a 9N shear force on the joint-wing seam was predicted at cruise speed) and other tail loads were also so low such that a 3-mm pin of any material would technically be strong enough, however it was deemed prudent to make the structure stronger rather than weaker to help prevent damage in the event of a crash and a steel pin material was selected.

Tail Joint Stress	
Lift from Half of Elevater (n)	1.1040
Tail Cl	0.2000
Moment	0.0997
Force at joint	9.9749

It was also desirable to integrate servos into the tail joint as creating hard-servo mounting points in our prototype aircraft had proven difficult and non-aerodynamic. Changes to elevator and rudder control surfaces that occurred through flight testing meant the tail servos were larger than initially planned, although they a tight fit it was possible for them to fit inside the wing. Again a 3-d printed and aluminum joint set was devised. These early designs, although partially integrated into the prototype fiberglass aircraft, proved to be insufficiently engineered as they were either too heavy, or lacking the necessary functions.
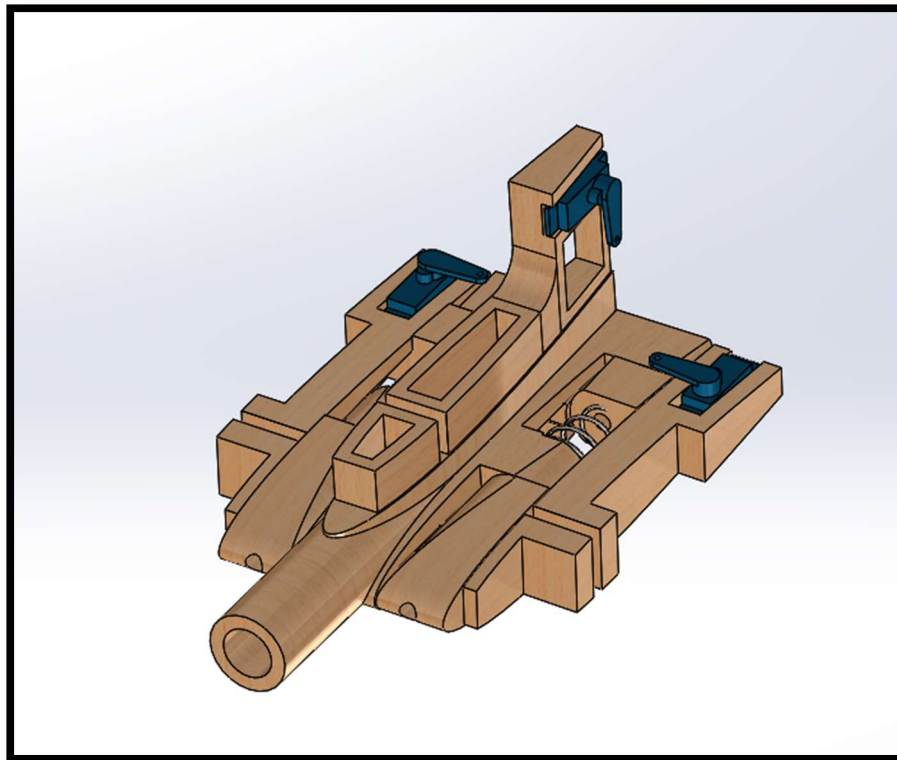
FIGURE 34: SOLIDWORKS MODEL OF A 3-D PRINTED TAIL JOINT ASSEMBLY

After the successful implementation, and manufacturing of an aluminum wing joint, the tail joint was redesigned to incorporate lessons learned. Larger servos were integrated, and wholly machined aluminum joints were designed. Due to the low aerodynamic forces on the tail it was decided to use a sliding-locking joint where the horizontal tail surface would be pulled forward to unlock, and rotated into the stowed position. To lock from the stowed position, the horizontal tail mere had to be rotated to the horizontal position and a spring would push it into a locked, horizontal state. This type of locking mechanism eliminated the need to machine a "Latch" in addition to the mounting components, this ultimately saved weight. Although this type of sliding latch might have had a tendency to have more play, the tails low aspect ratio ultimately meant that the small amount of compliance was not cause for concern. After the joints had been completed, the amount of compliance was significantly lower than expected. All aluminum tail components were machined out of one block of stock, as we primarily had one size stock available, and each of the pieces was relatively small.
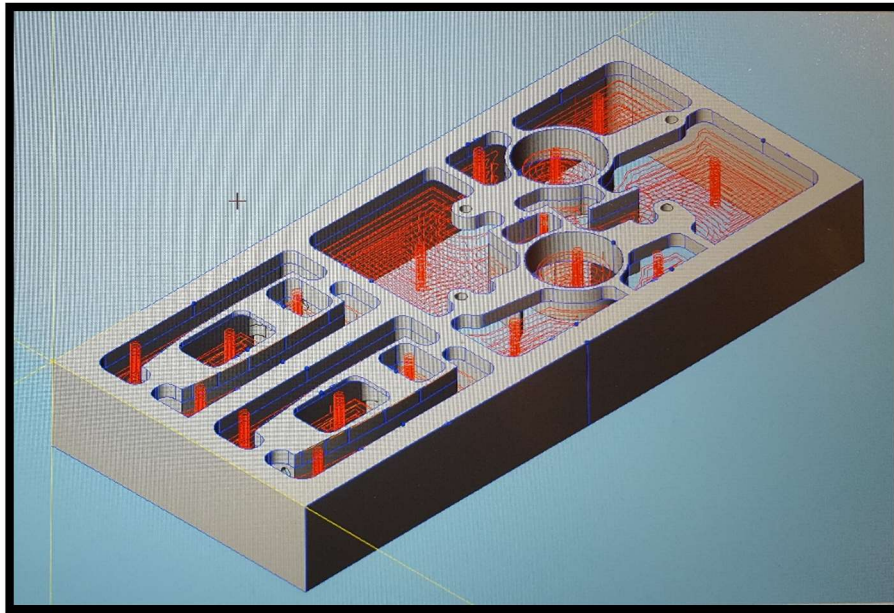
FIGURE 35: MACHINE TOOL PATH CREATED IN ESPRIT FOR THE MACHINED TAIL PIECES

After the aluminum tail joints pieces had been machined, and attempted to be fitted together, we realized some of the radii which were necessarily present after machining interfered with the joints function. Using hand files, clearance was created and the joints were made to function.   Due to the small space, the forward and aft portion of the pivot pin had to be separated, as it would otherwise interfere with

placement of the elevator servos. Available servo clearance was minimal even after the pivot pin was trimmed; mounting tail servos was not always a straightforward task. Due to the speed of design, it was not noticed that a counter-rotating set of servos would be required to actuate the independently servo controlled left and right elevator. Modifying a servo for counter-clockwise was possible, but a cause for a short 24 hour setback which may have been avoidable if this requirement noticed earlier. Although using all clock-wise actuated servos would have been ideal, symmetric design was convenient, aerodynamic and counter-clockwise HS-5070MH servos of the same specification are available commercially.

FIGURE 36: FINISHED BUT UN-ASSEMBLED ALUMINUM TAIL JOINT PIECES

The Tail Boom

The tail boom was based around a protruded carbon tube with an OD of 25 mm. To guarantee a snug close fit between the bushings and the tube, aluminum sleeves were fitted to the carbon tube so corresponding aluminum bushings could fit with minimal play. These aluminum sleeves also provided additional strength for the locking pin, and reinforcement where the tail boom entered the fuselage.

The aluminum sleeves were first turned to the exact ID and approximate OD, then they were glued to a length of carbon tube, and finally remounted on a lathe and turned down to their final outside diameter. It was necessary to create a plug that fit the ID of the tube so the tail boom and its corresponding aluminum sleeves could be mounted on the lathe without crushing the tube. Dissipating

the heat generated by turning was also necessary. As there was not a significantly thermal mass near the cutting region the tail boom/bushings heated up very quickly softening the glue holding them in place. Blowing a stream of compressed air over the part as it was turned proved to be an adequate, and clean way to cool the part as it was turned to its final OD on a manual lathe. Creating the bushings attached to the aircraft fuselage was a similar process to creating the tube-sleeve blanks. A final step was required to mill excess material away where the locking pin screwed into the rearmost bushing.

The Wing Rotating Joint

Initially the wings rotating joint was planned to be a shoulder bolt which fitted into a 3-d printed wing substructure. Although this method of construction was utilized in the prototype in combination with a Dual-Loc pad, it ultimately proved to be inadequate because servo wires needed to be routed from the wing into the fuselage. There was no easy way to modify the 3-d printed part to allow the passage of servo wires. At the time this problem had been realized a solution was needed quickly so an aluminum part was designed and machined. The 3-D printed part was also about as heavy as the finished aluminum rotating joint. Instead, a large aluminum bearing surface, bushings, and washer were machined out of a square, airfoil profiled block. The large center opening provided plentiful rom for servo wires and the large bearing area provided plentiful stiffness between the wing and fuselage. This joint was originally intended to be locked with a pull ring pin like the tail boom. This method of locking provided a way for the joint to cam out of position in the event of drag due to earth. This proved effective and useful on multiple flights.
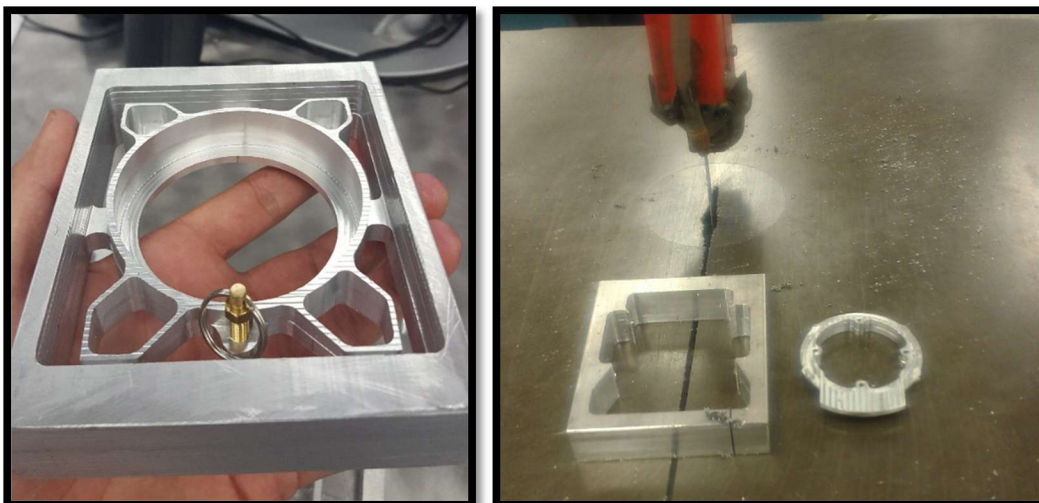
FIGURE 37: POST-CNC ROTATING WING JOINT SECTIONS

Test Plan

Ground Tests

The aircraft will undergo extensive testing once it is built. A "wingtip test" will be performed to ensure that the aircraft is statically stable. The aircraft will be placed on fulcrums at each end of the wing, to ensure that the center of gravity lies within the wing chord to ensure a statically stable aircraft.

Other ground tests will be conducted once the aircraft is built. Our aircraft relies extensively on folding and locking mechanisms designed and manufactured by the team. The folding mechanisms will be folded and unfolded many times to ensure continuous smooth operation. The locks will be subjected to forces that will simulate the forces encountered in flight. This will be conducted in a similar way to the wing twist tests already conducted. An asymmetrical load will be applied to the wingtip, with the hinge in place to be sure that it will hold. Our pivot will be designed to twist under high forces in a crash, as a safety mechanism to prevent the wing from breaking completely in the event of a crash. This will be tested by making sure the pivot can twist at a higher load when the locking pin is in place.

Once we are sure that all the folding and locking mechanisms are operational, the propulsion and control systems will be installed. First, the control servos, battery and receiver will be installed, and connected to each other. The control surfaces will be connected and adjusted to make sure they are properly aligned. Then the control deflections will be measured and compared to theoretical and simulated values. Once the control system is installed, the propulsion system will be installed and run through its paces to make sure it will function properly within our aircraft. Once all components are installed, the drop test from the competition will be performed on our aircraft.

Flight Tests

After those ground tests, we will proceed to flight tests. Before each flight test we will make sure to follow our preflight checklist. First we will perform several glide tests, to test the launch velocity of our aircraft and to perfect the technique for the running launch. These will be conducted in a grassy area, near a hill to allow for maximum glide range. Once we are certain we will be able to successfully launch,

glide, and recover the aircraft, we will perform several controlled glides, ensuring that our control system is capable of controlling our aircraft in flight. Once controlled glide tests are completed, we will test the propulsion system and begin powered flights.

Our powered flight tests will consist of two stages: developmental testing and operational testing. Most flight testing is done with these two stages. Developmental testing works according to the design specifications of the aircraft, and begins as the aircraft is being built. All of the testing done so far falls under the category of developmental testing. This stage ensures that the aircraft is safe to operate and identifies its safe operational limits. This is done by "pushing the envelope" and seeing what conditions the aircraft can still be controlled under. The aircraft will be tested first for roll, pitch and yaw control, and then those actions will be combined as the aircraft is put into turns, climbs and descents in short order.

Operational testing is done to ensure that the aircraft can perform the mission it is designed for. Our aircraft will fly each mission from the competition several times to ensure that it can fully complete each of these missions with each payload that it is capable of carrying. Once we are sure the aircraft can perform each mission, we will start trying to optimize and improve its performance. We will see how well our aircraft can perform in the competition by timing our missions and calculating the overall score for the aircraft we have built. Once we have a baseline score for our aircraft, we will be able to optimize the performance of our aircraft through continuous flight practice.

Test and Flight Checklist

Flight Test Goals

1. Ensure aircraft generates enough lift to take off and sustain flight
2. Ensure propulsion system generates enough thrust to accelerate to and sustain flight speeds for the required amount of time
3. Check rudder operation
4. Check elevator operation
5. Check aileron operation
6. Check flaps operation

7. Ensure aircraft can carry the required payload

8. Ensure the aircraft can fly for 5 minutes

9. Check top speed of aircraft

10. Check stall speed of aircraft

11. Check turn radius of aircraft

12. Fly all three missions for the competition

13. Optimize flight performance

14. Ensure fail safe mode works

Preflight Checklist

1. Assemble the aircraft

2. Ensure that safety/kill switch is set to "OFF"

3. Do a visual inspection of the structure, flight surfaces, and propulsion system to check for damage

4. Check the charge of the remote control battery

5. Check the charge of the main battery

6. Connect main battery to propulsion system

7. Check charge of control system battery

8. Connect control system battery to the control system

9. Check that all flight and control surfaces are locked in proper place

10. Check battery and servo connections again

11. Turn safety "ON"

12. Turn the remote control "ON" to low power

13. Check that the remote control is linked to the receiver on the aircraft

14. Test the control surface movements

15. Turn the remote control "ON" to full power

16. Walk 50-100ft away from the plane, and manipulate the control surfaces to do a range test on the controller

17. Anchor the plane to the ground or a test stand and rev the engine up to full power to test propulsion system

18. Aircraft is ready to fly

After step 11, if any problems are encountered, set the safety to "OFF" and fix the problem. If the problem is fixed within 10 minutes restart checklist from step 11, if the fix takes longer restart from step 1.

PERFORMANCE RESULTS

Subsystem and System Performance

Before manufacturing can begin, it is necessary to test all subsystems to ensure that they will meet the design requirements during flight. These subsystems included structural, propulsion, and aerodynamic tests.

Propulsion Testing

Before using the folding propeller to test, we performed wind tunnel testing for the regular propellers with both Park 480 and AXI 2820. After determining the requirements for the flights, and the preliminary motors, and propeller combinations, we performed wind tunnel tests to determine the best combination for the flight missions. The wind tunnel tests were performed in a lever arm rig, designed specifically to measure the thrust at different air speeds. Besides the thrust, voltage, amperage, and temperature readings were taken. The drag of the rig was measured and accounted for in the final calculations.

The wind tunnel temperature for all the tests was controlled and maintained at 69 degrees Fahrenheit. The following plots represent how power, static thrust, and current draw varied with air speed.
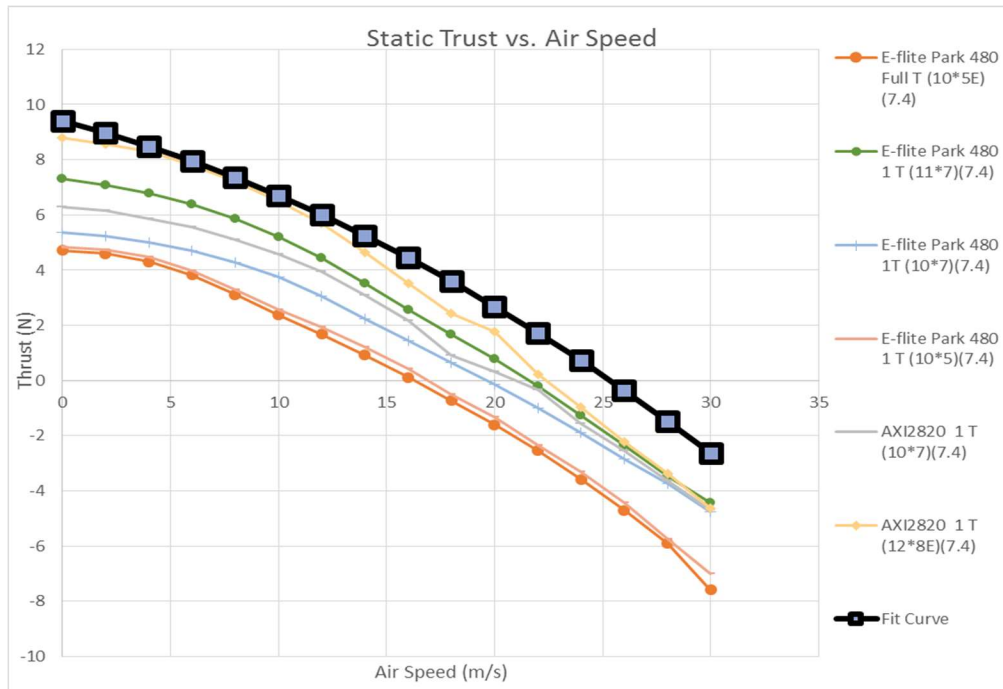
FIGURE 38: STATIC THRUST

The results shown gave us a better understand of how the static thrust was related to dynamic thrust. We created the fit curve shown above to estimate how much static thrust we need from a motor-propeller combination to achieve the required dynamic thrust. Based on the flight profile, the maximum thrust we need is 9.46 N. The first term in the legend indicates the motor used, and the second terms indicates how much the throttle on the controller was placed, and the third term is the propeller used, and the last term is the supply voltage of the battery. We also created similar figures for power. The fit curve for the power figure is set to 194W, which is the same as the highest power required in the flight profile. The wind tunnel set-up and the other testing results are also shown below.
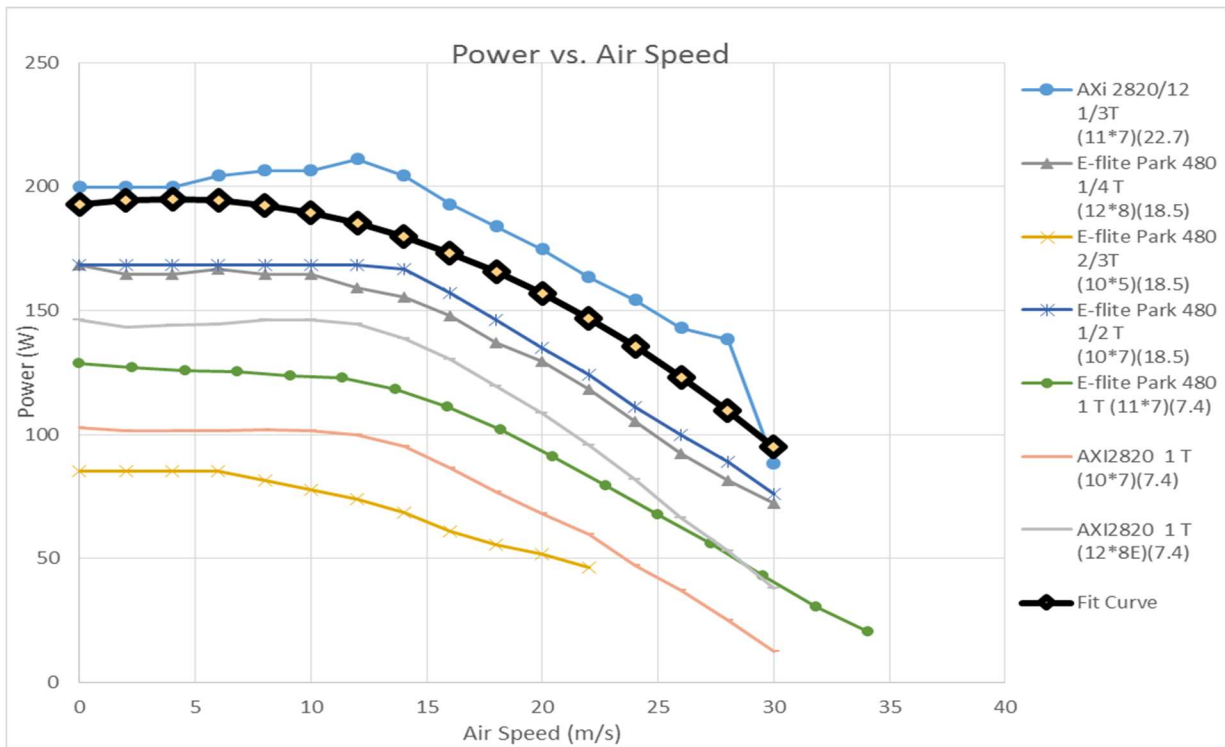
FIGURE 40: PROPULSION SYSTEM POWER
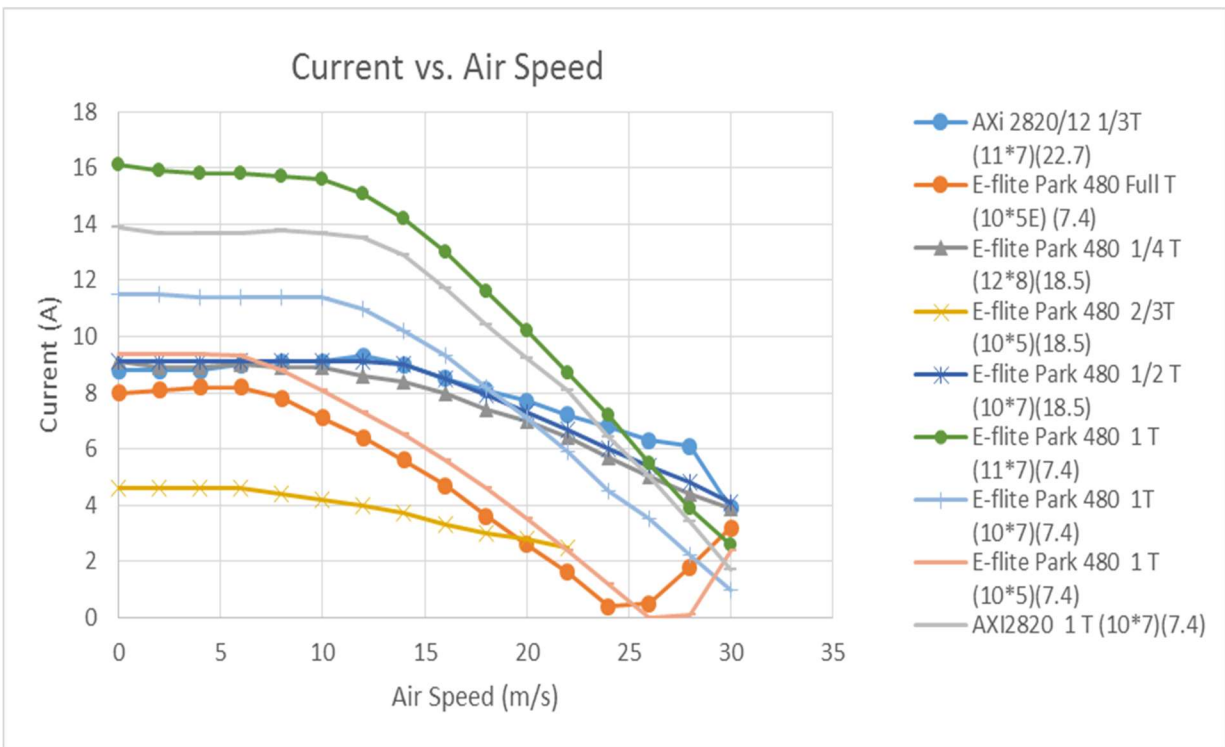
FIGURE 39: PROPULSION SYSTEM CURRENT DRAW

The current curve implies that the propellers with higher pitch angle draw have larger current draw. We narrow our selection of propeller to 10*6, 11*7, and 12*6.5.
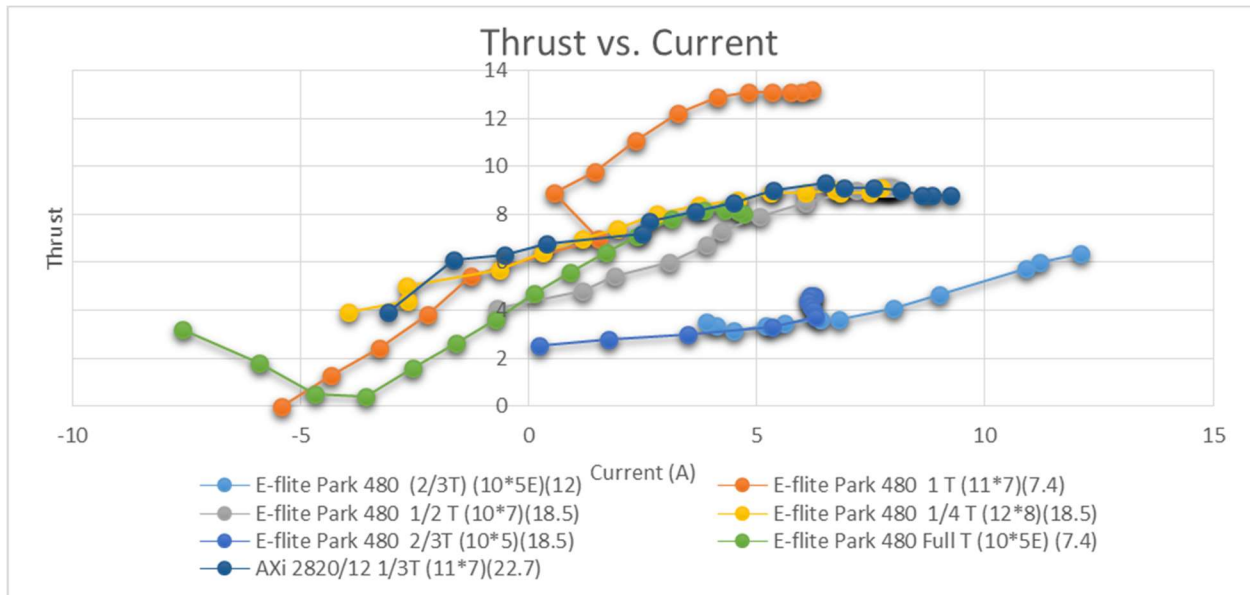
FIGURE 41: THRUST VS CURRENT

The thrust-to-current curve provides us the information that the static thrust can be raised by increasing the amperage value, so that we decided to choose a battery pack with a higher voltage to have a larger current accordingly.
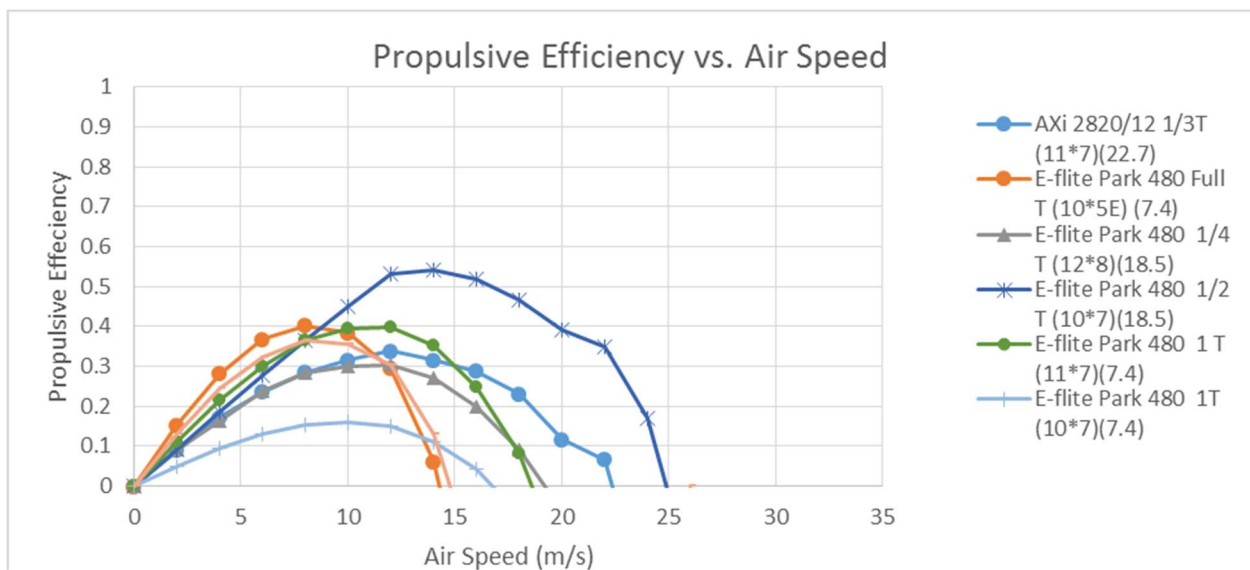
FIGURE 42: PROPULSIVE EFFICIENCY

The efficiency curve implies that the average efficiency the propulsion system will have is around 40% when at airspeed of about 10 m/s.
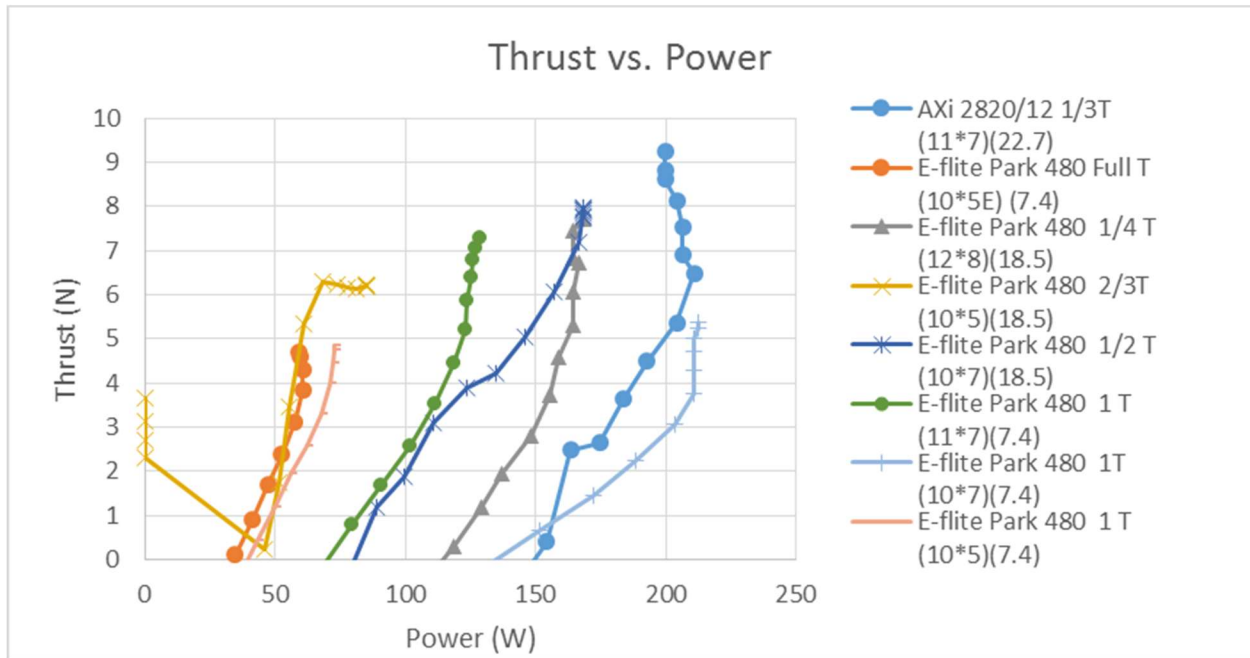
FIGURE 43: THRUST TO POWER

Aerodynamic Testing

Getting data to ensure the aerodynamics of our wing is important in ensure the flight capabilities of the UAV. If the lift coefficient of the wing doesn't match the expected value, the wing won't generate enough lift to carry the aircraft. In order to confirm the theoretical lift coefficients, a smaller 3D printed wing was designed and printed in order to fit into a wind tunnel. The wind tunnel was set to the same airspeed as the cruise speed of the aircraft, and lift and drag coefficients were then measured.

At the beginning of our tests, we ran into a problem where the height of the wind tunnel was too small to get a large range of angles of attacks Because of this, the lift and drag could only be measured between -0.25 degrees and 3.5 degrees. Because of this, it is difficult to extrapolate measured data. Additionally, there was no indicator of the zero angle inside the wind tunnel. The measurement tool did however give us information about the change in angle. However, we did our best to get a fit for both lift and drag vs. angles of attack

From the plot, we could see that our theoretical CL-alpha value of 5.27 was fairly close to the experimental value. We believe that the experimental value being larger than the theoretical value was due to the measurement tool under measuring changes in the angle of attack. The tool we were using is over fifty years old, and could possibly be inaccurate. The experiment CLo of 0.3596 was very close to our theoretical value of 0.32. The drag numbers were significantly higher than what we expected. This was most likely due to two reasons - the roughness of the 3D printed material and the support beam in the wind tunnel. We attempted to account for the drag of the bar in our calculations of the drag coefficient, but we believe there were 3D effects of the bar once the airfoil was added that couldn't be accounted for.
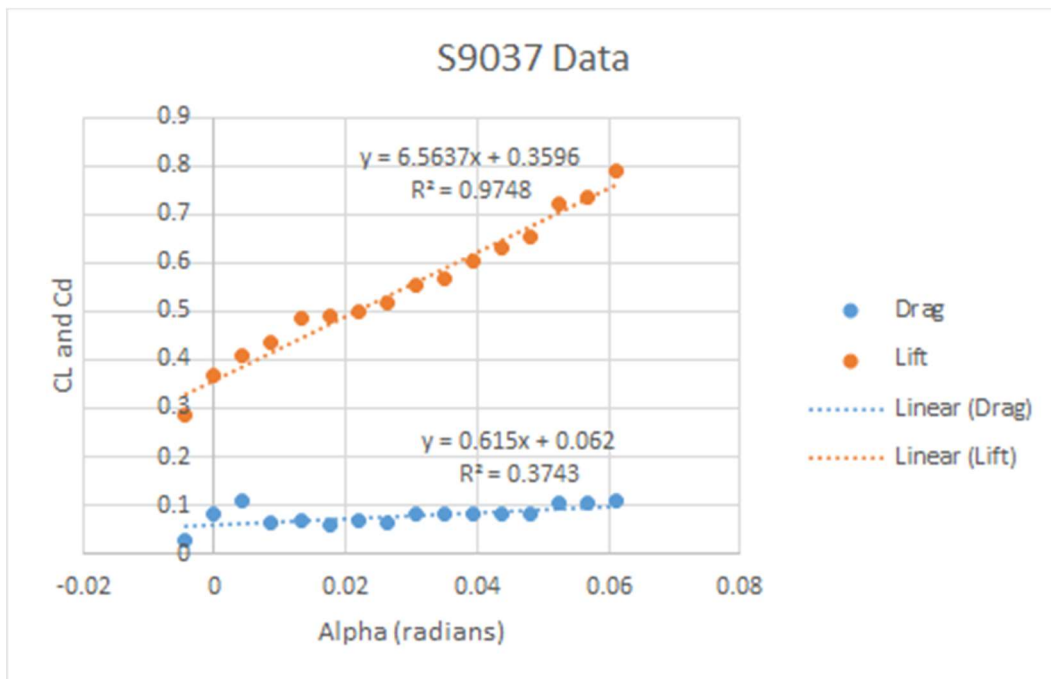
FIGURE 44: AERODYNAMICS WIND TUNNEL TESTING DATA ON S9037 AIRFOIL

Structural Testing

To choose the material we would use for the composite skin, we first evaluated the strength-to-weight ratio of our available materials (see Table 15).

				Material Testing			
Sample	Weave	Layers	Hardener	Normalized Weight (N/mm^2)	Average Elastic Modulus (N/mm^2)	Strength-to-Weight Ratio	Notes
Flat	3K Plain	1	PH3660	2953950.20	-	-	Fails visual inspection*
	3K Plain	1	PH3665	3121077.96	-	-	Fails visual inspection*
	3K Plain	2	PH3660	5933397.13	24981.77709	0.004210367	Fails just after 100 N
	3K Plain	2	PH3665	5900540.92	29978.13251	0.005080574	Fails before 100 N
	3K 2x2 Twill	1	PH3660	3063175.30	-	-	Fails visual inspection*
	3K 2x2 Twill	1	PH3665	2895140.38	-	-	Fails visual inspection*
	3K 2x2 Twill	2	PH3660	5661039.04	39358.87485	0.006952588	Fails just after 175 N
	3K 2x2 Twill	2	PH3665	5524964.21	49716.4735	0.008998515	Fails at 160 N
	6K 2x2 Twill	1	PH3660	4017994.91	162474.8164	0.04043679	Fails just after 100 N
	6K 2x2 Twill	1	PH3665	4354427.14	-	-	Fails visual inspection*
	6K 2x2 Twill	2	PH3660	8522630.61	474474.6046	0.055672318	Fails at 650 N
	6K 2x2 Twill	2	PH3665	9393352.08	421070.5365	0.04482644	Fails at 560 N
3D Print	N/A	N/A	N/A	28608484.77	11046919306	386.1413631	Carbon reinforced nylon
Foam	N/A	N/A	N/A	2736995.47	-	-	Only calculated Norm. Weight
Balsa	N/A	N/A	N/A	3055428.40	-	-	Only calculated Norm. Weight
Sandwich	3K Plain	3	PH3660	10554508.93	No Displacement**	80.5343011	Cracks at 600 N, Fails at 850 N
	3K Twill	3	PH3660	11853279.63	No Displacement**	71.71011116	Cracks at 600 N, Fails at 800 N
					Max Flat Sample Ratio:	0.055672318	2 Layers-6K 2x2 Twill-PH3660
					Max 2 Layer-3K Sample Ratio:	0.008998515	2 Layers-3K 2x2 Twill-PH3665

* Fails visual inspection means the sample failed before the force could be measured due to the instument's sensitivity

** Cannot measure vertical displacement because failure is localized; Strength-to-Weight Ratio in units of mm^2

We could not test every material possible, so we made some early assumptions about what materials made sense to use, so we could test them and find out what combinations of them had the most advantages. We considered 3 weaves of carbon fiber (3K Plain, 3K 2x2 Twill, and 6K 2x2 Twill), 1 to 3 layers of each material, and 2 types of hardeners (PH3660 and PH3665). PH3660 has a 1 hour setting time, and PH3665 has a 2 hour setting time. We chose epoxy (PR2032) on the basis that it was the lowest cost structural adhesive that was designed for carbon fiber-epoxy matrices in aerospace applications. We chose the hardeners that were designed for this adhesive and had reasonable setting times. We chose to test 1 to 3 layers because the weight cost of more than 3 layers was unacceptable for the size aircraft. We chose 3K Plain, 3K 2x2 Twill, and 6K 2x2 Twill because they were the only carbon fiber materials with bidirectional properties that would allow us to operate in this 1 to 3 layer range.

Once samples had been fabricated through the vacuum bagging process (see manufacturing plan), their dimensions and weight were measured to create a Normalized Weight. The samples were

then brought to a test stand where a three-point flexural test was conducted (see Figure X): a force was applied on the middle point of a sample that was supported on both ends from the opposite side (see Figure X).
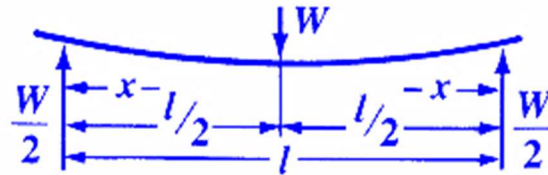
FIGURE 45: THREE-POINT FLEXURAL DIAGRAM

The force was then increased until the material failed. The dimensions of the test setup as well as the force used and measured displacement were all recorded. With these records, an Average Elastic Modulus was determined by using the following equations:

$$y = \frac{W * L^3}{(48 * E * I)} \rightarrow E = (W * I^3)/(48 * y * I)$$

Where: y = Max deflection at load (mm)

W = Force on Sample (N)

L = Test Length (mm)

E = Modulus of Elasticity (N/mm2)

I = Moment of Inertia = (t*w3)/12 (mm4); w = Test Width (mm) and t = Sample Thickness (mm)

This Average Elastic Modulus was then divided by the Normalized Weight to create a Strength-to-Weight ratio, which we used to analyze the results. We found that 3K plain was too weak compared to its 3K 2x2 Twill counterpart. We also found that 2 layers of 6K would be too heavy for the size of our aircraft. In doing so, our analysis identified 2x2 Twill with either 2 layers of 3K or 1 layer of 6K as the composite skin we should use during the manufacturing process.

However, other factors were considered for the final determination: we decided to use 3K Twill because we could manufacture a 0, 90, +45, -45° multi-directional composite for the skin, which would increase shear strength; furthermore, we decided to use PH3660 because was easier to work with than PH3665 and each hardener had similar properties when tested. We concluded that 2 Layers of 3K 2x2 Twill with PH3660 hardener would make the most sense to work with as a general purpose skin.

We also identified the need for thick, light weight material to use for wing ribs and a padded area to land on, if we continue with our plan to not use landing gear. We decided to manufacture a sandwich

that utilized a hard shell of carbon fiber for strength and a soft, lightweight core material for large, lightweight support. To select this material, we considered the same 3 weaves of carbon fiber (3K Plain, 3K 2x2 Twill, and 6K 2x2 Twill), and two core materials (balsa and FR4305 polyurethane foam). We chose the FR4305 as our foam because it was offered by the same distributor we had acquired our carbon fiber and epoxy from.

For the sandwich, we assumed 1 layer of 3K carbon fiber on either side is ⅛ in. of core material, and the PH3660 hardener due to weight and ease of manufacturing considerations. We chose foam as the core material because it had a lower Normalized Weight. We then produced 2 foam core samples which then underwent the three point flexural test. We chose 3K Plain as the shell material because it was able to withstand the highest force before cracking.

With our materials selected, we proceeded to manufacture and evaluate the strength of certain components of our aircraft design, like the wing panel. To characterize wing loading, we conducted a torsional rigidity and wing deflection test to determine 2 parameters ($G*I_0$ and $E*I$) that would allow us to create shear, moment, lift per unit span, angular deflection and wing deflection graphs using the scripting program, MATLAB. The test used a vice to turn an upside-down sample of our wing panel into a cantilever beam. The free end was loaded, and the resulting angular deflection and wing deflection were measured (see Figure X). Testing concluded at 6.8 kg, which is roughly three times our aircraft weight. Both Angular Deflection (see Figure X) and Wing Deflection (see Figure X) tested well within the acceptable range outlined in WPI's aero elasticity classes.
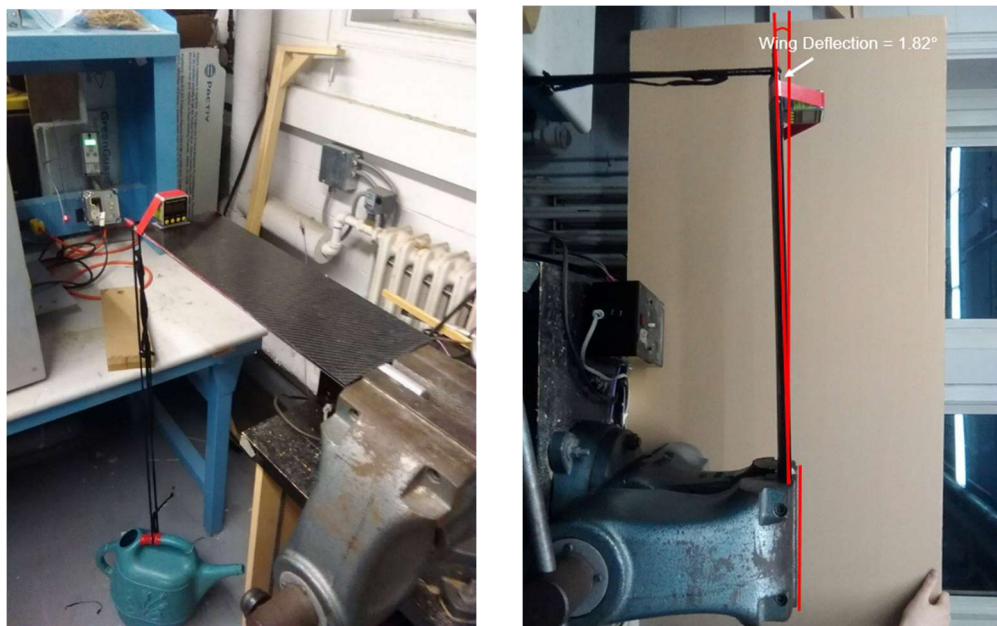
FIGURE 46: TORSIONAL RIGIDITY TESTING

To calculate the parameter G*I₀—the shear modulus of rigidity times the second moment of inertia—the length of the wing sample, the torque caused by the load, and the angular (torsional) deflection all must be know. The following equation was used.

$$\theta = (L_w * T)/(G * I0) \quad G * I0 = (L_w * T)/$$

Where: θ = angular shaft deflection (radians)

L_w = Length of Wing Panel (mm)

G*I0 = Shear Modulus of Rigidity*2nd Moment of Inertia

T = Torque = F*c/4; F = Force on Wing Panel (N) and c/4 = Distance from LE to Quarter Chord

To calculate the parameter E*I—the modulus of elasticity times the moment of inertia—the wing deflection at the free end, the force on the wing panel, and the length of the wing panel all must be known. The following equation was used.

$$\delta_{max} = \frac{P * L_w{}^3}{(3 * E * I)} \rightarrow E * I = (P * L_w{}^3)/(3 * \delta_{max})$$

Where: δ_{max} = Wing Deflection at Free End (mm)

P = Force on Wing Panel (N)

L_w = Length of Wing Panel (mm)

E*I = Elastic Modulus*Moment of Inertia (N*mm2)

TABLE 16: TORSIONAL RIGIDITY TESTING DATA

Cups	Total Weight (kg)	Total Weight (g)	Deflection (°)	Deflection (radians)	Shear Modulus*2nd Moment of Inertia (N*m^2)
0	0.3665	366.5	0.1	0.001745329	5.477065174
4	0.919691489	919.6914894	0.2	0.003490659	6.872046694
8	1.472882979	1472.882979	0.3	0.005235988	7.337040534
12	2.026074468	2026.074468	0.4	0.006981317	7.569537454
16	2.579265957	2579.265957	0.5	0.008726646	7.709035606
19	2.994159574	2994.159574	0.6	0.010471976	7.457574866
23	3.547351064	3547.351064	0.7	0.012217305	7.573211058
26	3.962244681	3962.244681	0.8	0.013962634	7.401593571
29	4.377138298	4377.138298	0.9	0.015707963	7.268113303
32	4.792031915	4792.031915	1	0.017453293	7.161329089
35	5.206925532	5206.925532	1.1	0.019198622	7.073960187
39	5.760117021	5760.117021	1.2	0.020943951	7.173382522
41	6.036712766	6036.712766	1.3	0.02268928	6.93954649
43	6.313308511	6313.308511	1.4	0.02443461	6.739115606
47	6.8665	6866.5	1.5	0.026179939	6.840976446
				Average	7.222604531
				Std Deviation	0.291915371

Wing deflection at free end was measured at the maximum load, 6.8 kg, and was found to be 1.82°, which was later converted to a length. Angular (torsional) deflection on the other hand was measured incrementally as the load on the wing panel was increased (by adding cups of water to the water vessel) and then averaged afterwards. This yielded a value of 7.223 N*m^2 with a std. deviation of 0.29 (Table X).

Using these results, our aircraft's general and performance characteristics, and scripts team members had made for WPI's aeroelasticity courses, we were able to generate 5 graphs that show wing loading in terms of shear, moment, lift per unit span, angular deflection and wing deflection. All the graphs show two lines, one that accounts for Prandtl's theory that wing lift drops off towards the wing tip, which is accurate, and one that doesn't account for this. This was done to show the influence of the Prandtl effect on wing loading. Figure X shows the lift per unit span along the wingspan of Gompei Volanti's wing.
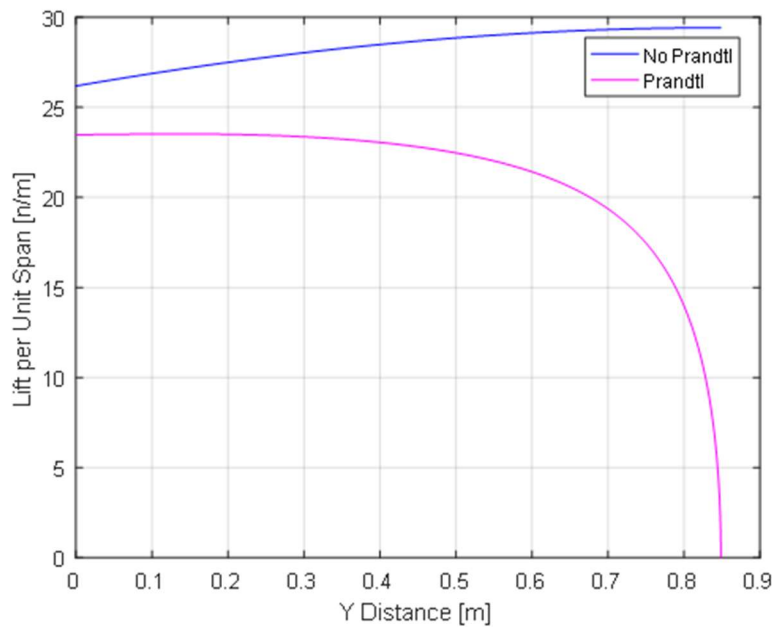
FIGURE 48: LIFT PER UNIT SPAN
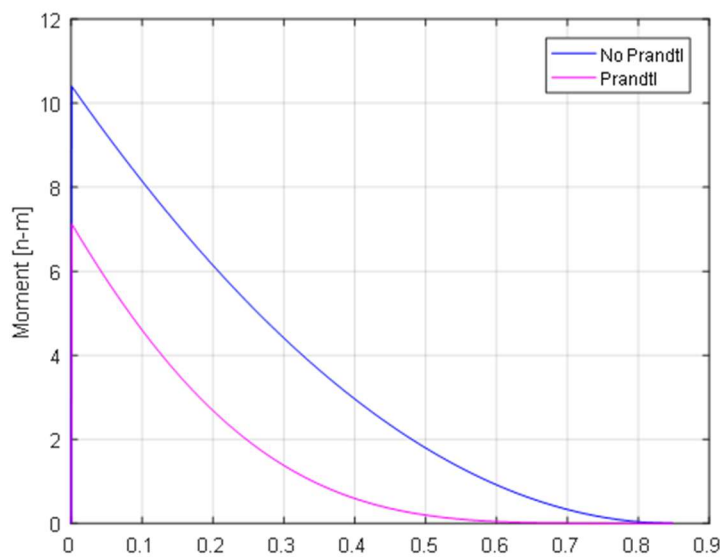
FIGURE 47: WING MOMENT

The figure shows very clearly the rapid decrease in lift generated (from its maximum of 23 N/m) as the wing approaches the tip, which is the most marked impact of the Prandtl effect.

Figure X shows the twisting moment along the wingspan of Gompei Volanti's wing. Like shear, the twisting moment on the wing peaks near the root at about 7 N-m, and decreases towards zero at the tip of the wing. Again, the Prandtl effect decreases this moment considerably.

As can be seen in Figure 31, shear on the wing peaks near the root at about 18 N, and decreases towards zero at the tip of the wing. The Prandtl effect decreases this shear considerably.
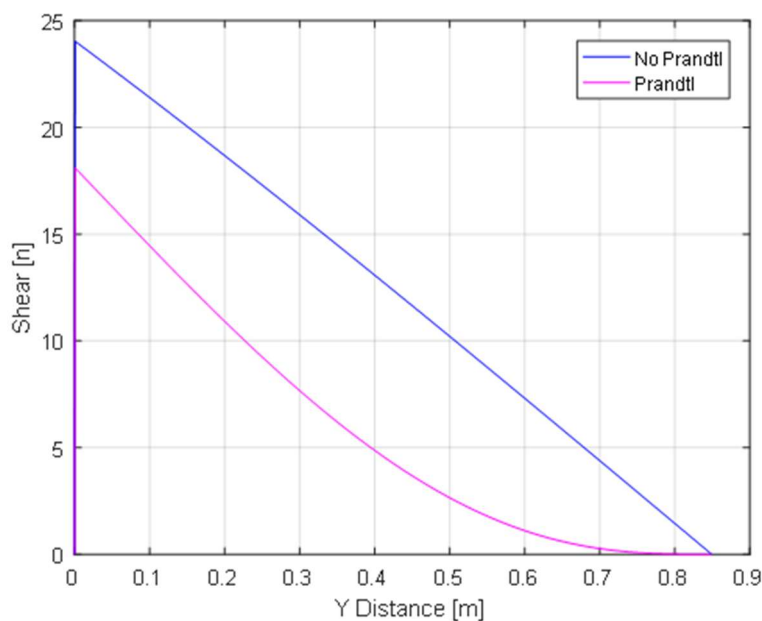
FIGURE 49 WING SHEAR

Figure X shows the angular (torsional) deflection along the wingspan of Gompei Volanti's wing. The angular deflection grows until it reaches a limit at about 0.16° at about two-thirds the way to the tip of the wing. The Prandtl effect decreases this angular deflection considerable and changes the maximum angular deflection from being at the tip of the wing to at the two-thirds marker.
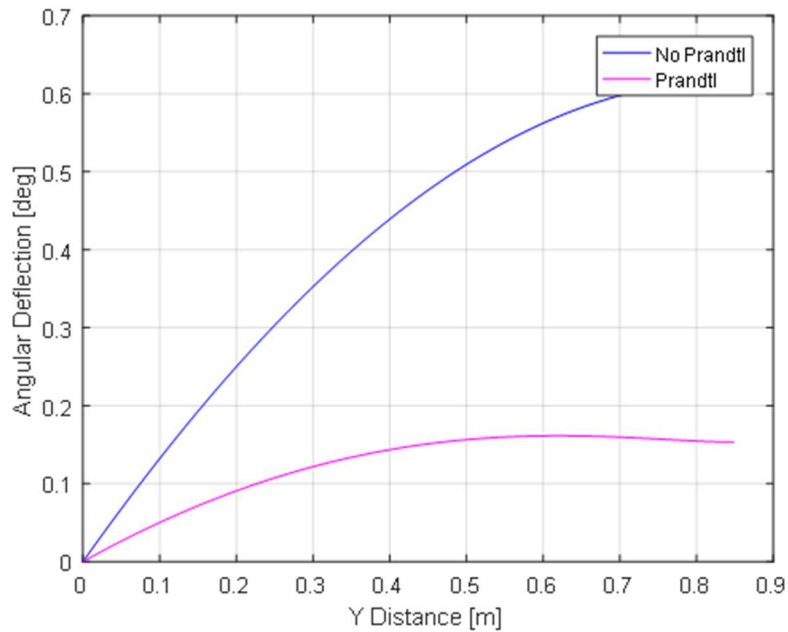
FIGURE 50: WING ANGULAR DEFLECTION

Figures 33 shows the wing deflection as angular deflection along the wingspan of Gompei Volanti's wing. The wing deflection grows exponentially at first but levels out about halfway to the tip of the wing, eventually reaching a maximum of 23 millimeters at the tip of the wing. Again, the Prandtl effect significantly decreases this wing deflection.
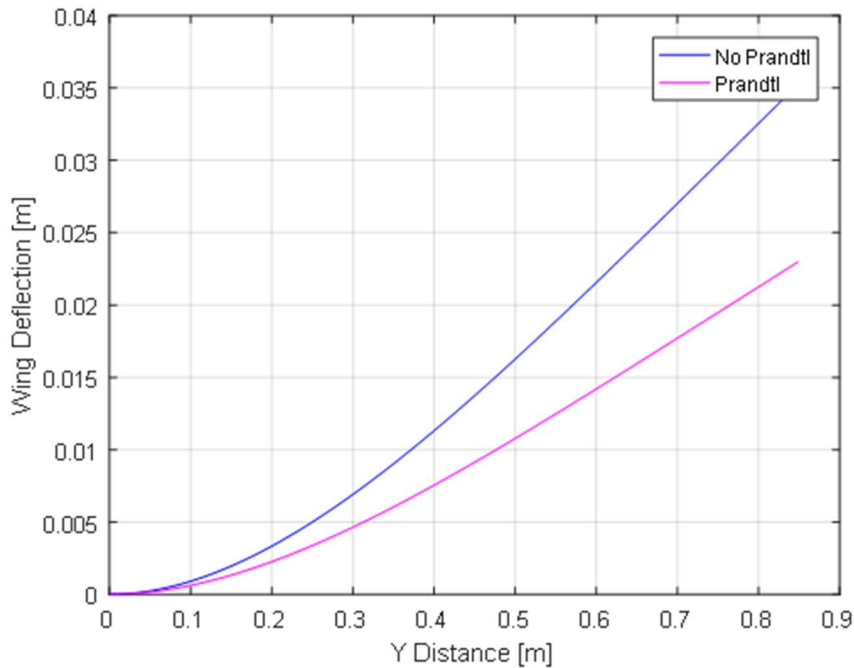
FIGURE 51: WING DEFLECTION

Figure 34 is simply intended to show a more accurate representation of how much the wing is deflecting, since its x-axis and y-axis are on the same scale. It is worthy of noting that this 23 millimeter deflection generates a 1.55° deflection that is very close to the 1.82° deflection in the torsional rigidity and wing deflection test. With our wing structure, Gompei Volanti will be able to handle the stresses associated with this deflection with ease, as our wing panel did so in the torsional rigidity test.
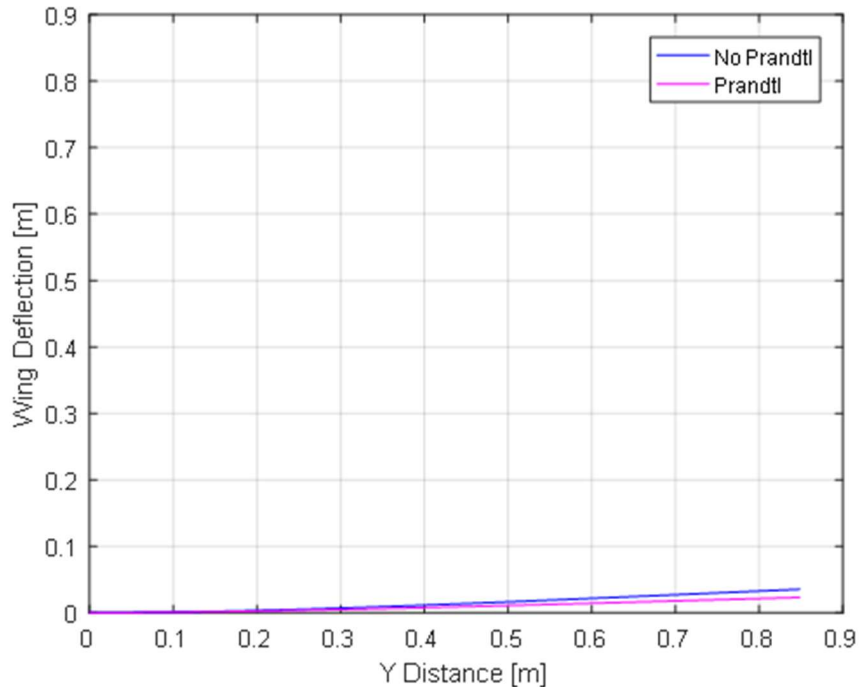
FIGURE 52: WING DEFLECT AS COMPARED TO BASELINE

Flight Testing

The team flew both the prototype and actual aircraft several times. The fiberglass prototype was heavier than the actual aircraft, and therefore underpowered. The first flight with the prototype was in a straight line, and it was determined that the elevators did not provide enough moment to sufficiently control the pitch of the aircraft. In response to this, the team built a new tail with larger elevators and rudder, which also had an increased range of motion. These new control surfaces proved to be sufficient enough and the second test flight was proceeding well, until the left wingtip of the aircraft impacted a tree during a turn. The fiberglass skin held up to the collision, breaking away at a glued seam, as it was

designed to do. The balsa wood spar inside the wing did not fare as well, shattering on impact. The team was able to repair the left wingtip, using a carbon fiber sandwich as a replacement spar for the left side of the wing. The prototype's third test flight took place on a windy day, and a sudden crosswind gust soon after takeoff causing a controlled flight into terrain. The right wing hit the ground first, causing much of the same damage as the collision with the tree. The balsa wood spar was shattered and the wing broke off at another glued seam. The team repaired this wing again, but the decision was made to proceed with construction of the final carbon fiber aircraft. The three flight tests of the prototype were judged to be successes, despite the two collisions with terrain. The flights proved that our design was capable of controlled flight. One of the lessons learned from the prototype was that we needed a neater leading edge on our airfoils, so a leading edge mold was made and integrated into production of the next aircraft.

The carbon fiber aircraft was underpowered and unbalanced at first; it took a few flights and hard landings to solve these problems. The aircraft made several straight line flights and landings. On these flights, panels would occasionally come unglued, but nothing catastrophic happened. On the third test flight of the carbon fiber aircraft, the right wingtip impacted the ground and the force sheared the upper fuselage in half. This allowed us to revisit our center of gravity calculations, and when the wing was attached to a new fuselage it was in a slightly different location, which we hoped would fix our stability problems. On the next test flight, the aircraft pitched up suddenly due to the new center of gravity, and the pilot was almost able to perform a full loop and recover the aircraft, but it impacted the ground nose first. There was significant damage, but only two new bulkheads needed to be made, and a few days later the aircraft was ready to fly again. On its fifth, test flight the plane flew a perfect lap around a soccer field. After this flight, the blistering speed of the plane became apparent, and the pilot needed a nearly 100 yard glide in order to safely land the plane. For the sixth and final flight of the aircraft, we brought the plane to a wide open field, loaded it with three hockey pucks and launched it. The plane flew one regulation lap, and the pilot brought it in for a landing. Unfortunately, he misjudged his speed and the landing was a little hot. The plane folded on impact as it was designed to do, with the wing rotating and knocking the vertical tail off. As the old saying goes, "any landing you can walk away from is a good landing," and the aircraft was repaired within four hours. It has not been flown since, as the team decided to preserve it for display. The airplane is currently in flying condition.

CONCLUSION

A MAV was built to meet the specifications for the 2017 AIAA DBF competition, as it demonstrated a capability to fold into a tube, fly after a hand launch, and carry a payload. General aircraft configuration was assessed by comparing alternative designs, and selecting the most viable, highest performing variant. The aircraft was sized based on a series of tests, theoretical equations, and design guidelines. Specific aircraft design was determined using detailed design criteria, in addition to lessons learned during flight tests. Composite structures were manufactured to provide a lightweight, strong structure/skin for the aircraft. Aluminum joints were designed and manufactured to meet the folding requirements of the design. Standard remote control equipment was sized through theory, extensive testing, and flight tests. All of these elements came together into a successful MQP and a highly competitive folding MAV.

RECOMMENDATIONS

Deciding on an aircraft configuration can be difficult, identifying critical design flaws by preliminary analysis can speed this process along. In particular performing a basic CG estimate for a particular micro aerial vehicle can help eliminate unstable candidates. Plan more time for manufacturing and flight testing and flight test design revision. While theoretical calculation and design guidelines are useful in creating a flyable aircraft, real world flight testing will provide immediate feedback whether the aircraft specifications are acceptable.

Identify critical skills, and improving those skills in weakest areas early on in the design process will help lead to more successful project. In particular, CAD skills while present in the team were not widespread enough to aid in developing the aircraft design. While composite manufacturing skills were ultimately excellent, cutting and gluing the composite parts together, although acceptable, would have benefited from further improvement.

Reducing the scope of the project by selecting a simpler aircraft configuration, which is easier to analyze and manufacture can be beneficial to meeting project goals if critical skills, or prior experience with aircraft design are nonexistent.

Discussing the project goals, timeline, and funding by meeting with the appropriate faculty early in the design process will ensure successful project. Aligning project goals, deadlines, and funding limits between the appropriate parties will help avoid conflict later in the year.

Include underclassmen in the future aircraft design projects so they can develop the skills, and experience designing aircraft. Having prior experience and knowledge of the typical roadblocks these projects face will ultimately lead to a better performing aircraft and tendency to meet project deadlines. This will also provide an opportunity for students to exercise the theory learned in class in the development of a model aircraft. Instituting an open door policy makes it easy for underclassmen to stay involved, and those who are truly dedicated to the project will make great contributions and ultimately become leaders in future projects.

References

[1] T. Eshel, "Switchblade - Miniature Loitering Weapon," Defense Update, 2011. [Online]. Available: http://defense-update.com/products/s/switchblade_31122010.html. [Accessed 20 February 2017].

[2] Next Media Animation, "US used 'kamikaze' drone in Afghanistan," Next Media Animation, 19 October 2011. [Online]. Available: https://www.youtube.com/watch?v=VdRjYkEU-N4. [Accessed 20 February 2017].

[3] L. Parnas, "An Agricultural Bloom," The Drone Perspective, 3 March 2016. [Online]. Available: https://thedroneperspective.wordpress.com/2016/03/03/an-agricultural-bloom-2/. [Accessed 20 February 2017].

[4] AeroVironment, "Unmanned Aircraft Systems," AeroVironment, [Online]. Available: https://www.avinc.com/uas/adc/switchblade. [Accessed 20 February 2017].

[5] D. P. Raymer, Aircraft Design: A Conceptual Approach, American Institute of Aeronautics, 2012.

[6] L. Benson, "Beam Deflection," 2015. [Online]. Available: https://www.slideshare.net/LisaBenson2/8-beam-deflection. [Accessed 20 2 2017].

[7] J. Anderson, Fundamentals of Aerodynamics, McGraw-Hill Education, 2010.

[8] J. Anderson, Aircraft Performance & Design, McGraw-Hill Education, 1998.

[9] "Torsional Deflection of a Shaft," [Online]. Available: http://www.engineersedge.com/mechanics_machines/torsional_deflection_of_shaft_13120.htm. [Accessed 20 2 2017].

[10] "Beam Bending," [Online]. Available: http://www.engineersedge.com/beam_bending/beam_bending2e.htm. [Accessed 20 2 2017].

[11] "Area Moment of Inertia," [Online]. Available: http://www.engineeringtoolbox.com/area-moment-inertia-d_1328.html. [Accessed 20 2 2017].

APPENDIX

Scoring Code –

```
clc;
clear;
clear all;
close all;

air_density = 1.08;
kinematic_viscosity = 1.46*10^-5;
launch_velocity = 9;
load_factor = 1;
turnloadfactor = 2;
batterysafetyfactor = 1.2;
numberofcells = 9;
batteryconstant = 4.17557434536678*10^-6;

%% Data holders
actual_empty_weight_r = [];
scoreable_empty_weight_r = [];
scoreable_velocity = [];
score_r = [];
velocity_score=[];
velocity_weight=[];
wing_areas_weight = [];
wing_ares_score = [];
actual_empty_weight_rs = [];
velocity_r_score = [];
highestscore = 0;

%% Material Info
Density_Aluminum = 2700;
Density_Resin = 1134;
threed_Printer_Density = 1315.40723;
Volume_FractionWovenFiberTotal= 0.45;
Volume_FractionMattFiberTotal = 0.2;
Carbon_FiberThickness3kPlain =  0.0003048;
Carbon_FiberThickness3kTwill =  0.0002794;
Carbon_FiberThickness6kTwill =  0.0004318;
Carbon_FiberWeight3kPlainFiber = 0.193263;
Carbon_Fiber0Weight3kTwillFiber = 0.193263;
Carbon_FiberWeight6kTwillFiber = 0.3695;
Carbon_FiberWeight3kPlain = 0.3834;
Carbon_FiberWeight3kTwill = 0.3675;
Carbon_FiberWeight6kTwill =0.6388;
NumberofLayers = 3;

Tube_Length = 0.72;
Tube_Diameter = 0.18;
```

```matlab
Cap_Weight = 0.2138;
Tube_Weight = 0.5202;
Total_Weight = 0.7340;

%% Ranges
pucks_r = 3:1:3;
velocity_r = 12:0.2:28;
empty_weight_r = 1.3:0.02:8;

%% Tail info
Volume_Ratio_Horizontal = 0.70;
Volume_Ratio_Vertical_Tail = 0.04;
Horiztonal_Tail_Chord_To_Tube_Diameter = 0.70;
Aspect_Ratio_Vertical = 1.80;
Taper_Ratio_Vertical_Tail = 1.00;
Tail_Distance_To_Tube_Length = 1.00;

%% Areas
global Elevator_area;
Elevator_area = 0.05;
global Rudder_area;
Rudder_area = 0.03;
global Tailboom_area;
Tailboom_area = 0.05;
global Fuselage_Wetted_Area;
Fuselage_Wetted_Area = 0.15;
global Fuselage_Frontal_Area;
Fuselage_Frontal_Area = 0.01;
global wing_wetted_area;
global AR;

%% Weights
puck_weight = 170/1000;
controls_battery_weight=57/1000;
servo_weight=9/1000;
reciever_weight=9/1000;
switch_weight=10/1000;
speed_control_weight=30/1000;

%% Coefficients
global fuselage_cd;
fuselage_cd = 0.05;
global parasitic_wing_cd;
parasitic_wing_cd = 0.02;
Cl_max = 1.4;
global e;
e = 0.83;
AR = 12;
k = (4/3)/(pi*e*AR);
Cl_max_i = Cl_max/(1+Cl_max*k);
Cl_o = 0.17;
ClAlpha = 6.28;
```

```
global Cl;
global skin_friction_coeff;
global wing_area;

global q;
%% Iterators
for N_pucks = pucks_r
    disp(N_pucks);
    for empty_weight = empty_weight_r
        for velocity = velocity_r
            total_weight = (empty_weight+puck_weight*N_pucks);
            %% Initial Calculations
            q = 0.5*air_density*velocity^2;
            Cl = Cl_max_i*(launch_velocity^2/velocity^2);
            wing_area =
(empty_weight+puck_weight*N_pucks)*9.8*2*load_factor/(air_density*velo
city^2*Cl);
            span = sqrt(AR*wing_area);
            chordlength = wing_area/span;
            ReynoldsNum =
air_density*velocity*chordlength/kinematic_viscosity;
            aoa = (Cl - Cl_o)/ClAlpha*180/pi;
            skin_friction_coeff = 1.328/(ReynoldsNum)^0.5;
            wing_wetted_area = 2 * wing_area;
            elevator_wetted_area = 2 * Elevator_area;
            rudder_wetted_area = 2*Rudder_area;
            % end of Initial Calculations
            %% Landing
            landingvelocity = 13;
            landingclimb = -3;
            q = 0.5*air_density*landingvelocity^2;
            ReynoldsNum =
air_density*landingvelocity*chordlength/kinematic_viscosity;
            skin_friction_coeff = 1.328/(ReynoldsNum)^0.5;
            total_landingdrag = totaldrag();
            landingthrust =
total_landingdrag+total_weight*sin(landingclimb*pi/180);
            landingstaticthrust =
thrusttostatic(landingthrust,landingvelocity);
            landingwattage = -0.1457*landingvelocity^2 +
1.1039*(landingvelocity) + thrusttowatts(landingstaticthrust);
            landingtime = 8;
            landingenergy = landingtime*landingwattage;
            % end of landing
            %% Turn
            turnvelocity = 14;
            q = 0.5*air_density*turnvelocity^2;
            ReynoldsNum =
air_density*turnvelocity*chordlength/kinematic_viscosity;
            skin_friction_coeff = 1.328/(ReynoldsNum)^0.5;
            turnclimb = 2;
            turnbank = 60;
```

```
            turnradius = turnvelocity^2/(9.8*sqrt(turnloadfactor^2-
1));
            turnthrust =
totaldrag()+total_weight*sin(turnclimb*pi/180);
            turnstaticthrust =
thrusttostatic(turnthrust,turnvelocity);
            turnwattage = -0.1457*turnvelocity^2 +
1.1039*(turnvelocity) + thrusttowatts(turnstaticthrust);
            turntime = turnradius*4*pi/turnvelocity;
            turnenergy = turntime*turnwattage;
            %% Takeoff
            takeoffvelocity = 9;
            q = 0.5*air_density*takeoffvelocity^2;
            ReynoldsNum =
air_density*takeoffvelocity*chordlength/kinematic_viscosity;
            skin_friction_coeff = 1.328/(ReynoldsNum)^0.5;
            takeoffthrust = totaldrag();
            takeoffstaticthrust =
thrusttostatic(takeoffthrust,takeoffvelocity);
            takeoffwattage = -0.1457*takeoffvelocity^2 +
1.1039*(takeoffvelocity) + thrusttowatts(takeoffstaticthrust);
            takeofftime = 1.2;
            takeoffenergy = takeofftime*takeoffwattage;
            %% Climb
            climbvelocity = 14;
            climbangle = 20;
            q = 0.5*air_density*climbvelocity^2;
            ReynoldsNum =
air_density*climbvelocity*chordlength/kinematic_viscosity;
            skin_friction_coeff = 1.328/(ReynoldsNum)^0.5;
            climbthrust =
sin(climbangle*pi/180)*total_weight*9.8+totaldrag();
            climbstaticthrust =
thrusttostatic(climbthrust,climbvelocity);
            climbwattage = -0.1457*climbvelocity^2 +
1.1039*(climbvelocity) + thrusttowatts(climbstaticthrust);
            altitude = 35;
            climbdistance = altitude/tan(climbangle*pi/180);
            climbtime =
altitude/(sin(climbangle*pi/180)*climbvelocity);
            climbenergy = climbtime*climbwattage;
            % end of Climb
            %% Cruise
            q = 0.5*air_density*velocity^2;
            ReynoldsNum =
air_density*velocity*chordlength/kinematic_viscosity;
            skin_friction_coeff = 1.328/(ReynoldsNum)^0.5;
            total_drag = totaldrag();
            cruisestaticthrust = thrusttostatic(total_drag,velocity);
            cruisewattage = -0.1457*velocity^2 + 1.1039*(velocity) +
thrusttowatts(cruisestaticthrust);
            loverd = total_weight*9.8/total_drag;
```

87

```
            cruisetime = 0.3048*2000/velocity;
            cruiseenergy = cruisetime*cruisewattage;
            % end of cruise
            %%
            maxthrust =
max([cruisestaticthrust,climbstaticthrust,turnstaticthrust,landingstat
icthrust,takeoffstaticthrust]);
            N_Laps = floor((5*60-climbtime-landingtime-
takeofftime)/(cruisetime+turntime));
            totalenergy =
batterysafetyfactor*(landingenergy+(turnenergy+cruiseenergy)*N_Laps+cl
imbenergy+takeoffenergy);
            voltage = 1.2*numberofcells;
            %% Tail Calculations
            tube_length = 0.36*span;
            Tail_Distance = Tail_Distance_To_Tube_Length *
tube_length;

Horizontal_Tail_Surface_Area=Volume_Ratio_Horizontal*chordlength*wing_
area/Tail_Distance;

Vertical_Tail_Surface_Area=Volume_Ratio_Vertical_Tail*span*wing_area/T
ail_Distance;
            tube_diameter = 1.08*chordlength;
            MeanHorizontalChord =
tube_diameter*Horiztonal_Tail_Chord_To_Tube_Diameter;
            Span_Horizontal_Tail =
Horizontal_Tail_Surface_Area/MeanHorizontalChord;
            HeightofVerticalTail =
sqrt(Aspect_Ratio_Vertical*Vertical_Tail_Surface_Area);
            RootChordVerticalTail=
(2*Vertical_Tail_Surface_Area)/((Taper_Ratio_Vertical_Tail+1)*Heightof
VerticalTail);
            TipChordVerticalTail =
RootChordVerticalTail*Taper_Ratio_Vertical_Tail;
            %
            %% Weight
            batteryweight = totalenergy*batteryconstant;
            pucks_weight = puck_weight*N_pucks;
            frontwings_weight =
NumberofLayers*Carbon_FiberWeight3kTwill*wing_area;
            fuselage_weight =
NumberofLayers*Carbon_FiberWeight3kTwill*Fuselage_Wetted_Area;
            tail_boom_weight =
NumberofLayers*Carbon_FiberWeight3kTwill*Tailboom_area;
            verticaltail_weight =
NumberofLayers*Carbon_FiberWeight3kTwill*Rudder_area;
            horizontaltail_weight =
NumberofLayers*Carbon_FiberWeight3kTwill*Elevator_area;
            wing_pivots_weight = 1*0.042;
            wing_hinges_weight = 2*0.051;
            tail_pivots_weight = 1*0.021;
```

```
            tail_hinges_weight = 1*0.025;
            light_servos_weight = 5*0.009;
            medium_servos_weight = 0*0.035;
            servo_extensions_weight = 4*0.007;
            servo_horns_weight = 5*0.005;
            controls_battery_weight = 0.057;
            controls_reciever_weight = 0.012;
            switch_weight = 0.01;
            prop_esc_weight = 0.035;
            prop_motor_weight = 3*(0.0426*maxthrust-0.325)/1000;
            prop_prop_weight = 0.025;
            prop_wiring_weight = 0.02;
            prop_switch_weight = 0.02;
            prop_fuse_weight = 0.02;

            actual_empty_weight =
batteryweight+frontwings_weight+fuselage_weight+tail_boom_weight+verti
caltail_weight +horizontaltail_weight +wing_pivots_weight
+wing_hinges_weight+tail_pivots_weight+tail_hinges_weight+light_servos
_weight+medium_servos_weight+servo_extensions_weight+servo_horns_weigh
t+controls_battery_weight+controls_reciever_weight+switch_weight+prop_
esc_weight+prop_motor_weight+prop_prop_weight+prop_wiring_weight+prop_
switch_weight+prop_fuse_weight;
            vstall =
((2*total_weight*9.8)/(Cl_max_i*wing_area*air_density))^0.5;
            if(actual_empty_weight<empty_weight)
                M1 = 1;
                M2 =
2*(90/(cruisetime*3+takeofftime+climbtime+turntime*3+landingtime));
                M3 = 4*((N_pucks*N_Laps)/(28))+2;
                tube_length = 0.36*span;
                tube_diameter = 1.08*chordlength;
                cap_weight =
(tube_diameter*pi*0.0001*threed_Printer_Density+tube_diameter^2/4*pi*C
arbon_FiberWeight6kTwill*2)*2;
                tube_weight =
pi*tube_length*tube_diameter*2*Carbon_FiberWeight6kTwill;
                tube_total_weight = tube_weight+cap_weight;
                RAC = (actual_empty_weight+tube_total_weight) *
(tube_length + pi*tube_diameter);
                W_R_S = 95;
                T_M_S = M1 + M2 + M3;
                score = W_R_S*T_M_S/RAC;
                scoreable_empty_weight_r = [scoreable_empty_weight_r
actual_empty_weight];
                velocity_score = [velocity_score velocity];
                score_r = [score_r score];
                if(score>highestscore)
                    highestscore = score;
                    save planeconfig.mat
                end
            end
```

```
        end
    end
    scatter(scoreable_empty_weight_r,score_r,6,'filled');
    hold on
    scoreable_empty_weight_r = [];
    score_r = [];
end
legend('hide')
legend('3 Pucks','4 Pucks','5 Pucks')
xlabel('Empty Weight (kg)')
ylabel('Score')
clc; clear all;
load planeconfig.mat;
```

Wing Aeroelasticity Code –

```
close all
clc
clear
%% This code was created as a part of HW and Exams for AE 5382, taken under
Prof. Sergey Averkin at WPI in 2016 and may or may (?) not be legally
considered intellectual propery of Alex Brown, it is more likely considered
educational material.I am not responsible in any case, for any damages, that
may result from the usage of this program. Satisfaction and saftey is not
guarenteed.
%% User Notes
% Progam will not notice if stall angle of attack is exceeded.
% Program uses cantelervered wing (1/2 a wing for a traditional plane)

%% listing all variables
r=1;        % Percentage of the wing with flap.
alpha_root=5*pi/180; % Angle of attatch at wing root
Clb=1.83;  % coeffecient lift of flap
Cmb=-0.3512; % coeffecient moment of flap
Bf=15*pi/180;% flap deflection angle
L=1;        % Length of cantilevered wing
AR=9;       % Aspect Ratio (assumed full wing)
GJ=5; % Torsional stiffness of wing (code does not work properly? with GJ=1
EI=40; % Bending Stiffness of the wing
Ao=2*pi;   % Lift-angle Slope
c=2*L/AR;  % chord (from aspect ratio and span)
e=.3*c;    % Distance between wing elastic axis and aeroydynamic center  ---
assumed elastic axis was at wing center c/2 and lift is aplied at aerodynamic
cetner c/4
p=1.08;  % Air/fluid density
u=10;      % Velocity
q=.5*p*u^2;% dynamic pressure
n=1000;     % number of discrete divisions
m=n+1;     % dimensions of matrix
phinom=pi/2;
phi=(phinom*ones(1,m)-((0:((phinom-10^-6)/(n)):(phinom-10^-6))));
%% Making the [B] matrix
Alex Brown Made this
B=zeros(m);
```

```matlab
bag=0;
 for j=(1:1:n);
        for f=(1:1:j);
            bag=bag+1;
        end
        B(j+1,j+1)=bag;
        bag=0;
        B(j+1,(j+1:n+1))= B(j+1,j+1).*ones(1,n-j+1);
        B((j+1:n+1),j+1)= B(j+1,j+1).*ones(n-j+1,1);
   end;

%% Making Vertical Displacement Matrix's (B111 and B123)
 B111=zeros(m);
 bag=0;
for j=(1:1:n);
        B111(j+1,(j+1:m))=1;
end;
 B_111=zeros(m);
 bag=0;
for j=(1:1:n);
        B_111(j+1,(2:j+1))=1;
end;
 B123=zeros(m);
for j=(1:1:n);
    for f=(1:1:n);
            if(f+j<m+1)
                B123(j+1,f+j) = f;
            end
    end
end;

%% Making [COO] matrix
COO=L/(n*GJ).*B;
%% Making the Prandtl [COO] matrix
COOp=zeros(m);
bin=0;
for j=(2:1:m)
    phij=phi(j);
    phij1=phi(j-1);
    bin=cos(phij)-cos(phij1)+bin;
    COOp(j,j)=bin;
    COOp(j,(j:m))= COOp(j,j).*ones(1,m-j+1);
    COOp((j:m),j)= COOp(j,j).*ones(m-j+1,1);
end
COOp=L/(GJ).*COOp;
%% Making the [A] matrix
%simple [A]
A=Ao*c.*eye(m);

%Prandtl aerdynamic matrix, [Ap] and its inverse [Api]

bless=zeros(m);
evil=zeros(m);
god=zeros(m);
 for j=(1:1:m);
    phin=phi(j);
    bless(j,j)=1/sin(phin);
```

91

```matlab
    for f=(1:1:m)
        evil(j,f)=(2*f-1)*sin((2*f-1)*phin);
        god(j,f)=sin((2*f-1)*phin);
    end
 end
 Api=1/(Ao*c).*eye(m)  +  (1/(8*L)).*bless*evil/god; %
 Ap=inv(Api);

%% Making the [Wi] and [eWi] matrix
Wi=L/n.*eye(m);
Wi(1,1)=0;
eWi=e*L/n.*eye(m);

% for Prandtl
Wip=zeros(m);
for j=(2:1:m)
    phij=phi(j);
    phij1=phi(j-1);
    Wip(j,j)=cos(phij)-cos(phij1);
end
Wip=Wip.*L;
eWip=Wip.*e;
%% Making the [Ar] (Alpha-r) and CLb (Flap Coeffecient Lift) and Flap
Coeffecient Moment Vector
Ar=alpha_root.*ones(m,1); %Angle of attack at root
xb=zeros(m,1);
xb(1:(round(n*r)+1),1)=1;
CLB=xb*(Clb*Bf/Ao);
CMB=xb*Cmb;
% making same matricies for prandtl
CLBp=ones(m,1)*(Clb*Bf/Ao);
CMBp=ones(m,1)*Cmb;
for f=(1:1:m)
    if r < cos(phi(f))
        CLBp(f,1)=0;
        CMBp(f,1)=0;
    end
end

%% Making the [P] and [H] matricies (equivlant to [RHS] and [LHS]respectively
from lecture 5)
P=q.*COO*(eWi*A*(Ar+CLB)+c^2.*Wi*CMB);
P1=q.*COOp*(eWip*Ap*(Ar+CLBp)+c^2.*Wip*CMBp);
H=eye(m)-q.*COO*eWi*A;
H1=eye(m)-q.*COOp*eWip*Ap;
%% Solving
O=H\P;
O1=H1\P1;
%% Eigen Values & Divergence Speed
qd=1/(max(eig(COO*eWi*A))); %Divergence Dynamic Pressure (non prandtl)
Vd=(2*qd/p)^0.5; % Divergence Velocity (non prandtl)
qd1=1/(max(eig(COOp*eWip*Ap))); %Divergence Dynamic Pressure (prandtl) W/
Wingtip Vortex
Vd1=(2*qd1/p)^0.5; % Divergence Velocity (prandtl) w/ Wingtip Vortex
Divergence_Velocity_prandtl=Vd1
Divergence_Velocity_non_prandtl=Vd;
%% Lift Distribution
```

92

```matlab
Lift_span=q.*A*(O+Ar+CLB);
Lift1_span=q.*Ap*(O1+Ar+CLBp);

%% Total Lift (non-prandtl)
x5=L/n;
Total_Lift=sum(Lift_span.*x5)
Total_Lift_kg=Total_Lift/9.8
%% The Exact Solution
y1=(q*c*Ao*e/GJ)^0.5;
u1=(Clb*e+c*Cmb)/(Ao*e);
x=(0:L/n:L);
x1=L*cos(phi);
O2= -u1*(1-cos(y1.*x)-sin(y1.*x)*tan(y1*L));
Lift2_span=q.*c.*((Ao.*(O2+1.*pi./180.*ones(1,m)))+Clb.*Bf.*ones(1,m));
%% Making Shear and Moment Matrices (prandtl)
Increments=zeros(m,1);
for j=(1:1:m)
Increments(j)=Wip(j,j);
end
B123p = zeros(m);
for j=(1:1:m);
    for f=(1:1:m);
            if(f>=j)
                B123p(j,f) = sum(Increments(j:f));
            end
    end
    B123p(1,j)=0;
end;
B111p = zeros(m);
for j=(1:1:n);
    for f=(1:1:n);
            if(f<=j)
                B111p(f+1,j+1) = Wip(j+1,j+1);
            end
    end
end;

B_111p = zeros(m);
for j=(1:1:n);
    for f=(1:1:n);
            if(f>=j)
                B_111p(f+1,j+1) = Wip(j+1,j+1);
            end
    end
end;
%% Calculating Shear & Moment
%non-prandtl
Shear=L/n*B111*Lift_span;
Moment=(L/n)^2*B123*Lift_span;
Dv_Dx=L/(n*EI)*B_111*Moment;
Vertical_Deflection=L/m*B_111*Dv_Dx;
%prandtl
Shear_p=B111p*Lift1_span;
Moment_p=B123p*(Lift1_span.*Increments);
Dv_Dx_p=(1/EI)*B_111p*Moment_p;
Vertical_Deflection_p=B_111p*Dv_Dx_p;
```

```matlab
%% Plotting Angular Deflection
%plot(x,O2.*180/pi,'r'); %actual Solution
%hold on
plot(x,O'.*180/pi,'b'); %without prandtl
grid on
hold on
plot(x1,O1'.*180/pi,'m');%with prandtl
legend('No Prandtl','Prandtl')
xlabel(' Y Distance [m] ')
ylabel('Angular Deflection [deg]')


%% Plotting Lift Per Unit Span
figure
%plot(x,Lift2_span,'r'); % Exact Full Flap Solution
%hold on
plot(x,Lift_span','b'); %Without Prandtl
grid on
hold on
plot(x1,Lift1_span','m');%with prandtl
legend('No Prandtl','Prandtl')
xlabel(' Y Distance [m] ')
ylabel('Lift per Unit Span [n/m]')

%% Plotting Vertical Deflection
figure
plot(x,Vertical_Deflection,'b')
grid on
hold on
plot(x1,Vertical_Deflection_p,'m')
xlabel(' Y Distance [m] ')
ylabel('Wing Deflection [m]')
legend('No Prandtl','Prandtl')
%% Plotting Moments
figure
plot(x,Moment,'b');
hold on
grid on
plot(x,Moment_p,'m');
xlabel(' Y Distance [m] ')
ylabel('Moment [n-m]')
legend('No Prandtl','Prandtl')
%% Plotting Shear

figure
plot(x,Shear,'b');
hold on
grid on
plot(x,Shear_p,'m');
xlabel(' Y Distance [m] ')
ylabel('Shear [n]')
legend('No Prandtl','Prandtl')
```

94

Drag Calculator Code –

```matlab
% Jamie Donahue
% DBF - Aerodyanmics Calculator
% 4/9/2017

clc;
clear;
close all;

%% CONVERSION TABLES
deg2rad = pi/180; % Converts degrees to radians

%% AIRCRAFT WEIGHT + SPEED
% Weight Characteristics
EW = 0.2905 + 0.230 + 0.2377 + 0.3334 + 0.2325 + 0.057 + 0.354 + 0.0416 +
0.193; % Aircraft Empty Weight (kg)
wo = EW - 0.193 - 0.354; % Empty weight without motor, battery, or prop
W_pay = 3*0.170097; % Payload Weight (kg) - 3 Hockey Pucks
W_max = EW + W_pay; % Total Max Weight (kg)
L = W_max*9.81; % Lift Force (N)

% Velocity Characteristics
V_c = 0:1:25; % Cruise velocity (m/s)
V_s = 10.5; % Stall velocity (m/s) --> Estimated max throwing speed
R = 287; % Gas Constant (kg/J*K)
gamma = 1.4; % Air constant
Temp = 294; % Temperature (K)
M = V_c/sqrt(gamma*R*Temp); % Mach number

%% AIRCRAFT WING GEOMETERY
% Straight Wing
b = 0.58*3 - 0.09; % Wing span (m)
c = 0.145; % Chord length (m)
S_w = b*c; % Wing Area (m^2)
AR = b^2/S_w; % Aspect Ratio;

%% AIRCRAFT TAIL GEOMETERY
% Horizontal Tail
b_ht = 2*0.15; % Span (m)
c_ht = 0.16; % Chord (m)
S_ht = b_ht*c_ht; % Horizontal Tail Area (m^2)

% Vertical Tail
b_vt = 0.14; % Span (m)
c_vt = 0.16; % Chord (m)
S_vt = b_vt*c_vt; % Vertical Tail Area (m^2)

% Total Tail (Vertical + Horizontal)
St_total = S_ht + S_vt; % Total Tail Area (m^2)

%% AIRCRAFT FUSELAGE GEOMETERY
S_f = 0.075*0.075; % Fuselage Frontal Area (m^2)

%% LIFT CHARACTERISTICS
rho = 1.0760; % Typical density in Tuscon, AZ during April (kg/m^3)

CL_c = L./(0.5*rho*V_c.^2*S_w); % Required Cruise CL
```

```matlab
CL_to = L./(0.5*rho*V_s.^2*S_w); % Required TO CL


%% DRAG CHARACTERISTICS
% Constants
e = 1.78*(1-0.045*AR^0.68) - 0.64; % Oswald Efficency Factor --> Chapter 3.
Drag Force and its Coefficent (pg.9)
u = 1.46E-5; % Kinematic Viscosity of Air (m^2/s)

% Geometery
c_bar = c; % Wing MAC (m)
c_ht_bar = c_ht; % Horizontal Tail MAC (m)
c_vt_bar = c_vt; % Vertical Tail MAC (m)
FL = 0.57; % Fuselage Length (m)
FD = 0.075; % Fuselage Diamter (m)
d_joint = 0.02; % Joint diameter (m)

    % Calculate individual Reynolds numbers for each component
        % 1. Wing --> Li = c_w bar
         Re_w = rho*V_c.^2*c_bar/u;
        % 2. Horz tail --> Li = c_ht_bar
         Re_ht = rho*V_c.^2*c_ht_bar/u;
        % 3. Ver tail --> Li = c_vt_bar
         Re_vt = rho*V_c.^2*c_vt_bar/u;
        % 4. Fuselage --> Li = Fuselage Length
         Re_f = rho*V_c.^2*FL/u;
        % 5. Joints
         Re_joint = rho*V_c.^2*d_joint/u;

t_c = 0.012; % Thickness of Wing, HT, and VT Airfoils
L_nose = 0.04; % Nose Length (m)

% Wetted Areas
Sw_wet = 2*(1 + 0.2*(t_c))*S_w; % Wetted Wing Area (m^2)
Sht_wet = 0.72*S_ht; % HT Wetted Tail Area (m^2)
Svt_wet = 0.72*S_vt; % Vt Wetted Tail Area (m^2)
Sf_wet = 0.75*S_f*L_nose; % Wetted Fuselage Frontal Area (m^2)
Sj_wet = 0.72*d_joint ; % Wetted Joint Area (m^2)
S_wet = 2*(Sw_wet + Sht_wet + Svt_wet + Sf_wet + Sj_wet); % Total Wetted Area
(ft^2)

% Drag Coefficent Calculations

Cf_w = 0.455./(log(Re_w).^2.58); % Skin Friction Wing Coefficent (Turbulent
Flow)
Cf_ht = 0.455./(log(Re_ht).^2.58); % Skin Friction HT Coefficent (Turbulent
Flow)
Cf_vt = 0.455./(log(Re_vt).^2.58); % Skin Friction VT Coefficent (Turbulent
Flow)
Cf_f = 0.455./(log(Re_f).^2.58); % Skin Friction Fuselage Coefficent
(Turbulent Flow)
Cf_joint = 0.455./(log(Re_joint).^2.58); % Skin Friction Weapon 1 Coefficent
(Turbulent Flow)

f_tcw = 1 + 2.7*(t_c) + 100*(t_c)^4; % Based on 12% thick airfoil
f_tcht = 1 + 2.7*(t_c) + 100*(t_c)^4; % Based on 12% thick airfoil
f_tcvt = 1 + 2.7*(t_c) + 100*(t_c)^4; % Based on 12% thick airfoil
```

```matlab
f_ld = 1 + 60/(FL/FD)^3 + 0.0025*(FL/FD); % Fuselage length-to-diameter ratio
f_m = 1 - 0.08*M.^1.45; % Mach number function

Cd_min_w = 0.0085; % Minimum Drag Coefficent for wing (From airfoil analysis)
Cd_min_ht = 0.008; % Minimum Drag Coefficent for HT (From airfoil analysis)
Cd_min_vt = 0.008; % Minimum Drag Coefficent for VT (From airfoil analysis)

Cd_f = Cf_f.*f_ld.*f_m*(Sf_wet/S_w); % Fuselage Drag Coefficent --> Chapter
3. Drag Force and its Coefficent (pg.13)
Cd_w = Cf_w.*f_tcw.*f_m*(Sw_wet/S_w)*(Cd_min_w/0.004)^0.4; % Wing Drag
Coefficent
Cd_ht = Cf_ht.*f_tcht.*f_m*(Sht_wet/S_w)*(Cd_min_ht/0.004)^0.4; % Horizontal
Tail Drag Coefficent
Cd_vt = Cf_vt.*f_tcvt.*f_m*(Svt_wet/S_w)*(Cd_min_vt/0.004)^0.4; % Vertical
Tail Drag Coefficent
Cd_joint = Cf_joint.*f_tcw.*f_m*(Sj_wet/S_w); % Joint Drag Coefficent
Cd_hld = 0.0217; % High Lift Devices (Flap) Drag Coefficent --> From Airfoil
Analysis (Change in Cd due to flap)

Cd_o = Cd_f + Cd_w + Cd_ht + Cd_vt + Cd_joint + Cd_hld; % Parastic Drag
Coefficent

k = 1/(pi*e*AR); % Induced Drag Factor Correction
Cd_ic = k*CL_c.^2; % Cruise Induced Drag Coefficent
Cd_ito = k*CL_to_c.^2; % Take-off Induced Drag Coefficent


Cd_c = Cd_o + Cd_ic; % Cruise Total Drag Coefficent
Cd_to = Cd_o + Cd_ito; % Take-off Total Drag Coefficent
%% Thrust-Drag Plot

V_max = 0:1:25; % Variable Cruise Velocity (m/s)

Di_c = 0.5*rho*V_max.^2.*S_w.*Cd_ic; % Cruise Induced Drag (N)
Do_c = 0.5*rho*V_max.^2.*S_w.*Cd_o; % Cruise Zero-Lift Drag (N)
D_c = Di_c + Do_c; % Cruise Total Drag Force (N)

Vs_max = 9.6:1:34.6; % Variable Stall Velocity (m/s)

Di_to = 0.5*rho*Vs_max.^2.*S_w.*Cd_ito; % Take-off Induced Drag (lbs)
Do_to = 0.5*rho*Vs_max.^2.*S_w.*Cd_o; % Take-off Zero-Lift Drag (lbs)
D_to = Di_to + Do_to; % Take-off Total Drag Force (lbs)

Thrust_c = D_c;
Thrust_to = D_to;

figure
plot(V_max,D_c, 'b')
hold on
plot(V_max, Thrust_c, 'r')
plot(V_max, Thrust_c, 'r*')
title('Cruise Speed vs Drag')
xlabel('Cruise Speed (m/s)')
ylabel('Drag(N) + Thrust (N)')
legend('Drag', 'Thrust')
grid on
hold off
```

```matlab
figure
plot(Vs_max,D_to, 'b')
hold on
plot(Vs_max, Thrust_to, 'r')
plot(Vs_max, Thrust_to, 'r*')
title('T/O Speed vs Drag')
xlabel('T/O Speed (m/s)')
ylabel('Drag(N) + Thrust (N)')
legend('Drag', 'Thrust')
grid on
hold off

V_check = V_max - V_c;
```

Total Drag Code –

```matlab
function totaldrag = totaldrag
global q;
global Elevator_area;
global Rudder_area;
global Tailboom_area;
elevator_wetted_area = 2*Elevator_area;
rudder_wetted_area = 2*Rudder_area;
global Fuselage_Wetted_Area;
global Fuselage_Frontal_Area;
global wing_wetted_area;
global AR;
global e;
global skin_friction_coeff;
global Cl;
global fuselage_cd;
global wing_area;
global parasitic_wing_cd;
wetted_area_drag =
q*(wing_wetted_area+elevator_wetted_area+Fuselage_Wetted_Area+rudder_w
etted_area+Tailboom_area)*skin_friction_coeff;
induced_wing_cd = Cl^2/(pi*AR*e);
fuselage_pressure_drag = q*fuselage_cd*Fuselage_Frontal_Area;
induced_wing_drag = q*induced_wing_cd*wing_area;
wing_parasitic_drag = q*wing_area*parasitic_wing_cd;
totaldrag = wing_parasitic_drag + induced_wing_drag +
fuselage_pressure_drag+wetted_area_drag;
```
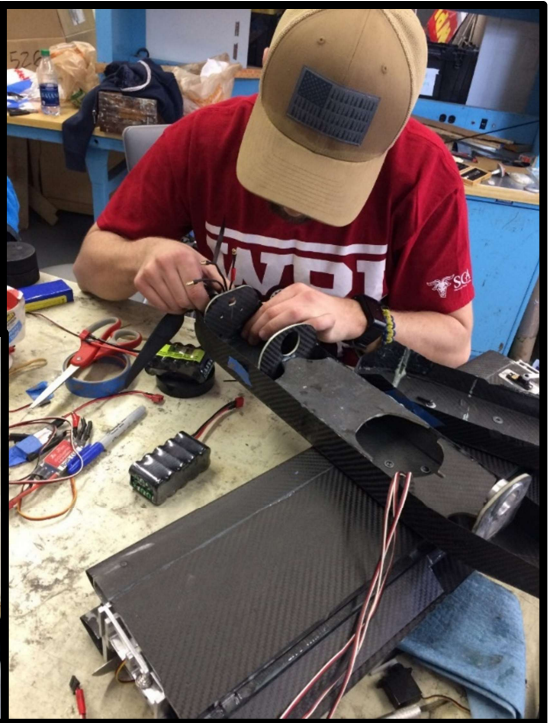
Aircraft Composite Weight Calculater	
Input	**Numbers**
Density of Aluminum	2700
Density of Resin (kg/M^3)	1134
3-D Printer Density (Kg/M^3)	1056.26823
Volume Fraction Woven (Fiber/Total)	0.45
Volume Fraction Matt (Fiber/Total)	0.2
Carbon Fiber Thickness(3k Plain) (M)	0.0003048
Carbon Fiber Thickness (3k Twill)(M)	0.0002794
Carbon Fiber Thickness (6k Twill)(M)	0.0004318
Carbon Fiber Weight (3k Plain)(Kg/M^2) (Fiber only)	0.193263
Carbon Fiber Weight (3k Twill)(Kg/M^2)(Fiber only)	0.193263
Carbon Fiber Weight (6k Twill)(Kg/M^2) (Fiber only)	0.3695
Carbon Fiber Weight(3k Plain) (Kg/M^2)	0.3182
Carbon Fiber Weight (3k Twill) (Kg/M^2)	0.2951
Carbon Fiber Weight (6k Twill) (Kg/M^2)	0.4439
Number of Carbon Fiber Layers per plan form area 3k	4.2500
Rib Distance	0.05

Aircraft Propulsion Calculater					
Input	**Cruise**	**Takeoff**	**Climb**	**Turn**	**Landing Run**
Velocity (m/s)	22.2500	9.5000	12.3500	20.0000	13.0000
Climb Angle (degree)	X	X	20	2	-3
Bank Angle (degree)	0.0000	0.0000		60.0000	0.0000
Turning Radius (m)	X	X	X	23.5653	X
Thrust (N)	1.6696	1.4652	8.5774	2.3212	1.0681
Static Thrust(N)	9.4604	3.9922	12.0948	9.0272	4.8264
Static Thrust (g)	965.3468	407.3653	1234.1614	921.1414	492.4932
Static Wattage (W)	193.5774	63.1377	286.9561	180.1229	77.5073
Wattage (W)	146.0085	60.4753	278.3668	143.9209	67.2347
Altitude (m)	X	X	35	X	X
Time (s)	27.3978	12	8.286085345	14.8065	8
Repeat	6.0000	1	1	6.0000	1
Energy (J)	24001.8329	725.7035	2306.5709	12785.8066	537.8776

Battery Weight Calculater

Input			Output	
Safety Factor (#)		2	Energy (j)	80715.58303
Number of cells in Series (#)		9	Weight(kg)	0.3370
Constant (kg/J)		4.18E-06	Voltage (V)	10.8
			Voltage	10.8
			Capacity (A-s)	7473.6651
			Capacity in mAh	2076.018082

Score Predictor

Our Team	Score	Imaginary Team	Score	Best (time) or (laps*pucks)
M1	1	M1	1	X
M2	1.1620	M2	2	90
M3	4.5714	M3	6	28
RAC	3.4889	RAC	1	
Report	95	Report	100	
Total Score	183.3476	Total Score	900.0000	

Aircraft Trim & Stability Calculator (Carrying Pucks)

Input	Cruise	Takeoff	Climb	Turn	Landing Run
Cmac (Zero Lift Pitching Moment)	0.0600	0.0070	0.0070	0.0070	0.0070
a (Lift Curve Slope (Wing) 3d)	5.2700	5.2700	5.2700	5.2700	5.2700
at (Lift Curve Slope (Tail) 3d)	5.4200	5.4200	5.4200	5.4200	5.4200
Wing Area	0.2973	0.2973	0.2973	0.2973	0.2973
Tail Area	0.0415	0.0415	0.0415	0.0415	0.0415
stance Between Aerodynamic Centers (LT ba	0.6188	0.6188	0.6188	0.6188	0.6188
Chord Length	0.1769	0.1769	0.1769	0.1769	0.1769
h	0.5000	0.5000	0.5000	0.5000	0.5000
hac	0.2500	0.2500	0.2500	0.2500	0.2500
Incidence Angle (degrees) (It)	-1.0000	-1.0000	-1.0000	-1.0000	-1.0000
dԑ/dα	0.0400	0.0400	0.0400	0.0400	0.0400
Lift Force	23.0275	23.0275	23.0275	46.0550	23.0275
Density	1.0760	1.0760	1.0760	1.0760	1.0760
Velocity	22.2500	9.5000	12.3500	20.0000	13.0000
Elevator Effectiveness	2.0400	2.0400	2.0400	2.0400	2.0400
Downwash angle ԑ0 (Degrees)	0.0000	0.0000	0.0000	0.0000	0.0000
Vh bar (Horizontal Wing Volume Ratio)	0.4877	0.4877	0.4877	0.4877	0.4877
Lt (Distance Between CG and tail AC)	0.5746	0.5746	0.5746	0.5746	0.5746
CM0 (Moment at Zero Angle of Attack)	0.1028	0.0498	0.0498	0.0498	0.0498
ā	5.9955	5.9955	5.9955	5.9955	5.9955
Cmα (Moment Curve Slope)	-1.0389	-1.0389	-1.0389	-1.0389	-1.0389
Clo (Lift Coefficient at Zero AoA)	-0.0132	-0.0132	-0.0132	-0.0132	-0.0132
Cl total (Total Lift Coefficient)	0.2908	1.5953	0.9440	0.7199	0.8519
Moment Curve Slope (Elevator)	-0.9239	-0.9239	-0.9239	-0.9239	-0.9239
Lift Coefficient (Elevator)	0.2844	0.2844	0.2844	0.2844	0.2844
Incidence Angle (radians)	-0.0175	-0.0175	-0.0175	-0.0175	-0.0175
Angle of Attack (Trim) (rads)	-0.0118	0.2209	0.1062	0.0667	0.0900
Elevator Deflection (Trim) (rads)	0.0574	-0.2617	-0.1327	-0.0883	-0.1144
Angle of Attack (Trim) (degs)	**-0.6753**	**12.6584**	**6.0830**	**3.8209**	**5.1539**
Elevator Deflection (Trim) (degs)	**3.2860**	**-14.9952**	**-7.6009**	**-5.0570**	**-6.5561**
Neutral Point hn	0.6733	0.6733	0.6733	0.6733	0.6733
Static margin (Better be positive)	0.1733	0.1733	0.1733	0.1733	0.1733
alpha wb trim numerator	-0.2516	-1.4719	-0.8701	-0.6631	-0.7851
elevator deflection numerator	-0.3007	1.3723	0.6956	0.4628	0.6000
denominator	-5.2436	-5.2436	-5.2436	-5.2436	-5.2436

Aircraft Aerodynamics Calculater					
Input	Cruise	Takeoff	Climb	Turn	Landing Run
Wing Planform Area (M^2)	0.2973	0.2973	0.2973	0.2973	0.2973
Elevator Planform Area (M^2)	0.0415	0.0415	0.0415	0.0415	0.0415
Rudder Planform Area (M^2)	0.0276	0.0276	0.0276	0.0276	0.0276
Fuselage Length/Tube Length	0.80	0.8000	0.8000	0.8000	0.8000
Fusalage Wetted Area (M^2)	0.1535	0.1535	0.1535	0.1535	0.1535
Fusalage Frontal Area(M^2)	0.0060	0.0060	0.0060	0.0060	0.0060
Tail Boom Wetted Area	0.05	0.0500	0.0500	0.0500	0.0500
Average Chord Length (m)	0.1769	0.1769	0.1769	0.1769	0.1769
Span (m)	1.6805	1.6805	1.6805	1.6805	1.6805
Fusalage Cd	0.05	0.0500	0.0500	0.0500	0.0500
Aircraft Weight(kg)	2.20	2.2000	2.2000	2.2000	2.2000
Airspeed (m/s)	22.25	9.5000	12.35	20.00	13.00
Oswald Effeciency Factor	0.83	0.83	0.83	0.83	0.83
Parasitic Wing Cd0	0.01	0.01	0.01	0.01	0.01
CL_o	0.32	0.32	0.32	0.32	0.32
Density of Air (kg/m^3)	1.08	1.08	1.08	1.08	1.08
Kinematic Viscosity of Air (m^2/s)	1.46E-05	1.46E-05	1.46E-05	1.46E-05	1.46E-05
Cl-alpha	5.27	5.27	5.27	5.27	5.27
Cl-Max Safety Factor	0.94	0.94	0.94	0.94	0.94
Cl max	1.59	1.59	1.59	1.59	1.59
Design Stall Speed	9.50	9.50	9.50	9.50	9.50
Dynamic Pressure (N/m^2)	266	49	82	215	91
Reynolds Number	290076.01	123852.68	161008.48	260742.48	169482.61
Skin Friction Coeffecient	0.0025	0.0038	0.0033	0.0026	0.0032
k	0.040369041	0.0404	0.0404	0.0404	0.0404
Induced Clmax	1.4937	1.4937	1.4937	1.4937	1.4937
Induced Cl	0.2693	1.4087	0.8534	0.6562	0.7728
Wing Wetted Area	0.5946	0.5946	0.5946	0.5946	0.5946
Elevator Wetted Area	0.0829	0.0829	0.0829	0.0829	0.0829
Rudder Wetted Area	0.0551	0.0551	0.0551	0.0551	0.0551
Load Factor	1.0000	1.0000	1.0000	2.0000	1.0000
Lift (N)	21.5600	21.5600	21.5600	43.1200	21.5600
Aspect Ratio	9.5000	9.5000	9.5000	9.5000	9.5000
AoA (Radians)	-0.0087	0.2075	0.1022	0.0647	0.0869
Predicted Aircraft Weight (kg)	2.3497	2.3497	2.3497	2.3497	2.3497
AoA (Degrees)	-0.4965	11.8909	5.8532	3.7091	4.9769
CL	0.2723	1.4937	0.8838	0.6740	0.7976
Induced Wing Cd	0.0029	0.0801	0.0294	0.0174	0.0241
Wetted Area Drag (N)	0.6148	0.1715	0.2542	0.5239	0.2746
Fuselage Pressure Drag (N)	0.0802	0.0146	0.0247	0.0648	0.0274
Induced Wing Drag (N)	0.2319	1.1564	0.7172	1.1119	0.6516
Wing Parasitic Drag (N)	0.7428	0.1227	0.2073	0.5438	0.2298
Cd0 (total)	0.0104	0.0095	0.0095	0.0095	0.0095
Total Drag (N)	1.6696	1.4652	1.2034	2.2444	1.1833
Total Drag(Kg)	0.1704	0.1495	0.1228	0.2290	0.1207
Area to Meet Stall Speed	0.2973	0.2973	0.2973	0.2973	0.2973
Lift/Drag	12.9136	14.7149	17.9155	19.2122	18.2207
Vstall (m/s)	9.5000	9.5000	9.5000	13.4350	9.5000
Vstall (mph)	21.2509	21.2509	21.2509	30.0534	21.2509
Note:	FLAPS UP 2 DEGREES IN CRUISE				

Wing Panel Flap/Aileron Moment Calculater					
Input	Cruise	Takeoff	Climb	Turn	Landing Run
Dynamic Pressure (N/m^2)	266.3436	48.5545	82.0571	215.2000	90.9220
Percentage Control Surface	0.2000	0.2000	0.2000	0.2000	0.2000
Flap Area (m^2)	0.0198	0.0198	0.0198	0.0198	0.0198
Flap Chord (m)	0.0354	0.0354	0.0354	0.0354	0.0354
Flap Angle (deg)	20.0000	20.0000	20.0000	20.0000	20.0000
Flap angle (rad)	0.3491	0.3491	0.3491	0.3491	0.3491
Nondimensional Flap Torque	0.4974	0.4974	0.4974	0.4974	0.4974
Dimensional Flap Torque (n-m)	0.0929	0.0169	0.0286	0.0751	0.0317
Dimensional Flap Torque (n-cm)	9.2892	1.6934	2.8619	7.5055	3.1711
Dimensional Flap Torque (kg-cm)	0.9479	0.1728	0.2920	0.7659	0.3236
Saftey Factor	2.0000	2.0000	2.0000	2.0000	2.0000
Servo Arm (mm)	9.0000	9.0000	9.0000	9.0000	9.0000
Control Horn Arm (mm)	12.0000	12.0000	12.0000	12.0000	12.0000
Adjusted Torque (kg-cm)	1.4218	0.2592	0.4380	1.1488	0.4854
Mimumim Stall Torque (kg-cm)	2.8436	Suggested Servo:	3 x	HS-5070MH	

Tail Calculations	
Volume Ratio Horizontal	0.5
Volume Ratio Vertical Tail	0.04
Horiztonal Tail Chord/Tube Diameter	0.58
Aspect Ratio Vertical	1.02
Taper Ratio Vertical Tail	1.00
Tail Distance/Tube Length	0.80
Tail Distance	0.6343
Elevater Surface Area	0.0415
Elevater Span	0.3614
Elevater Chord	0.1147
Rudder Surface Area	0.0276
Rudder Height	0.1682
Rudder Root Chord	0.1639
Rudder Tip Chord	0.1639